

ESO ELT
Basic Reference Design
1st Phase (Jan.-April 2006)

ESO/Community Working Groups

WG3 - ELT Site Evaluation Working Group Final Report

13 April 2006

WG3 Composition

Chair:

Roland Gredel gredel@caha.es

Deputy Chair:

Marc Sarazin msarazin@eso.org

Secretary:

Gautier Mathys gmathys@eso.org

Immo Appenzeller I.Appenzeller@lsw.uni-heidelberg.de

Vincent Coude du Foresto Vincent.Foresto@obspm.fr

Casiana Munoz-Tunon cmt@iac.es

Sergio Ortolani ortolani@pd.astro.it

Andreas Quirrenbach quirrenb@strw.leinduniv.nl

Jean Vernin vernin@unice.fr

Richard Wilson r.w.wilson@durham.ac.uk

Roberto Gilmozzi rgilmozz@eso.org

Ferdinando Patat fpatat@eso.org

Ralf Siebenmorgen rsiebenm@eso.org

Jorge Melnick jmelnick@eso.org

WGs Coordinator:

Guy Monnet gmonnet@eso.org

Table of Content

Executive Summary

Tables:

- **8**-Potential sites
- **11**-Available instrumentation
- **13**-Relevant parameters for science
- **19**-Requirements for site characterization

Main Document (page number, title, author):

- I. General considerations, site characterization
 - **21**-Search for potential sites (Marc Sarazin)
 - **25**-Available instrumentation for site characterization (Casiana Munoz Tunon)
 - **34**-Site characterization at Dome C (Jean Vernin)
- II. Relevant site parameters for UV/optical observations
 - **42**-Impact of optical and NIR sky brightness on site evaluation (Ferdinando Patat)
 - **60**-Site requirements for UV observations (Roberto Gilmozzi)
 - **65**-Site requirements for Quant-Eye (Sergio Ortolani)
 - **68**-Site requirements for CODEX (Gauthier Mathys)
 - **71**-Site requirements for EPICS (Vincent Coude du Foresto)
- III. Relevant site parameters for NIR-MIR-submm observations
 - **76**-Atmospheric parameters in the 1-1000 μm regime (Ralf Siebenmorgen & Ulli Kaeufl)
 - **85**-Site requirements for ONIRICA (Andreas Quirrenbach)
 - **87**-Site requirements for MOMFIS (Immo Appenzeller)
 - **89**-Critical dependences of site properties for MOAO (Richard Wilson)
- IV. Appendix: contributed papers
 - **96**-Considerations on contrails (Holger Pedersen)
 - **104**-Synergy considerations for the ELT site (Peter Shaver & Marco Zwaan)
 - **107**-NaI profiles (Joerg Gumbel)

WG3 - ELT Site Evaluation Working Group

Executive Summary

The WG3 has been tasked to categorize site characteristics, to list all sites considered throughout the world (including Antarctica), and compile the presently available information. The working group met twice at the ESO premises in Garching on Jan 13, 2006 and Feb 7, 2006. The main conclusions are presented in Tables 1 – 4 below, which provide a list of sites with relevant sources of information (Table 1), the instruments available for site characterization together with the parameters measured (Table 2), and an assessment of the importance of the various site characterization parameters for individual science cases (Tables 3 and 4). The information given in Tables 1 – 4 is based on comprehensive reports prepared by the working group members which are included below. In addition to these reports, contributions were solicited from Dr. Shaver (ESO), Dr. Pedersen (Copenhagen), and Dr. Gumbel (MISU Stockholm), which address issues related to ELT-ALMA synergies, contrails, and NaI profiles, respectively (cf. Appendix).

The ranking of the site characterization parameters for the various science cases has been derived by use of the science cases as given in the OWL blue book and the various instrument studies available there. At the time of the writing (Feb 28, 2006), the science case and the instruments are under scrutiny and may be re-defined by the ELT working groups. The present ranking may thus require modifications and adjustments once the results from the other working groups become available.

Introduction and Table of Content

Probably the most important issue concerning the ELT site selection is the need of a comprehensive and homogeneous data base which covers a long enough time period (years/decades). The data which is available to date is heterogeneous to a large extent, and an effort needs to be undertaken to re-analyze the available data in a consistent way.

Among the various parameters used in the characterization of an astronomical sites, those related to seeing and atmospheric turbulence are of highest importance, as they critically affect the design of the AO system. It is thus of utmost importance that the ranked list of site parameters is re-visited once the AO and science working groups have re-defined the former OWL requirements. Equally important are sky brightness and transparency in the UV and IR and the amount of water vapor in the atmosphere (PWV), as some of these parameters may open up new observing windows from the ground. Note however that both wavelength regimes, UV and IR, may have largely different site requirements. For mid-IR observations, turbulence in the water vapor containing layers only is important, whereas for UV and near-IR observations, dry-air turbulence is important as well. Similarly, a site with a large fraction of nights with very good seeing, compared with a

site with a similar median seeing but fewer very poor nights, is preferred for an instrument such as ONIRICA, but such a site may not be ideal for most of the other instruments which require good seeing in average. A large sky coverage is most relevant for instruments such as QuantEye, whereas a high geographical latitude is of some advantage for instruments such as CODEX. It may thus be difficult to balance the requirements and select a site which is good for all wavelength regimes. If the ELT is designed to serve a single science case, the selection of an optimal site is more straightforward.

Ground wind speed, the frequency and strength of precipitations, soil properties and seismicity will affect the telescope and enclosure design, and the local topography, the energy cost, the proximity of medical facilities such as hospitals will largely determine the cost for logistics, construction and operation. Those parameters are largely independent of the science case and need to be re-discussed in iteration with the results from WG4 (telescope design).

Last but not least, ESO's experience in Chile shows that large variations in cloudiness occur on time scales of less than a decade. The ideal sites in today's climate may thus not be ideal in a few decades from now. The use of general circulation models (eg FriOWL) is thus required to estimate the effects of climate change.

The present document is structured as follows:

- I. General considerations, site characterization
 - Search for potential sites (Marc Sarazin)
 - Available instrumentation for site characterization (Casiana Munoz Tunon)
 - Site characterization at Dome C (Jean Vernin)
- II. Relevant site parameters for UV/optical observations
 - Impact of optical and NIR sky brightness on site evaluation (Ferdinando Patat)
 - Site requirements for UV observations (Roberto Gilmozzi)
 - Site requirements for Quant-Eye (Sergio Ortolani)
 - Site requirements for CODEX (Gauthier Mathys)
 - Site requirements for EPICS (Vincent Coude de Forresto)
- III. Relevant site parameters for NIR-MIR-submm observations
 - Atmospheric parameters in the 1-1000 μm regime (Ralf Siebenmorgen & Ulli Kaeufl)
 - Site requirements for ONIRICA (Andreas Quirrenbach)
 - Site requirements for MOMFIS (Immo Appenzeller)
 - Critical dependences of site properties for MOAO (Richard Wilson)
- IV. Appendix: contributed papers
 - Considerations on contrails (Holger Pedersen)
 - Synergy considerations for the ELT site (Peter Shaver & Marco Zwaan)
 - NaI profiles (Joerg Gumbel)

Future Instrumentation to be deployed

First and foremost, access to the existing databases is needed to derive at a robust characterization and comparison of site parameters of sites which suffer already from extensive site testing. In that respect Dr. Gary Sanders (TMT) has been contacted who will discuss with the TMT board whether the TMT database will eventually be made available to ESO.

GL turbulence profile, outer scale L_0

The design of the various adaptive optics instruments (in particular the required DM actuator stroke) will critically depend on the outer scale (L_0) and the shape of the cutoff. Equally important is the shape of the surface layer turbulence profile up to the height of the telescope, this is critical and needs a solution to monitor the GL. L_0 can presently only be measured with the GSM (and VLTI, but that is not a deployable instrument yet; or a small 8m interferometer?).

Atmospheric extinction and PWV

Remote sensing does not provide accurate values of the atmospheric extinction (and the PWV). A differential LIDAR has been developed by the Forschungszentrum Karlsruhe in order to measure the vertical structure of the water vapor content up to an altitude of 12 km. The system is presently being used at the Schneefernerhaus/Zugspitze but it is too complex and too expensive to be replicated (Dr. Trickl/Institut fuer Umweltforschung).

OH airglow

It has been proposed to measure and characterize the OH airglow at the various sites (those without NIR infrastructure) via a transportable spectrometer (G. Finger, ESO). This suggestion is strongly endorsed by this working group.

NaI column densities

It has been suggested that the NaI column densities suffer from strong seasonal variations (Ageorges & Els, SPIE Vol 5490, 1041 (2004)). NaI profiles are retrieved from ODIN by measurements of the sodium dayglow at 589 nm. In a first step, Dr. Gumbel (MISU Stockholm) has retrieved NaI column densities as a function of time (see figure). There is no geographical longitude dependence of NaI column densities. The group at MISU is in progress to construct a sodium reference atmosphere, based on satellite and LIDAR measurements and on numerical modeling. The model is to be prepared for the upcoming COSPAR conference in July and will be made available to this group.

Table 1: Site List

Site	Latitude N.	Longitude E.	Altitude (m. a.s.l.)		Location	Owner Country
Dome C	-75.1	-123.4	3233		Antarctica	International
Grand Benare	-21.1	55.42	2896		La Reunion Island	France
Tolar	-21.95	-70.08	2290		Atacama Fault	Chile
Chajnantor	-22.98	-67.63	5100		Andes	Chile
Gamsberg	-23.34	16.23	2347		Namib Desert	Namibia
Macon	-24.5	-67.29	4500-5400		N-W Puña	Argentina
La Chira	-24.52	-70.37	2559		Atacama Fault	Chile
Armazones	-24.58	-70.18	3064		Atacama Fault	Chile
Paranal	-24.62	-70.4	2636		Atacama Fault	Chile
La Silla	-29.25	-70.73	2400		Andes	Chile
Mauna Kea	19.83	-155.47	4580		Big Island, Hawaii	USA
Izaña	28.3	16.5	2367		Tenerife, Canary Islands	Spain
Roque de los Muchachos	28.77	17.88	2396		La Palma, Canary Islands	Spain
Lekst	29.8	-9.04	2359		Anti-Atlas	Morocco
Yanbajing	30.11	90.53	4500		Tibet	China
San Pedro Martir	31.05	-115.49	2980		Baja California	Mexico
Hanle	32.78	78.97	4500		Himalaya	India
Maidanak	38.68	66.9	2600		Pamir	Uzbekistan
Greenland Summit	72.57	-38.28	3225		Greenland Ice Cap	Denmark

Site	Data Source 1	Data Source 2	Nearest City (km, kha)
Dome C	University of Nice	Meteo	Saint Denis (100,100)
Grand Benare	ESO		Tocopilla (17, 23)
Tolar	TMT		Calama (100, 126)
Chajnantor	ESO-NRAO	NRO	Windhoek (100, 233)
Gamsberg	MPI Heidelberg/ESO		Salta (200, 468)
Macon	Observatorio de Cordoba	ESO	Antofagasta (120, 485)
La Chira	ESO		Antofagasta (140, 485)
Armazones	ESO/TMT		Antofagasta (140, 485)
Paranal	ESO		La Serena (120, 296)
La Silla	ESO		
Mauna Kea	TMT	ESO	
Izaña	IAC	Meteo	La Laguna/Santa Cruz (?,360)
Roque de los Muchachos	IAC	ESO	
Lekst	University of Marrakech	ELT-DS WP12000	Agadir (80, 679)
Yangbajing	Lhasa 2004 Workshop	Cloud/PWV Satellite analysis	
San Pedro Martir	UNAM	TMT	
Hanle	Indian Institute of Astrophysics	Cloud/PWV Satellite analysis	
Maidanak	Uzbek Academy of Science	ESO	Shahrisabz (100, 53)
Greenland Summit	ESO		Ilulissat (Jacobshavn) (600, 4)

Table 2: Available Site Instrumentation

	G-SCIDAR	SLODAR	MASS	DIMM	LIDAR	SODAR	GSM	Equiped Balloons	AWS	DustMeter	Climate D.Arch.	GOME	TOMS	MET9	MODIS	satellites	"Ad hoc" Telescopes	International Networks	BB seismographs (in situ)
Integrated Seeing	X	X	X (1)	X		X (1)	X	X											
Seeing (Long term)			X (1)	X		X(1)													
tauo	X						X	X											
theta	X	X	X				X	X											
Scintillation	X	X	X	X			X												
CN2(h)	X							X											
Cn2 para Deltah		X	X			X(1)													
V(h)	X							X											
V(h) (in the BL)	X				(2)	X													
V200mbar								X		X									
Na (content)					X						TBE					TBE	X		
Na (height, t)					X						TBE						X		
PWV											X			X	X	X			
Ozone (content)											X	X							
Temporal variation(Ozone)											X	X							
Ground meteo									X										
Local aerosols					X				X										
Aerosols (h)					X														
Integrated aerosols														TBE	TBE				
Sky Background																	X		
Extinction														TBE	TBE		X		
Cloudiness and fog														X	TBE		X		
Seismicity																		X	X
Microseismicity																			
Ground tilmeter																	X	X	
(1) Parcial. Mass does not SEE below 1Km y SODAR is "blind "above several kms.																			
(2) LIDAR Doppler																			
GOME= Global Ozone Monitoring Experiment																			
TBE= To Be Explored																			

Table 3: ELT Instrument vs. Site Parameter
with assessment of the critical character of each parameter

Table III

Instrument	UV observations	CODEX
Wavelength Range	< 0.4 nm	0.4 - 0.6
AO type		none; seeing correcting active optics only
PWV		II
Seeing statistics, long term		II
Integrated seeing, Fried r(0)		II; slit losses and contamination of target spectrum by faint objects nearby
Cn2(h)		I
Theta(0)		I
tau(0)		II
Outer scale		II
NaI layer		III
Extinction	I+; 280-320 nm below 270 Dobson O ₃	I
Sky Brightness		I
Light pollution		I
Cloudiness, ConTrails		I
Precipitations		I
Temp/Wind profile ground		I
Seismicity		II; high stability of optical beam required
ALMA/ELT, latitude difference		

I+ Critical parameter, enables additional wavelength regimes

I Critical parameter, quadratic or higher dependence on performance

II Important parameter, linear dependence on performance

III Performance little/not affected

Table III

Instrument	QUANTEYE	EPICS
Wavelength Range	BVR	0.6-1.7
AO type	none	XAO
PWV	II	I
Seeing statistics, long term	II	I
Integrated seeing, Fried r(0)	II; low scintillation	I; number of actuators and computing power scales with r0-2
Cn2(h)	II; low scintillation	I; Strehl ratio
Theta(0)	III; photon statistics on sources	III; XAO on star
tau(0)	II	II; computing power scales with 1/t
Outer scale	II	II
NaI layer	III	I
Extinction	I	II; LGS Rayleigh scattering into science field
Sky Brightness	I	II
Light pollution	I	I
Cloudiness, ConTrails	I	I
Precipitations	I	I
Temp/Wind profile ground	I; avoid high frequencies from wind shake	I
Seismicity	I; microseismicity	II
ALMA/ELT, latitude difference		

I+ Critical parameter, enables additional wavelength regimes

I Critical parameter, quadratic or higher dependence on performance

II Important parameter, linear dependence on performance

III Performance little/not affected

Table III

Instrument	MOMFIS
Wavelength Range	1 - 2.5 μ
AO type	MOAO
PWV	I+; JHK separation disappears
Seeing statistics, long term	I
Integrated seeing, Fried $r(0)$	I; number of actuators and computing power scales with r_0^2
$C_n^2(h)$	I; field dependent PSF
Theta(0)	I
tau(0)	I; AO system bandwidth
Outer scale	II
NaI layer	I
Extinction	II
Sky Brightness	I; low OH, low thermal emission in K
Light pollution	II
Cloudiness, ConTrails	I
Precipitations	I
Temp/Wind profile ground	II; internal metrology, control of main optical elements
Seismicity	II; internal metrology and control of main optical elements
ALMA/ELT, latitude difference	

I+ Critical parameter, enables additional wavelength regimes

I Critical parameter, quadratic or higher dependence on performance

II Important parameter, linear dependence on performance

III Performance little/not affected

Table III

Instrument	ONIRICA	T-OWL
Wavelength Range	1 - 2.5 μ m	2 - 27 μ m
AO type	MCAO, GLAO	GLAO
PWV	I+; JHK separation disappears	I+; new MIR/FIR windows
Seeing statistics, long term	I+; works only in 10-30% of best seeing	I
Integrated seeing, Fried r(0)	I; number of actuators and computing power scales with r0-2	II; lower number of actuators needed
Cn2(h)	I; field dependent PSF	II
Theta(0)	I	II
tau(0)	I; AO system bandwidth	I; AO system bandwidth
Outer scale	II	III
NaI layer	I	I
Extinction	II	II
Sky Brightness	I/I+; OH emission	I
Light pollution	II	III
Cloudiness, ConTrails	I	II
Precipitations	I	II
Temp/Wind profile ground	I	I
Seismicity	II	II
ALMA/ELT, latitude difference		

I+ Critical parameter, enables additional wavelength regimes

I Critical parameter, quadratic or higher dependence on performance

II Important parameter, linear dependence on performance

III Performance little/not affected

Table III

Instrument	SCOWL	ALMA-ELT
Wavelength Range	sub-mm	
AO type	none	
PWV	I+; new MIR/FIR windows	
Seeing statistics, long term	II	
Integrated seeing, Fried r(0)	II	
Cn2(h)	II	
Theta(0)	II	
tau(0)	II	
Outer scale	III	
Nal layer	III	
Extinction	III	
Sky Brightness	I	
Light pollution	III	
Cloudiness, ConTrails	III	
Precipitations	II	
Temp/Wind profile ground	I	
Seismicity	II	
ALMA/ELT, latitude difference		I

I+ Critical parameter, enables additional wavelength regimes

I Critical parameter, quadratic or higher dependence on performance

II Important parameter, linear dependence on performance

III Performance little/not affected

Table 4: Required Site Instrumentation

required accuracy, dependence on location, need for further action, etc.

Table IV

Parameter	Total	CODEX	QUANTEY	EPICS	MOMFIS	ONIRICA	T-OWL	SCOWL
PWV	5.02	0.01	0.01	1	1	1	1	1
Integrated Seeing	4.03	0.01	0.01	1	1	1	1	0.01
Cn2(h)	4.03	1	0.01	1	1	1	0.01	0.01
Theta(0)	3.02	1	0	0	1	1	0.01	0.01
tau(0)	3.04	0.01	0.01	0.01	1	1	1	0.01
Outer scale	0.05	0.01	0.01	0.01	0.01	0.01	0	0
NaI layer	4	0	0	1	1	1	1	0
Extinction	2.04	1	1	0.01	0.01	0.01	0.01	0
Sky Brightness	6.01	1	1	0.01	1	1	1	1
Light pollution	3.02	1	1	1	0.01	0.01	0	0
Cloudiness, ConTrails	5.01	1	1	1	1	1	0.01	0
Precipitations	5.01	1	1	1	1	1	0.01	0
Temp/Wind profile ground	6.01	1	1	1	0.01	1	1	1
Seismicity	0.07	0.01	0.01	0.01	0.01	0.01	0.01	0.01
ALMA & ELT latitude difference	0	0	0	0	0	0	0	0
Total Sensitivity to Site		8.05	6.06	8.05	9.05	10.04	6.06	3.05

Parameter Notation per Instrument (from Table 3)

USED FOR RANKING ONLY (X.Y): means X parameters are critical, Y are important

1 Critical parameter, enables additional wavelength regimes

1 Critical parameter, quadratic or higher dependence on performance

0.01 Important parameter, linear dependence on performance

0 Performance little/not affected

Table IV

Parameter	Resolution	Variability	Forecast
PWV	0.1mmH2O	10 min	
Integrated Seeing	0.1arcsec	1 min	
Cn2(h)	0.1 E-13 m ^{1/3}	1 min	
Theta(0)	0.1 arcsec	1 min	
tau(0)	0.1 ms	1 min	
Outer scale	1 m		
NaI layer	10km horizontal	1 min	
Extinction			
Sky Brightness			
Light pollution			
Cloudiness, ConTrails			
Precipitations			
Temp/Wind profile ground			
Seismicity			

From MOAO/GLAO requirements (Wilson):

	Surface Layer (<100m)	Ground Layer (<1km)	Free Atmosphere (>1km)	Global
Vertical Resolution				
Cn2(h)	5 m	50 m	0.5-2 km	
V(h) - turbulence velocity				2 km
L0(h)				2 km

Site Considerations for ELTs

Marc Sarazin¹

¹European Southern Observatory, Karlsschwarzschildstr. 2, D85748 Garching, Germany
email: msarazin@eso.org

Abstract. The ESO strategy for short listing ELT candidate sites is reviewed using a specially designed tool which allows the simultaneous use of existing database of various relevant parameters.

Keywords. atmospheric effects, site testing

1. Introduction

Several projects of ELTs have started a few years ago and prompted new site surveys worldwide. Among them the TMT has certainly the most ambitious site testing campaign underway (Schoeck (2004)). Thanks to an excellent collaboration, TMT and ESO site characterization efforts are often complementary and a strong case is made for deploying similar, if not identical, instrumentation on the candidate sites. Moreover, any new instrument in development is systematically cross-compared to the existing standards. Thanks to a straightforward merging of the various database, it is hoped that the candidates studied for both projects can be ultimately cross-compared. Because of the high cost of the site characterization instrumentation, the number of candidates has to be reduced to a few. Identifying potential candidates is however hardly a rational process and many factors others than science performance may sometimes blur the picture. How to be sure that areas with strong potential have not been left over? To answer this question, a more systematic approach described in this paper has been attempted at ESO with the development of a dedicated geographical information tool.

2. Preliminary Global Analysis

A tool dedicated to tracking climatic trends, FRIOWL has been developed by the Department of Geography of the University of Fribourg (<http://archive.eso.org/friowl>, Graham *et al.* (2004)). This tool has also a first function of helping to locate the most promising areas worldwide on the basis of the long term average value of pre-selected parameters. FRIOWL is a geographical information system with a spatial resolution of 2.5^0 (300 km), composed of several layers containing a minimum of 15 years of data stored as monthly averages. The study of the temporal variability of the layers gives later access to the seasonal and long term climatology of the areas containing selected sites. The nature of the layers has been chosen among the available material according to the expected sensitivity of ELT science to the various atmospheric parameters. In addition to topography, FRIOWL is currently composed of 11 layers among which total cloud cover and precipitable water vapour. Other layers are specific to observation like the high altitude wind speed (figure 1), related to the temporal coherence of the wavefront in adaptive optics (Sarazin & Tokovinin (2002)) and the aerosol index (figure 2) which is believed to be related to atmospheric extinction, however in a still debated way (Siher *et al.* (2004), Varela *et al.* (2004)).

It is possible to combine the layers with different weights so as to compose dedicated maps of suitability. An example is given in figure 3 where topography, PWV and cloudiness have been used as reference parameters for IR astronomy. It is easy to see that only a few regions on earth are suitable, which are however wide enough to provide many candidates which then are compared using the full parameter space. The wider the observation spectrum of the astronomical facility, the more layers must be added and the narrower the choice becomes. For instance in UV and V photometry, the central Saharan regions where the desert sand is pumped upwards before traveling to Europe, Brazil or to the Middle East depending on the seasons, have to be discarded for their high aerosol contamination.

In order to identify the best candidates within an area, the low spatial resolution information can be complemented by the direct use of satellite imagery. With a resolution about the size of the observable sky of a ground based facility, the technique developed by Erasmus (2006) has proven its usefulness.

3. Site Short listing

Most existing observatories housing international facilities are high standards natural candidates for future projects unless they suffer from lack of space or environmental restriction. For this reason, several ELT sites surveys are currently conducted on well known places such as La Campanas in Chile (GMT), San Pedro Martir in Mexico (TMT) and Roque de los Muchachos in Canary Islands (OWL). At Mauna Kea (Hawaii), second choice areas are compared to the summit ridge (TMT). At the VLT Observatory of Paranal (Chile), ESO plans to characterize a summit 20 km to the North (La Chira) for OWL, while TMT studies an earlier candidate of the VLT site survey (Armazones) 20 km further to the East.

Other existing observatories studied at the opportunity of earlier projects like the 8 m generation can be re-activated and short-listed. They must appear more attractive either because of the new science goals, additional technical constraints, or because earlier handicaps (e.g. political instability, difficulty of access, etc.) have been reduced. This could be the case of Maidanak (Uzbekistan), known for its good seeing and very low wind at ground level, should wind load be considered as a major ELT telescope design driver.

Similarly entirely new sites can be introduced. However, the risk being higher, they have to present a well identified benefit for the project. This is the case of high elevation mountains studied by TMT in Chile for their low precipitable water vapor (PWV) content. This is also the case of the Macon ridge in NW Argentina studied by Cordoba Observatory and ESO which, in addition to low PWV, presents a twice lower seismic risk than Paranal. Note that we have considered until now only countries which have a long tradition in astronomy with a well developed scientific community. It is also possible, even recommended from the point of view of the dissemination of Science, to address the case of emerging countries. A few locally motivated individuals can indeed become reliable partners and provide the necessary logistics for a large scale site survey. A good example is Morocco, steadily moving since about a decade from a core of astronomers trained abroad, towards the construction of a national observing facility close to the University of Marrakech (Oukaimeden). On this basis, and with the perspective of a lower weather downtime than in the Canary Islands during Winter, the anti-Atlas mountain ridge is also considered for the siting of the European ELT.

Finally, if justified by science, the extreme conditions are not anymore excluded for large facilities. The path was shown by ALMA, with the planned operation at 5000 m

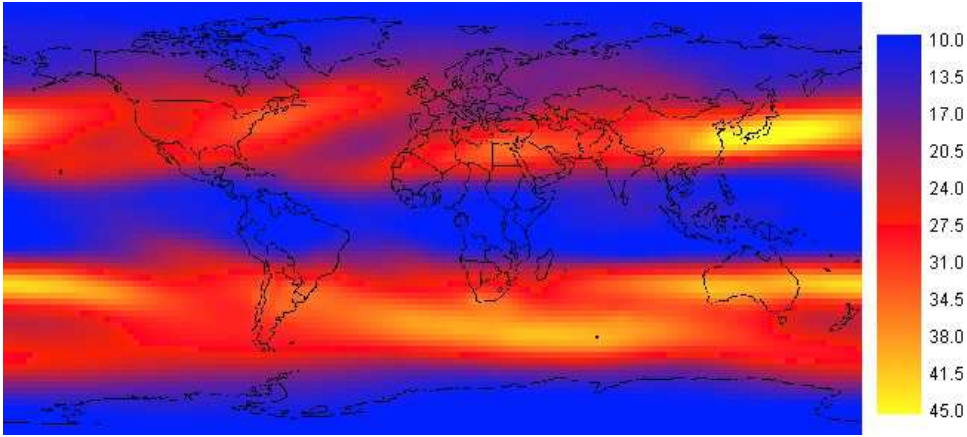


Figure 1. Mean Wind Speed at 200mB (≈ 12 km a.s.l) in m/s for the period 1979-1993, 2.5° square pixels

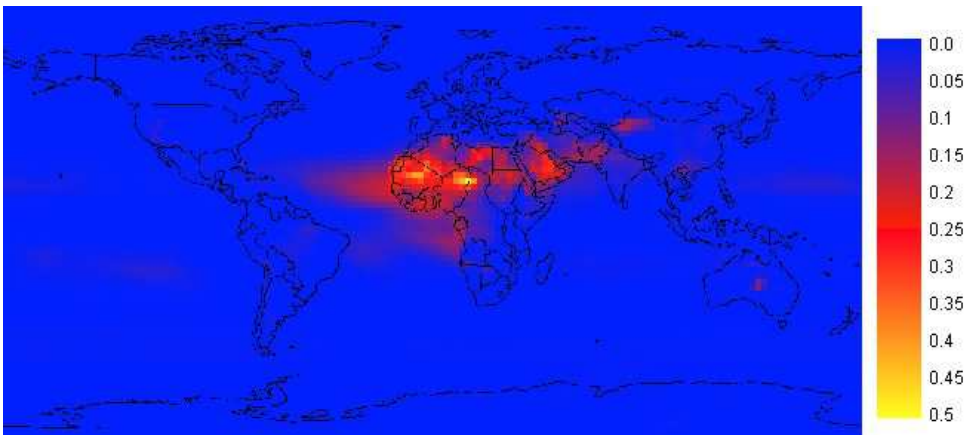


Figure 2. Mean aerosol index (arbitrary scale) as measured by TOMS UV satellite for the period 1980-2002, 2.5° square pixels

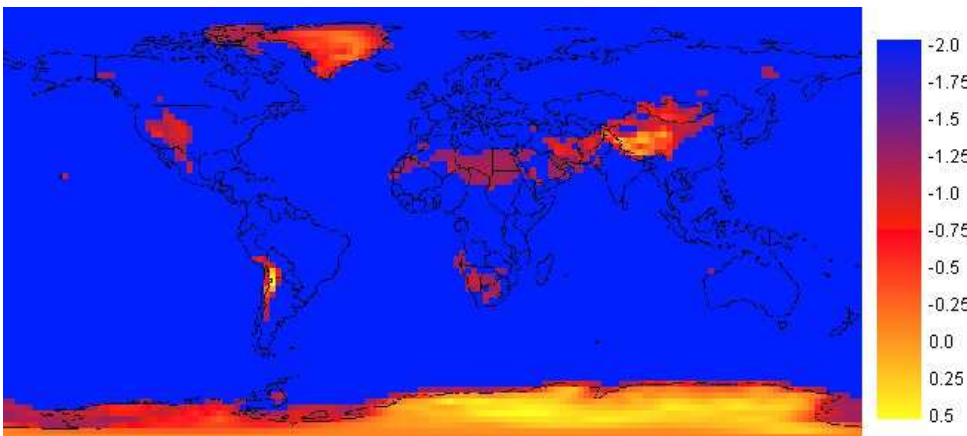


Figure 3. Overlay distinguishing areas providing both high summits and low cloudiness as well as low PWV (arbitrary scale) 2.5° square pixels

altitude of an highly sophisticated instrumentation fed by an array of 50 movable large size antennas. This is also be the case of the new Antarctic scientific station of Concordia at Dome C, which could offer so favorable observing conditions that even a smaller ELT located there could become scientifically competitive. Dome C is the object of an intensive site testing activity led by Nice University (France), with the collaboration of many institutes worldwide, among them the University of New South Wales from Australia.

While the US project are mostly privately funded, European astronomy is composed of a constellation of institutes which nevertheless managed to converge towards a single funding request to the European Commission FP6 framework program. This gave birth to The ELT Design Study, a technology development programme undertaken under ESO's lead by institutes and companies in Europe which will span over the 2005-2008 period. The study covers the development of enabling technologies and concepts required for the eventual design and construction of a European extremely large optical and infrared telescope, with a diameter in the 50- to 100-m range. Site characterization, exploratory instruments designs, and an assessment of the performance of a segmented aperture exposed to wind on a representative site are also included. Considering the available funds, the site characterization workpackage under the responsibility of Nice University (IAC and ESO as deputies) has been limited to 4 continental sites (Chile, Canary Islands, Argentina, Morocco) and Dome C in Antarctica. It also includes actions for a better understanding of the physics of the turbulence at large scales, proposed by Arcetri Observatory.

4. Conclusion

Considering a limited set of atmospheric parameters relevant for astronomy, it is easy to show that the potentially interesting areas on the planet are well identified. Moreover, not surprisingly, most of them are already the theater of professional astronomical observing. Finding new candidates is nevertheless possible when required by science or design constrains.

Within the next 3 years, more than 10 sites shall be characterized by the various ELT groups. And because much care was taken to use instruments which, if not always identical, are very similar and in any case repeatedly cross-calibrated, the data accumulated can easily be merged and the sites cross compared for the benefit of all institutions.

References

- Erasmus A. 2006, *these proceedings*
- Graham, E., Sarazin, M., Beniston, M., Collet, C., Hayoz, M., Neun, M. 2004, *Proceedings of the SPIE*, Volume 5489, pp. 102-112
- Sarazin, M., Tokovinin, A. 2002, *ESO Conference and Workshop Proceedings*, Volume 58, pp. 321-328
- Schoeck M. 2004, *Proceedings of the SPIE*, Volume 5489, pp. 95-101
- Siher, E., Ortolani, S., Sarazin, M., Benkhaldoun, Z. 2004, *Proceedings of the SPIE*, Volume 5489, pp. 138-145
- Varela, M., A., Fuensalida, J., J., Muñoz-Tuñón, C., Rodriguez Espinosa, J., M., Garcia-Lorenzo, B., M., Cuevas, E. 2004, *Proceedings of the SPIE*, Volume 5489, pp. 245-255

Instruments and tools for site testing

(prepared for GW3-ESO- Site Evaluation; February 2006)

Casiana Muñoz-Tuñón (cmt@iac.es), Begoña García Lorenzo, & Antonia Varela
Instituto de Astrofísica de Canarias (IAC)¹

This document compiles parameters relevant for astronomical site evaluation and a brief description of instruments currently available for their measurement. We have selected only those for which instruments and methods are available and, to a reasonable extent, standardized.

The parameters included in this document are:

1. Vertical structure of the atmospheric turbulence.
2. Humidity and precipitable water vapour.
3. Wind speed and direction; vertical profile in the BL.
4. Sodium layer.
5. Ground deformations and seismicity.
6. Seeing or atmospheric coherence length.
7. Airborne aerosols, including the chemical composition of dust, particle size distribution and abrasive characteristics.
8. Cloudiness, fog and dust.
9. Atmospheric extinction.
10. Long-term meteorological parameters.

1. Vertical structure of the atmospheric turbulence

Different remote sensing techniques have been implemented to monitor the vertical structure of atmospheric turbulence. The instruments suitable for achieving the Cn² profiles are: SCIDAR, SLODAR and MASS. SCIDAR is the one which provides the best vertical resolution, covering the whole vertical scale, from the ground layer. MASS samples the vertical profiles in several slices (about 5) and therefore gives a low resolution sampling of the turbulence vertical profile. However, it is the one which is nowadays automatized thereby allowing long term measurements, with the limitation of being "blind" in the first Km.

Techniques measuring the refractive index "in situ" are also standard and have also been successfully proven, using equipped balloons. However, the resources required make them useful for intensive campaigns only and inadequate for systematic, prolonged measurements.

1.1 SCIntillation Detection and Ranging (SCIDAR)

SCIDAR (Vernin) has proved to be the best contrasted, efficient and extended technique from ground level for atmospheric turbulence measurements. Table 1 summarizes the main characteristics of SCIDAR instruments. Several teams are using the SCIDAR technique nowadays (see the list below):

<http://www.iac.es/project/gare/esp/index.html>
<http://www.astrosmo.unam.mx/~r.avila/Scidar/>
<http://www.eso.org/gen-fac/pubs/astclim/lasilla/asm/scidar/>

Intensive campaigns of SCIDAR observations have taken place in some astronomical sites such as San Pedro Mártir (Mexico), La Silla (Chile) or Mauna Kea (Hawaii, USA).

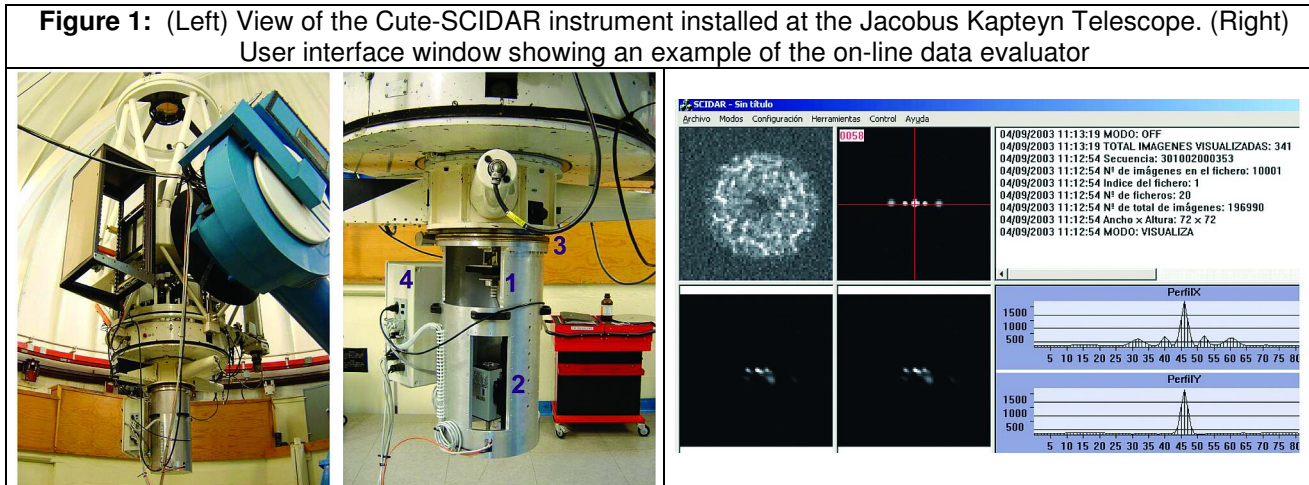
Long-term monitoring observations started during 2003 at the Observatorio del Roque de los Muchachos (ORM) on the Island of La Palma (Spain) and Observatorio del Teide (OT) on Tenerife (Spain).

An updated version of SCIDAR (Cute-SCIDAR), which aims at being more flexible and user friendly, is being developed at the IAC (Instituto de Astrofísica de Canarias), in collaboration with LUAN (Laboratoire Universitaire d'Astrophysique de Nice).

¹ Thanks to Jesús J. Fuensalida, Julio A. Castro Almazán & Antonio Darwich for their help in the compilation.

Figure 1 shows a view of the *Cute-SCIDAR*, an automatically controlled SCIDAR instrument, installed at the Jacobus Kapteyn Telescope (JKT), at ORM and its user interface window, showing an example of the on-line data evaluator.

Table 1: Main characteristics of instruments based on the SCIDAR technique	
SCIntillation Detection and Ranging (SCIDAR)	
Altitude resolution	$\sim \sqrt{\lambda(h-h_c)/(2\lambda)} \sim 200\text{-}500\text{m}$
Temporal Resolution	~ 2 profiles/min
Operation mode	one observer (highly automated system)
Telescope	Larger than 1 meter
Uses light from	a double star (Single star SCIDAR is in progress)



The SCIDAR technique is explained in different papers and measurements of the vertical turbulence profiles using this technique have also been published. We list here some references:

- Ávila, Masciadri, Vernin, & Sánchez, PASP, 116, 778 (2004)
- Coburn, Garnier, & Dainty, SPIE, 5981, 105 (2005)
- Fuensalida, et al., SPIE, 5572, 1 (2004)
- Klueckers, V., et al, A&A Suppl. Ser., 130, 141 (1998)
- Vernin, J., & Roddier, F., J. Opt. Soc. Am., 63 (1973)

1.2. SLOpe Detection and Ranging (SLODAR)

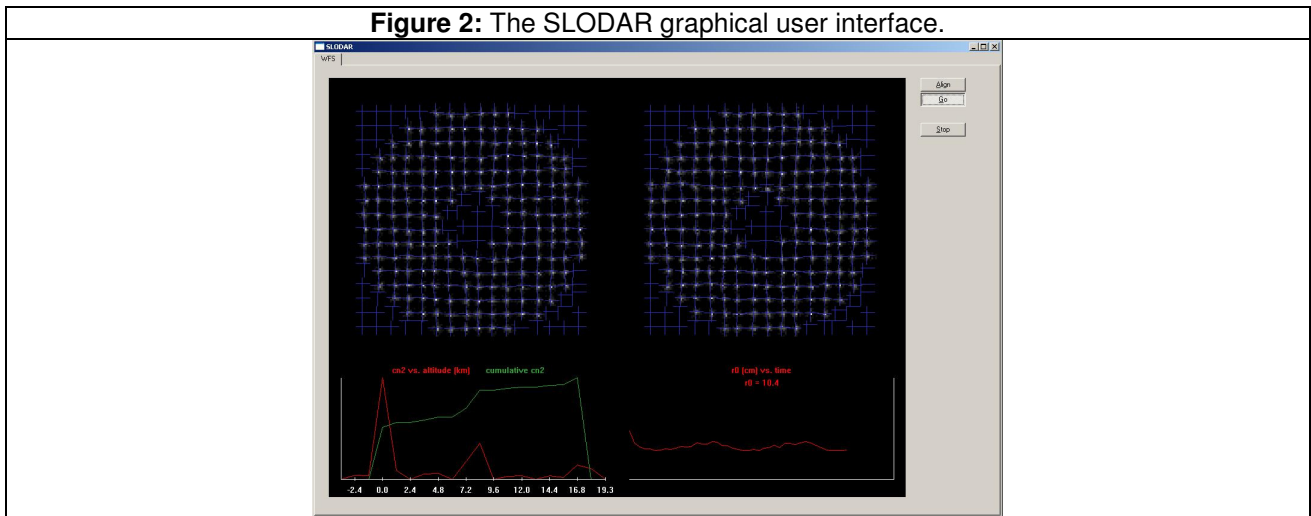
SLODAR (Wilson) is, so far, the less extended technique for the vertical turbulence profile measurement of the listed techniques in this document, but it is becoming more popular thanks to its portability and possible automatism.

Table 2 summarizes the main characteristics of SLODAR instruments. More information about SLODAR can be found at: <http://www.cfai.dur.ac.uk/fix/projects/slodar/>

Table 2: Main characteristics SLODAR instrument	
SLOpe Detection and Ranging (SLODAR)	
Altitude resolution	$\sim D/n_{\text{sub}}/\lambda$ (~ 2 km with a portable Telescope)
Altitude range:	$\sim 0\text{-}n_{\text{sub}}\lambda H$ ($\sim 0\text{-}10$ km with a portable telescope)
Temporal Resolution	~ 2 profiles/min
Operation mode	one observer
Telescope	λ 40 cm
Uses light from	a double star

Intensive campaigns of SLODAR have taken place at some astronomical sites such as ORM (La Palma, Spain), Cerro Tololo (Chile) and Cerro Paranal (Chile).

Figure 2 shows the graphical user interface for data visualization of the SLODAR instrument.



The main references about SLODAR are the following:

- Wilson, MNRAS 337, 103 (2002)
- Wilson & Saunter, proc. SPIE 4839, 466 (2003)

1.3. Multi-Aperture Scintillation Sensor (MASS)

MASS (Tokovinin) is an instrument to measure the vertical distribution of turbulence in the atmosphere by analysing the scintillation (twinkling) of bright stars. Most information about this technique can be found at: <http://www.ctio.noao.edu/~atokovin/profiler/>

Intensive campaigns using MASS have been carried out at: Mt. Maidanak (Republic of Uzbekistan), Cerro Pachón and Tololol (Chile), Mauna Kea (Hawaii, USA) and Dome-C.

Table 3 summarizes the main characteristics of MASS.

Table 3: Main characteristics MASS instrument	
Multi-Aperture Scintillation Sensor (MASS)	
Altitude resolution	~ $\Delta h/h = 0.5$
Altitude range:	~ 0.5-16 km
Temporal Resolution	~ 1 profil/min
Operation mode	one observer/automatic
Telescope	~ 30 cm
Uses light from	a bright star

We list here some papers about MASS and its measurements.

- Tokovinin, NOAO-NSO Newsletter, Issue 77, 32-34, (2004)
- Kornilov, et al. SPIE, 4839, 837 (2003)
- Tokovinin, & Kornilov in: Astronomical Site Evaluation in the Visible and Radio Range, Eds. Benkhaldoun et al., AASP Conf. Ser. (2001)
- Tokovinin A.A.; ESO Report VLT-TRE-UNI-17416-008 (1998)

2. Humidity and precipitable water vapour

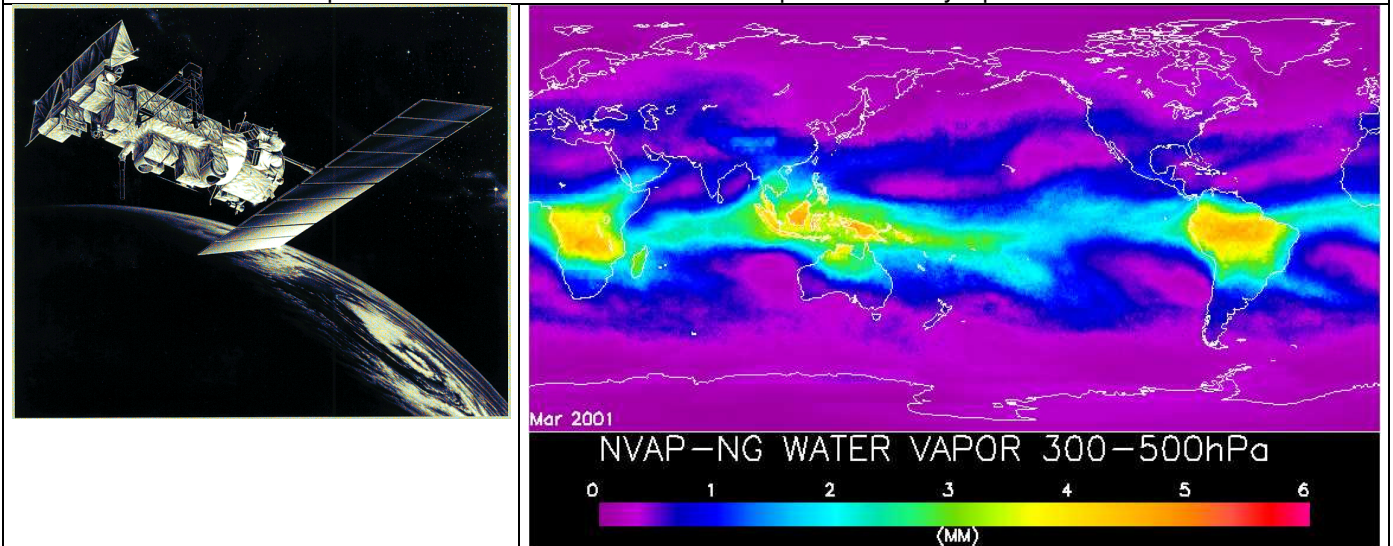
Different instruments and techniques can be used to measure the humidity and the precipitable water vapour in the atmosphere. The resources that can be used are: satellites and data diagnostic archives.

2.1. Satellites

Several satellites provide daily measurements of humidity and precipitable water vapour. Table 4 includes some of them, as well as their web pages and some characteristics of the data.

Table 4: Orbiting satellites with dedicate instruments for water vapour measurements and general characteristics of data	
Spatial resolution	~ 0.5 degrees
Temporal resolution:	~ twice/day
Altitude resolution:	~ 5 layers (from 850 to 200 mbar)
Temporal coverage:	~ 1998-2001
Satellites:	
<ul style="list-style-type: none"> ▪ Infrared Operational Satellite (TIROS) ▪ Operational Vertical Sounders (TOVS) ▪ Defence Meteorological Satellite Program (DMSP) 	http://www.met.fsu.edu/explores/Guide/tirosindex.html http://www.ozonelayer.noaa.gov/action/tovs.htm http://www.ngdc.noaa.gov/dmsp/index.html

Figure 3: (Left) One of NOAA's polar orbiting satellites carrying the TOVS instruments. (right) The mean water vapour between 300 and 500 hPa in the period January-April 2001.



2.2 Climate Diagnostic archives

Climate diagnostic archives maintain a large collection of datasets to support climate research. Climate diagnostic databases make such data freely accessible to the world, within the limits of their resources. The most popular is the Climate Diagnostic Center which combines data from different sources and climate sophisticated models (<http://www.cdc.noaa.gov/index.html>).

Table 5 shows the main characteristics of data from this database.

Table 5: Main characteristics of humidity and precipitable water data that can be obtained from the Climate Diagnostic Center database	
Spatial resolution	~ 2.5 degrees
Temporal resolution:	~ 4/day
Altitude resolution:	~ 8 layers and integrated (from 1000 to 200 mbar)
Temporal coverage:	~ 1940-noadays

Some references on these topics:

- García-Lorenzo et al. MNRAS, 356, 849 (2005)
- García-Lorenzo et al., SPIE, 5572, 68 (2004)
- Carrasco et al., PASP, 117, 104 (2005)
- Erasmus & Sarazin, (2002), ASP Conf. Ser., vol. 266, p.310-326.
- Erasmus & van Rooyen, Final Report to ESO, 14 February, (2006).

3. Wind speed and direction; vertical profile in the BL

Information about the wind's vertical profile can be obtained from SCIDAR and SLODAR measurements, as well as from climate diagnostic archives. SCIDAR's team is already developing procedures to gather the wind profiles. The algorithms are expected to be ready and suitable to be implemented along this year (Fuensalida, private communication).

The vertical profile in the boundary layer can be obtained from SODAR measurements.

3.1 *Velocity of turbulence layers measured using SCIDAR and SLODAR observations*

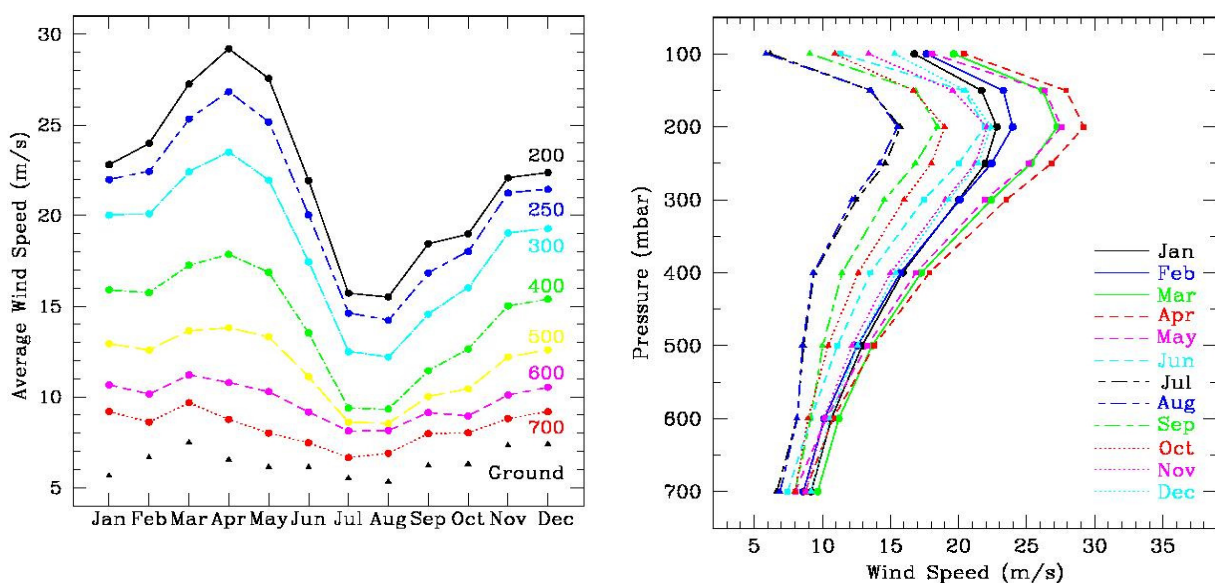
The wind speed and direction of turbulence layers can be measured from SCIDAR and SLODAR observations. The following references describe the different methods developed to derive the velocity of turbulence layers from SCIDAR observations:

- García-Lorenzo & Fuensalida, sent to MNRAS (2006)
- Prieur, Ávila, Daigne & Vernin, PASP, 116, 682 (2004)

For more details and references see sections 1.1 (SCIDAR) and 1.2 (SLODAR).

Climate Diagnostic Archives have proven to be very useful to obtain winds vertical profiles and several works have already been published concerning their use to analyze the wind profiles at different sites. In Figure 4 we show, as an example, the seasonal variation at ORM taken from Garcia-Lorenzo et al. 2005, MNRAS, 356, 849. In a previous paper the crosscalibration of this data set and local parameters using balloons was established (Chueca et al., 2004, MNRAS, 349, 627).

FIGURE 4. The monthly averaged wind velocity for the period 1980-2002 at the pressure levels indicated in the figure at ORM (from Garcia Lorenzo, et al., 2005, MNRAS, 356, 849). The paper also compiles results for La Silla, MaunaKea, Paranal and S. Pedro Martir.



3.2. SODAR

SODAR (sonic detection and ranging) systems are used to remotely measure the vertical turbulence structure and the wind profile of the lower layer of the atmosphere (Boundary Layer). Table 6 summarizes the main characteristics of the SODAR that is expected to start operation next summer at the Canary Islands' observatories.

Model:	Scintec FAS; model : XFAS
Size:	145 x 145 x 33 cm
Maximum height:	5000 m
Vertical resolution:	~ 20-500 m
Minimum height:	20 m

4. Mesospheric sodium layer density and height

The sodium layer's density and altitude can be measured through laser experiments from telescopes or from LIDAR measurements.

4.1. Laser experiments from telescopes

Several measurements of the mesospheric sodium layer, using laser beacons launched from telescopes, have been already carried out. For references consult the web pages and papers listed below :

http://op.ph.ic.ac.uk/jkt_lgs/

<http://www.iac.es/project/gare/esp/index.html>

- Michaille et al., MNRAS, 318, 139 (2000)
- Michaille et al., MNRAS, 328, 993 (2001)
- Chueca et al., SPIE, 5237, 261 (2004)

4.2. Light Detection and Ranging (LIDAR)

LIDAR systems are "laser radar systems". The time for the light to travel out to the target (mesospheric Na layer) and back to the LIDAR is used to determine the height of the layer. Usually LIDAR's are used in a monostatic configuration: laser beam is projected through the receiving telescope or is parallel to the optical axis. Typically, a pulsed dye laser is tuned to the Na D₂ resonant absorption line (589nm, orange). Backscattered photons are collected in a telescope and focused onto a photomultiplier tube. Typical plots from a LIDAR systems show the signal received vs. the altitude where the photons come from. The altitude is directly determined from the photons' "time of flight": as the detected light is recorded in sample bins the detector records the time since the laser was fired. Typical resolution may be 0.5km, or better. The density of Na may be determined from the ratio of the photon counts in the mesosphere region to those in the high stratosphere (~30km), where Rayleigh scattering occurs with air molecules, while no Mie scattering with aerosols is present. The Na column abundance ranges from a summer minimum of $\sim 3 \times 10^9 \text{ cm}^{-2}$ to a winter maximum of about 10^{10} cm^{-2} .

5. Ground deformations and seismicity

5.1 *Ground deformations* are induced by (a) barometric pressure loading and hydrologic loading: Rain and snow, (b) deformations induced by temperature changes and (c) magma motion at great depths that can produce landslides.

Ground deformations can be measured with:

- Tiltmeters (Low cost, very high accuracy)
- GPS
- Radar interferometer

Currently, continuous monitoring of ground deformations with enough precision are not yet available.

5.2 Seismicity is induced by regional tectonics, oceanic effects, volcanic and/or anthropogenic activity. Several different types can be found:

- Regional seismicity >1mb (Very low)
- Microseismicity
- Low frequency seismicity (volcanic tremors, oceanic effects, ...)

The seismicity is measured with broadband seismometers. In general, all countries monitor the regional seismicity (e.g. in Spain <http://www.ign.es>). However, a devoted network for very local seismicity is needed. At Paranal there are instruments installed to measure it (Gilmozzy, private communication) and at ORM some equipment has been used in the past (see for references Muñoz-Tuñón, 2002, ASP Conf. Ser., vol. 266, p.498-515. and <http://www.iac.es/project/sitesting/site.html> [there do a search for the keyword "seismicity"]).

6. Seeing or atmospheric coherence length

Different instruments have been developed to measure the atmospheric coherence length. In this section we take an overview of DIMM, MASS, MASS-DIMM, SCIDAR and GSM.

6.1. *Differential Image Motion Monitor (DIMM)*

For description of the technique and instrument we refer to:

Sarazin & Roddier, 1990, A&A, 227, 294.
Vernin & Muñoz-Tuñón, 1995, PASP, 107, 265.

The DIMM provides the full atmospheric seeing with an accuracy better than 0.1" with a sampling rate better than 1data/minute. The DIMM is the ideal instrument for long term monitoring of the image quality (e.g., see statistics at ORM in Muñoz-Tuñón et al., 1997, A&A Suppl. Ser., 125, 183-193.).

At la Silla, Paranal and ORM seeing is continuously been monitored using DIMMs. For further information see:

<http://www.iac.es/project/sitesting/site.html>
<http://www.ing.iac.es/ds/robodimm/>
<http://www.eso.org.com>

6.2. *Multi-Aperture Scintillation Sensor (MASS)*

The MASS measurements provide free atmosphere seeing, with a resolution. Monitoring campaigns are being carried out at several astronomical sites (<http://www.ctio.noao.edu/atokovinin/profiler/principle.html>). See also section 1.3 for further information.

6.3. *MASS-DIMM*

The instrument measures the full atmospheric seeing with a resolution better than 0".1, providing also information of the turbulence profile in 5 atmospheric slabs (from 1-16km). Monitoring campaigns are currently in progress at different astronomical sites. More information about MASS-DIMM can be found in <http://mass.ctio.noao.edu> and Tokovinin, NOAO-NSO Newsletter, Issue 77, 32-34, (2004)².

6. 4 *SCIDAR.*

Monitoring campaigns are currently working at ORM and OT (in the Canaries). See section 1.1 for further information and references. In the near future, Paranal will also be part of the list.

6.5. *GSM (Generalized Seeing Monitor)*

² Five MASS-DIMMS will be operating at Paranal N, ORM, Argentina, Observatorio del Teide (OT) and Morocco within the framework of the FP6 project *European Extremely Large Telescope Design Study*, within the Site Characterization WG.

The GSM provides the free atmosphere seeing with, and altitude resolution ranges from, 1 to 20 km. Several intensive campaigns at different observatories have been carried out. For more information, see the following web page: <http://www-luan.unice.fr/GSM/Bibliography.html>

Other techniques such as SLODAR or SSS (Single Star SCIDAR) also provide seeing values.

7. Airborne aerosols, including dust's chemical composition, particle size distribution and abrasive characteristics

7.1. Size and density

Portable Counter Particle (Pacific Scientific Instruments) are being used at Paranal and ORM to measure the size and density of local aerosols. They measure in 6 channels (0,3 – 0,5 -1 –3 – 5- 10 μ m) with a rate of 1 c.f.m. and the light source is a laser diode.

7.2. The vertical structure of aerosols (backscattering coefficient and optical aerosol depth)

This information can be obtained from LIDAR observations (INTA) with a 30 m resolution (NASA MPL-NET - AERONET).

7.3. UV aerosol index

The use of TOMS has been explored. TOMS (**T**otal **O**zone **M**apping **S**pectrometer), NASA; on board **Nimbus7: 1978-1993**; Meteor-3: 1991-1994; ADEOS, 1996-1997; **Earth-Probe: 1996-2004**. It has shown not to be adequate due to its poor spatial resolution: 1.25 $^{\circ}$ x 1 $^{\circ}$ (139 x 111km 2). It lacks of good resolution at lower atmosphere, making necessary the use of "in SITU" measurements (Varela et al., 2006, to be submitted to MNRAS)

More references: Varela et al., 2004, SPIE 5489, 245; SPIE 5571, 105; Siher et al., 2004, SPIE 5489, 138; Erasmus & van Rooyen, Final Report to ESO, 14 February, 2006.

8. Cloudiness, fog and dust (under study)

It is now been explored the use of other detectors on board different satellites (MET-9, MODIS) that operate in bands of astronomical interest (visible and NIR) and with higher spatial resolution (1km x 1km or better). Also useful are NCEP-NCAR data (see also Erasmus & van Rooyen, Final Report to ESO, 14 February, 2006).

- **MODIS**: Moderate Resolution Imaging Spectrometer, onboard Terra (1999) and Aqua (2002).
 - ✓ 36 spectral bands, from 0.47 to 14.24 μ m.
 - ✓ Includes two new channels 0.405 and 0.550 μ m
 - ✓ Spatial Resolution: 0.25, 0.50 and 1km
- **METEOSAT 9 (MSG – ESA)**. The main MSG instrument is called the Spinning Enhanced Visible and Infra-red Imager (SEVIRI). It builds up images of the Earth's surface and atmosphere in 12 different wavelengths once every 15 minutes, compared to three wavelengths once every 30 minutes for the comparable instrument on Meteosat. 1km horizontal image resolution.

9. Atmospheric extinction in visible and NIR

The different contributions to the total atmospheric extinction are summarized in the expression:

$$A(\lambda) = A_{Ray}(\lambda, h) + A_{Oz}(\lambda) + A_{Wv}(\lambda) + A_{aer}$$

For optical, NIR, and MIR, a dedicated telescope is required to determine properly the atmospheric extinction (e.g. Carlsberg Automatic Meridian Circle (CAMC) http://www.ast.cam.ac.uk/dwe/SRF/camc_extinction.html or Mercator at the ORM).

10. Long-term meteorological parameters

Meteorological parameters can be obtained in situ or through remote sensing techniques, such as those provided by climate diagnostic archives.

10.1. Ground (in situ) measurements, are provided by equipped meteorological masts, e.g. Automatic Weather Stations (AWS). Typical parameters provided by AWS are listed below:

- Air temperature 0.30-0.55°C
- Soil and Subsoil Temp. “
- Barometric Pressure 0.3mB
- Vapour pressure
- Relative Humidity 2%
- Wind Speed 0.3m/s for ws>3m/s
- Gusts 3% for ws>3m/s
- Wind direction 2%
- Rainfall 1%

For references and use in astronomy see, e.g., Mahoney, Muñoz-Tuñón, & A.M. Varela., *New Astronomy Reviews*, 42, 417 (1998).

10.2. Climate diagnostic archives

See section 2.3.

Find below the reference's list (in order of appearance in the document).

REFERENCES

- Ávila, Masciadri, Vernin, & Sánchez, *PASP*, 116, 778 (2004)
Coburn, Garnier, & Dainty, *SPIE*, 5981, 105, (2005)
Fuensalida, et al., *SPIE*, 5572, 1 (2004)
Klueckers, V., et al, *A&A Suppl. Ser.*, 130, 141 (1998)
Vernin, J., & Roddier, F., *J. Opt. Soc. Am.*, 63 (1973)
Wilson, *MNRAS* 337, 103 (2002)
Wilson & Saunter, *proc. SPIE* 4839, 466 (2003)
Tokovinin, *NOAO-NSO Newsletter*, Issue 77, 32-34, 2004
Kornilov, et al. *SPIE*, 4839, 837 (2003)
Tokovinin, & Kornilov in: *Astronomical Site Evaluation in the Visible and Radio Range*, Eds. Benkhaldoun et al., *AASP Conf. Ser.* (2001)
Tokovinin A.A.; *ESO Report VLT-TRE-UNI-17416-008* (1998)
Varela et al., submitted to *MNRAS* (2006)
García-Lorenzo et al. *MNRAS*, 356, 849 (2005)
García-Lorenzo et al., *SPIE*, 5572, 68 (2004)
Carrasco et al., *PASP*, 117, 104 (2005)
Erasmus & Sarazin, 2002, *ASP Conf. Ser.*, vol. 266, p.310-326.
Erasmus & van Rooyen, *Final Report to ESO*, 14 February, 2006.
García-Lorenzo & Fuensalida, send to *MNRAS* (2006)
Prieur, Ávila, Daigne & Vernin, *PASP*, 116, 682 (2004)
Michaille et al., *MNRAS*, 318, 139 (2000)
Chueca et al., 2004, *MNRAS*, 349, 627.
Michaille et al., *MNRAS*, 328, 993 (2001)
Chueca et al., *SPIE*, 5237, 261 (2004)
Muñoz-Tuñón, C., 2002, *ASP Conf. Ser.*, vol. 266, p.498-515.

Sarazin & Roddier, 1990, A&A, 227, 294.
Vernin & Muñoz-Tuñón, 1995, PASP, 107, 265.
Muñoz-Tuñón et al., 1997, A&A Suppl. Ser., 125, 183-193.
Tokovinin, NOAO-NSO Newsletter, Issue 77, 32-34, 2004 .
Varela et al., 2004, SPIE 5489, 245
Varela et al., 2004, SPIE 5571, 105
Siher et al., 2004, SPIE 5489, 138
Mahoney, Muñoz-Tuñón, & A.M. Varela., New Astronomy Reviews, 42, 417 (1998).

In the web...

<http://www.iac.es/project/gare/esp/index.html>
<http://www.astrosmo.unam.mx/~r.avila/Scidar/>
<http://www.eso.org/gen-fac/pubs/astclim/lasilla/asm/scidar/>
<http://www.cfai.dur.ac.uk/fix/projects/slodar/>
<http://www.ctio.noao.edu/~atokovin/profiler/>
<http://www.met.fsu.edu/explores/Guide/tirosindex.html>
<http://www.ozonelayer.noaa.gov/action/tovs.htm>
<http://www.ngdc.noaa.gov/dmsp/index.html>
http://op.ph.ic.ac.uk/jkt_lgs/
<http://www.iac.es/project/gare/esp/index.html>
<http://www.ign.es>
<http://www.iac.es/project/sitestesting/site.html>
<http://www.iac.es/project/sitestesting/site.html>
<http://www.ing.iac.es/ds/robodimm/>
<http://www.eso.org.com>
<http://www.ctio.noao.edu/atokovinin/profiler/principle.html>.
<http://mass.ctio.noao.edu>
<http://www-luan.unice.fr/GSM/Bibliography.html>
<http://www.ast.cam.ac.uk/~dwe/SRF/images/vextinction.gif>

More references (TBCompleted...)

“ESO workshop on Site Testing for Future Large Telescopes”**1983**, eds A. Ardeberg & L. Woltjer.
Vistas in Astronomy, “The Observatories of the Canaries” Vol. 28, **1985**, Murdin & Beer eds.
“Identification, Optimisation and Protection of Optical Telescopes Sites”, **1986**, Flagstaff.
“VLT site selection working group; final report”(no. 62), **1990** Sarazin, M., eds.
“Site properties of the Canarian Observatories” New Astron. Reviews, vol 42, **1998**, Muñoz-Tuñón, C., eds.
SITE2000/ IAU technical workshop. “Astronomical Site Evaluation in the Visible and Radio Range” ASP, vol. 266, 2002, Vernin, J, Behaldoum, Z & Muñoz-Tuñón, C., eds.

ELT Site evaluation WG3

Checking for Dôme C possibility

J. Vernin - LUAN, Nice University

February 21, 2006

1 Introduction

Here we try to elaborate the implications of going to Dôme C, Antarctica, to install a 30-60 m telescope. First we show how is it possible to reach Dôme, at what cost. Then, from our knowledge of the optical turbulence properties, we try to figure out what are the main advantages to go to Dôme C when compared to other mid-latitude “classical” sites. This knowledge is based upon one full Antarctic night, i.e. 2005. Unless it does not seem possible right now to have a valuable conclusion, we indicate what are the possible ways to investigate in order to take a decision about mid-latitude/Antarctica alternative. This short study is mainly devoted to High Angular Resolution astronomy, but one needs to take into account other properties such as extinction, light pollution, OH emission, auroras ... Dôme C, 75 S and 123 E, is situated at 3230 m altitude above one of the highest Antarctic plateaux, Dôme A being the highest summit, at 4200 m altitude. It is characterized by very low wintertime temperature (-50-80 C), very dry (~ 0.4 mm water vapor content), low wind (~ 2.6 m/s), see for exemple Aristidi et al, 2005, and references therein.

2 How Dôme C is reachable

Dôme C can be reached by different ways, as shown in Fig. 1. It can be reached either by the Italian or the French side, through Terra Nova (TN) or Dumont d’Urville (DDU) coastline bases. Terra Nova might be reached either by C130 plane or Italice boat, from New Zealand. Dumont d’Urville might be reached either by C130 or Astrolabe boat, from Hobart island, Tasmania, Australia. Then, Dôme C is accessible from TN or DDU with small Twin-Otter planes. But the only way to carry heavy loads to Dôme C is from DDU with the use of raids. C130 flights last ~ 8 hours to reach TN or DDU. Twin-Otter flights last $\sim 4-5$ hours to reach DC. A raid lasts 8-10 days to reach DC.

3 Costs

Here we give few estimates of prices to send material to Dôme C, as well as the size and load that can be shipped, estimates of the price of the construction of the winter base and finally the overall price of the Italo-French “Concordia” project.

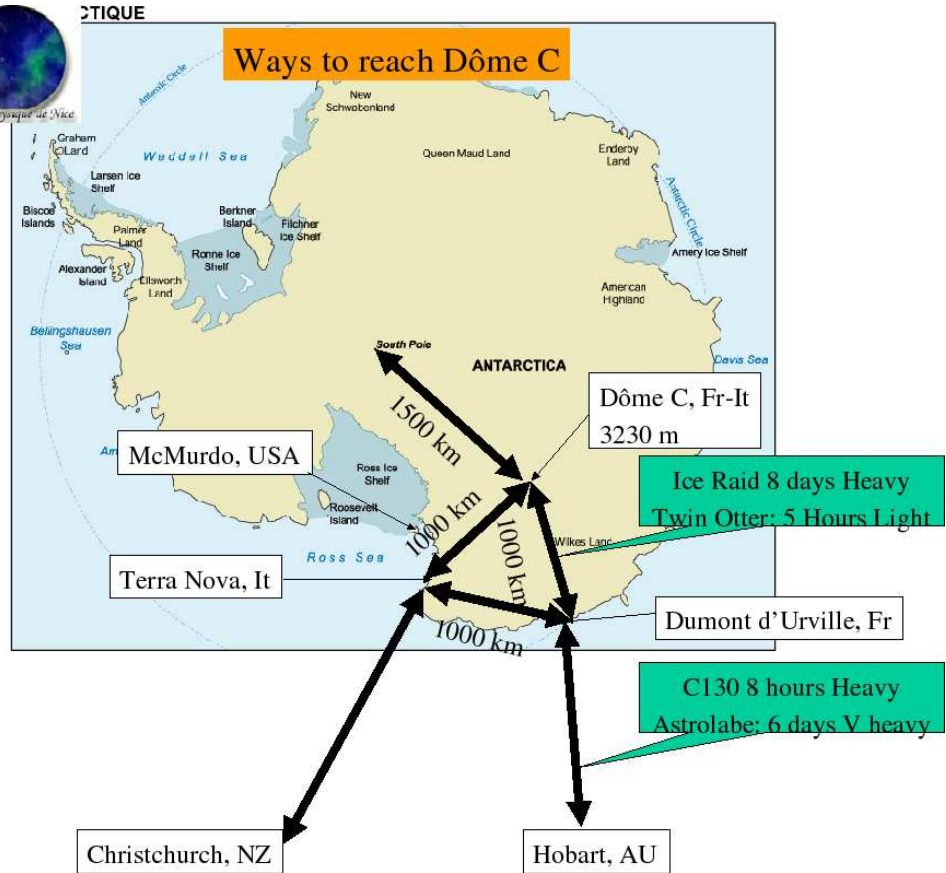


Figure 1: How to reach Dôme C

- Price: One ton can be shipped for 2500 €.
- Maximum size, load: Pieces as large as 10 per 4 per 4 m, and as heavy as 32 T can be delivered with the Astrolabe boat and then delivered at Dôme C. With 3 raids, during a summer season, about 450 T can be sent to DC.
- Buildings: 28 raids have been necessary to bring the 4000 T necessary to construct the whole base. Each building weights 300 T. The construction of the two building required 18 months and 9 people.
- Snow resistance: The snow resistance is about 2 T per m^2 .
- Concordia Project: The overall coast of the Concordia project is 35 M€

4 Optical turbulence parameters

Here, only optical turbulence parameters relevant to High Angular Resolution Astronomy will be discussed. But, clearly, if one wants to construct an astronomical observatory at DC, more detailed studies will be needed to access other

parameters such as sky transparency, extinction coefficients, cloudyness, light pollution, auroras, OH emission, seismicity, soil resistance... Up to now, few summer campaigns took place and only one winter campaign. During this last 2005 winter campaign, about 40 instrumented balloons were launched and two Differential Image Motion Monitors (DIMM) were used. To have more details for what concerns the summer and winter site testing campaigns at DC, one can read Agabi et al., 2006.

4.1 Intagrated parameters

4.1.1 Seeing

In Fig. 2, one can note that the median seeing, in most of mid-latitude “good” sites is around 0.6/1.0 arcsec (The statistic is made over few balloon launches and therefore the seeing might be different from DIMM measurements made during years. This study is based on Abahamid et al., 2004 and Abahamid et al.(to be published). For La Palma observatory see <http://www.otri.iac.es/sitestesting/index.php>, and for Paranal see <http://www.eso.org/gen-fac/pubs/astclim/paranal/seeing/> ...). One notes the very poor seeing at South Pole which is due to katabatic winds which induce a huge optical turbulence in the boundary layer (See Rodney et al., ,1999). This fact convinces us to investigate Dome C site since it is on top of a plateau, less exposed to katabatic winds. But, one notes that, as it was tha case at South Pole, the seeing is also poor at DC with a 1.58 arcsec median value. Our team shown that most of the turbulence comes from the first 30 m, and that, excluding the first 30 m layer, the seeing dropped down to 0.38 arcsec, which is, to our knowledge, the best seeing ever recorded. Anyway, it is not simple to imagine a structure 30 m high to overcome this turbulent layer. **This is a point which needs deep investigation.** For an ELT of 30-60 m diameter, one can think that such a telescope would have his mirror well above this layer, taking great precautions to do not disturb the flow in this layer.

Within the first 30 m, there is a steep gradient of the potential temperature of about +20 degrees. This is a very stable condition. But, as the wind increases from zero, at ice level, up to around 10 m/s, at 30 m, it creates kinetic energy which counter balances the thermal stability and helps the flow to degenerate into turbulence. The remaining optical turbulence is centered around 8-10 km ASL, which means 5-7 km above ice level.

4.1.2 Isoplanatic angle

In Fig. 3, one can note that θ_{AO} is about 2-3 arcsec in most of the mid-latitude sites and twice as large (about 5 arcsec) at Dome C, yielding an isoplanatic field of view 4 times larger. This Dome C better performance is independant of whether or not the telescope is above the turbulent layer.

4.1.3 Temporal coherence for Adaptive Optics

In mid-latitude sites the Adaptive Optics boiling time is around 4-6 ms, as seen in Fig. 4. At Dome C, τ_{AO} is 7 ms at ice level, but rises up to 11 ms above 30 m.

Seeing in various places (Balloons)

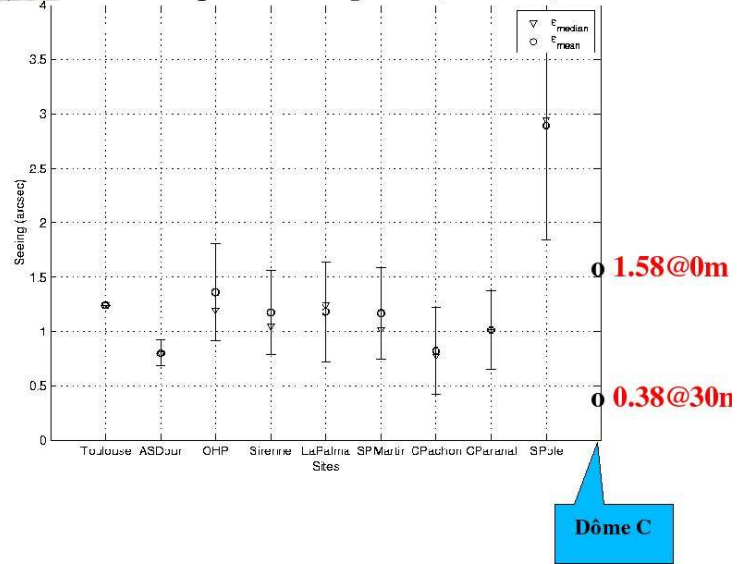


Figure 2: Seeing in various places

Isoplanatic angle for Adaptive Optics Θ_{AO} (Balloons)

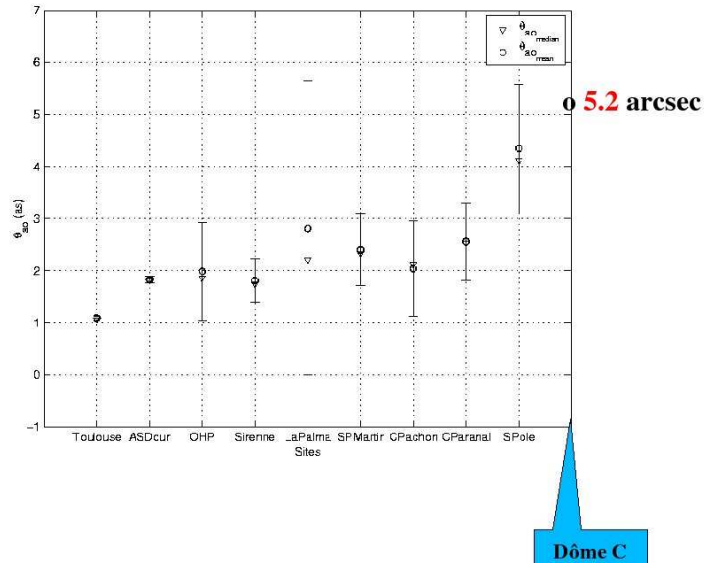


Figure 3: Isoplanatic angle in various places

Boiling time for Adaptive Optics τ_{AO}

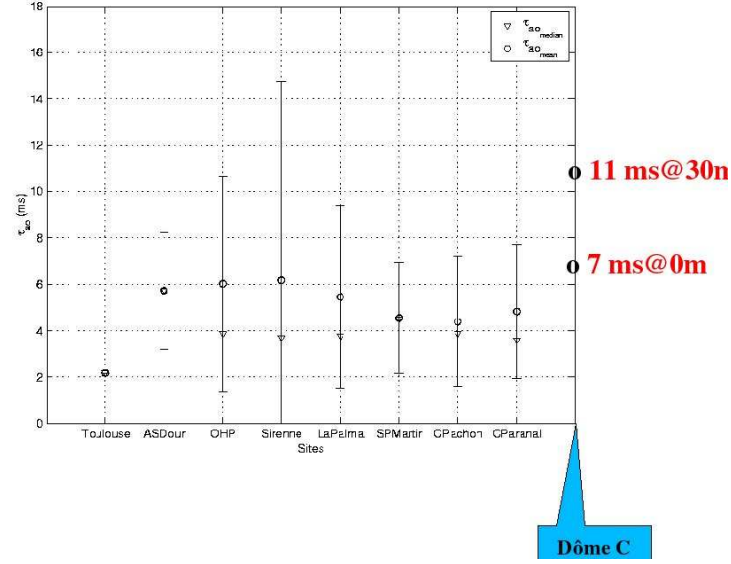


Figure 4: Temporal coherence for Adaptive Optics, in various places

4.1.4 Water vapor content

At mid-latitude sites, the water vapor content is comprized between 1 and 10 mm, even at high altitude and dry sites. This is due to the relative “warm” temperatures of those sites, where dry air contains a lot of water vapor. Conversely, at DC, where temperature is so cold, even a saturated air parcell contains a very small amount of water vapor. It is known that WVC is about 0.4 mm on the whole Antarctic plateau, being very favourable for IR and Sub-mm astronomy. More, it is known that the WVC is very steady, with time, helping background subtraction.

In summary, if one is able to overcome the bad influence of the first 30 m turbulent layer, a gain of more than 2 is expected for the 3 main parameters (seeing, θ_{AO} and τ_{AO}) which optimizes adaptive optics techniques. In comparison, at mid-latitude sites, rising the telescope high 30 m above ground layer would not change much those 3 parameters.

4.2 Optical turbulence profiles and implications on AO and MCAO

In Fig. 5 are shown two “typical” $C_N^2(h)$ profiles at a mid-latitude site and DC. At mid-latitude sites, boundary layer turbulence is concentrated within the first km whereas, at DC, optical turbulence is concentrated within only one thin (~ 30 m) slab. Then, in the rest of the atmosphere, the situation is more similar, except that, it seems that, at DC, most of the optical turbulence is distributed around 5 to 7 km above ice level. Again, this feature has an important con-

sequence if the telescope can be built 30 m above the ice, as explained before. For multi conjugated adaptive optics, this behavior is even more important. Indeed, at mid-latitude sites, most of the turbulence propagates within 3 to 4 major layers (see Tallon et al., 1992a, 1992b, and Vernin et al, 1994), meanwhile, at DC, when the telescope is placed above the ground layer turbulence, the main contribution comes from only one layer. Of course, this conclusion needs to be carefully explored, with the already existing balloon database.

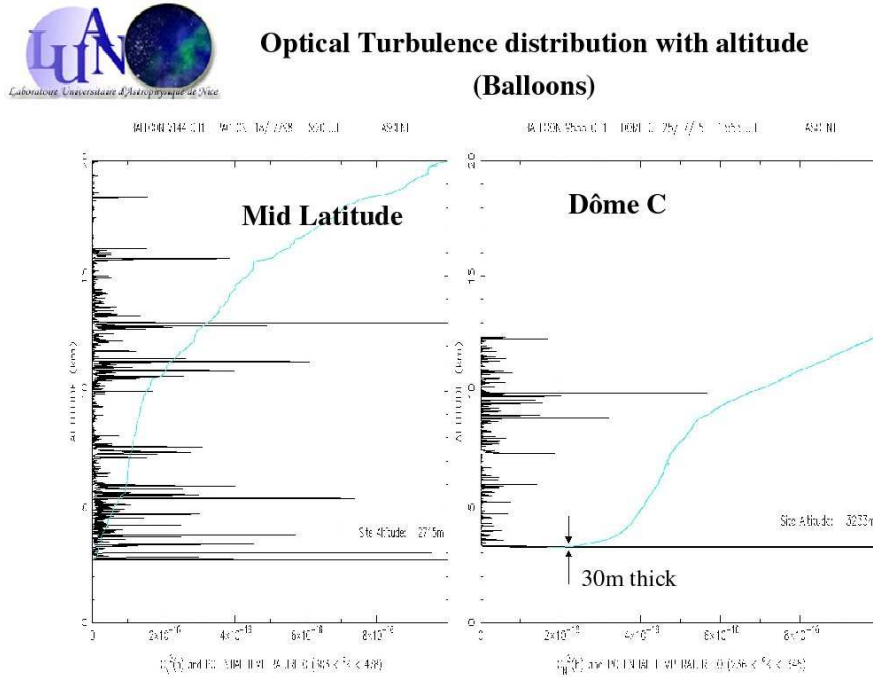


Figure 5: Typical optical turbulence profiles ($C_N^2(h)$) at mid-latitude (Left) and Dome C (right) sites

References

- [1] Agabi A. et al., 2006: First whole atmosphere nighttime seeing measurements at Dome C, Antarctica, To appear in PASP, vol.118
- [2] Aristidi E. et al., 2005: An analysis of temperatures and wind speeds above Dome C, Antarctica, A&A, **430**, 739
- [3] Abahamid A. et al., 2004: Seeing, outer scale of optical turbulence, and coherence outer scale at different astronomical sites using instruments on meteorological balloons, A&A, **422**, 1123
- [4] Marks R. et al., 1999: Measurement of optical seeing on the high Antarctic plateau, A&A, **134**, 161
- [5] Tallon M. et al., 1992a: in Proc. Laser guide star adaptive optics workshop, Fugate ed., Albuquerque (10-12 March)

- [6] Tallon M. et al., 1992b: in ESO Conf. on “Progress in telescope and instrumentation technologies”, Ulrich, M.H. ed., Garching (27-30 April)
- [7] Vernin J., 1994: Optical seeing at La Palma Observatory. II. Intensive site testing campaign at the Nordic Optical Telescope, *A&A*, **284**, 311

IMPACT OF OPTICAL AND NEAR-IR SKY BRIGHTNESS ON SITE EVALUATION

F. PATAT - ESO

(fpatat@eso.org)

1 Introduction

The presence of an emission background from the Earth's atmosphere is a transversal problem in the context of site evaluation, in the sense that it affects all instruments which operate in background-limited conditions. Of course the impact changes according to the different wavelength ranges covered and so does the dominating physical mechanism which is responsible for the radiation emission.

The night sky light as seen from ground is generated by two classes of sources:

- extra-terrestrial (unresolved stars/galaxies, diffuse galactic background, zodiacal light);
- terrestrial (airglow, auroral activity and thermal emission);

While the extra-terrestrial components vary only with the position on the sky and are therefore predictable, the terrestrial ones are known to depend on a large number of parameters (season, geographical position, solar cycle and so on) which interact in a largely unpredictable way. In fact, airglow contributes with a significant fraction to the global night sky emission and hence its variations have a strong effect on the overall brightness.

In this document I will discuss mostly the terrestrial component, since this may depend on the site location and, therefore, it has to be considered among the parameters that characterize a given site. We will also briefly mention the extra-terrestrial component, since the site latitude is directly related to the sky region covered by the observations and hence to the typical extra-terrestrial background (zodiacal light, galactic background).

An overview of the contributions by different sources to the sky brightness is given in Fig. 1.

2 Natural terrestrial components

The terrestrial component can be subdivided into two distinct phenomena, i.e. airglow and aurorae. The main emission features are summarized in Tab. 1 for the two classes, while spectra extending from $0.34 \mu\text{m}$ to $5 \mu\text{m}$ are presented in Figs. 2 and 3.

Table 1: Main night sky emissions in the optical and near-IR (compiled from [2], [18] and [20]).

Emitter	λ (nm)	Intensity		Notes
		Night (R)	Aurora (kR)	
OI	557.7	250	100	<100 R to > 500 R night-to-night variation
OI	630.0-636.4	100	2-100	sporadic enhancements in tropical night glow
OI	777.4	-	10	
OI	844.6	-	12	
NI	346.6	-	1	ICB III Aurora
NI	519.9	-	0.1-2	ICB III Aurora
NII	VIS,FUV	-	45	
NaI	589.0-589.6			NaD, strong seasonal variation
		30	1	summer
		200	1	winter
N ₂	IR	-	880	1st positive, ICB III Aurora
N ₂	UV	-	110	1st positive, ICB III Aurora
N ₂	Blue	100	55	Vegard-Kaplan bands, ICB III Aurora
N ₂ ⁺	NUV,VIS	-	150	1st negative, ICB III Aurora
N ₂ ⁺	630-890	-	630	Meinel bands, ICB III Aurora
O ₂	300-400	1500	-	Herzberg, and Chamberlain bands
O ₂	864.5	500	60	Atmospheric bands (0-1) R and P, ICB III Aurora
O ₂ ⁺	VIS,IR	-	26	1st negative, ICB III Aurora
OH	VIS	130	-	(5-0) (7-1) (7-2) (9-3) ... bands
OH	8342	2000	-	(6-2) band
OH	Total	4.5×10 ⁶		
NO ₂	400-700	250		nightglow pseudo-continuum
HeI	1083	-	1000	

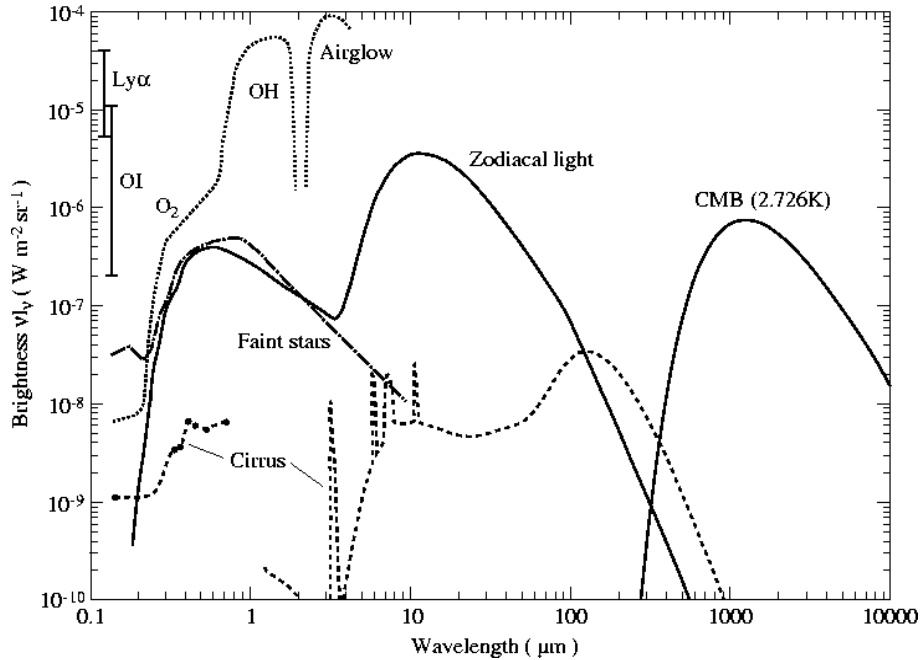


Figure 1: Overview of the night sky brightness outside of the lower terrestrial atmosphere and at high ecliptic latitudes (from [11]).

2.1 Airglow

Airglow (a.k.a. nightglow), is caused by ambient excitation (usually photochemical) of upper-atmosphere atoms and molecules (mesosphere, 85-90 km). The main parameters that govern the airglow brightness are as follows:

- geomagnetic latitude (?), season, solar activity, wavelength

A low resolution spectrum in the optical and near-IR domain is presented in Figs. 2 and 3. While the flux in the blue region ($\lambda < 5500\text{\AA}$) is produced by the so-called NO_2 pseudo-continuum, the red is totally dominated by the OH bands emission bands [2], which are also the responsible for the non-thermal emission in the IR (see for example [17]). Line atlases have been published both for the optical [9] and the IR [19]. The night sky emission is in general extremely variable even on short time scales and these fluctuations are stronger at longer wavelengths. In some passbands, like I and J, the OH bands show a steady decline in the first two hours after the end of evening twilight.

It is often mentioned in the literature that the airglow depends on the geomagnetic latitude (see for example [11], [1]). However, I could not find very precise statements, let alone direct measurements. For example, [20] states that the airglow is brighter at middle and high latitudes than at low latitudes and some emissions (like OI 6300, 6363 \AA) increase by a factor 2 [3]. At low and mid-latitudes there is a semi-annual variation in atomic hydrogen, which is in turn thought to be the responsible for the OH nightglow fluctuations [12]. At least in the optical, once one takes into account the effect of solar activity (which can give a variation of ~ 0.4 - 0.5 mag on a full solar cycle), all light pollution-free sites show very comparable night sky surface brightnesses (see [11], [13], [21]).

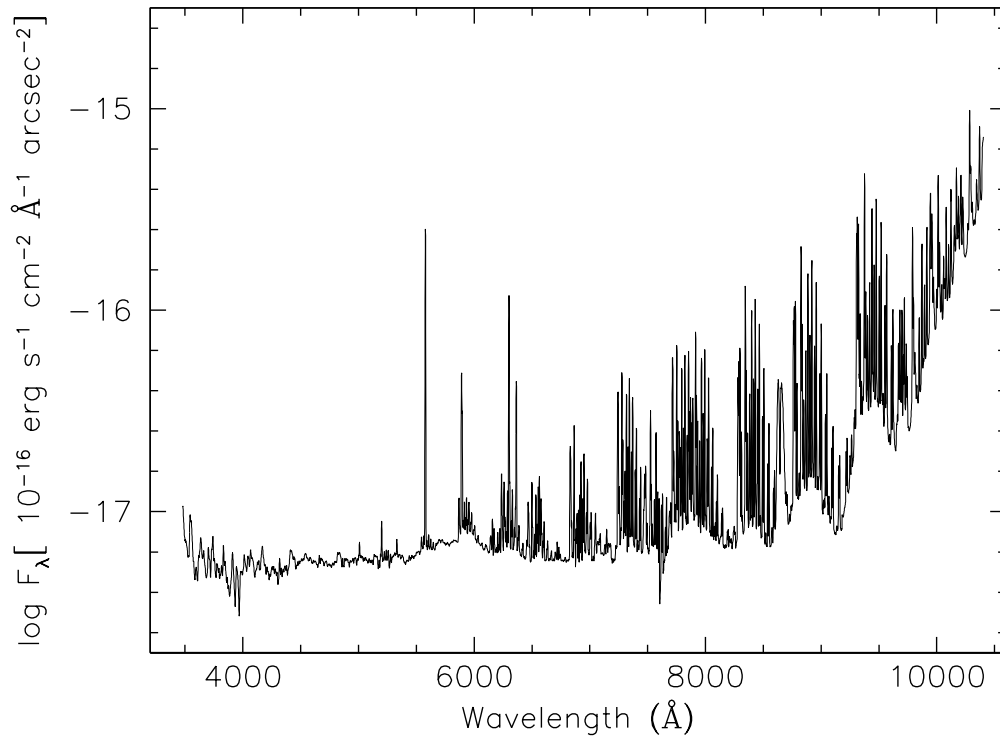


Figure 2: Optical night sky spectrum obtained at Paranal with FORS1 (resolution $\sim 5\text{\AA}$ FWHM).

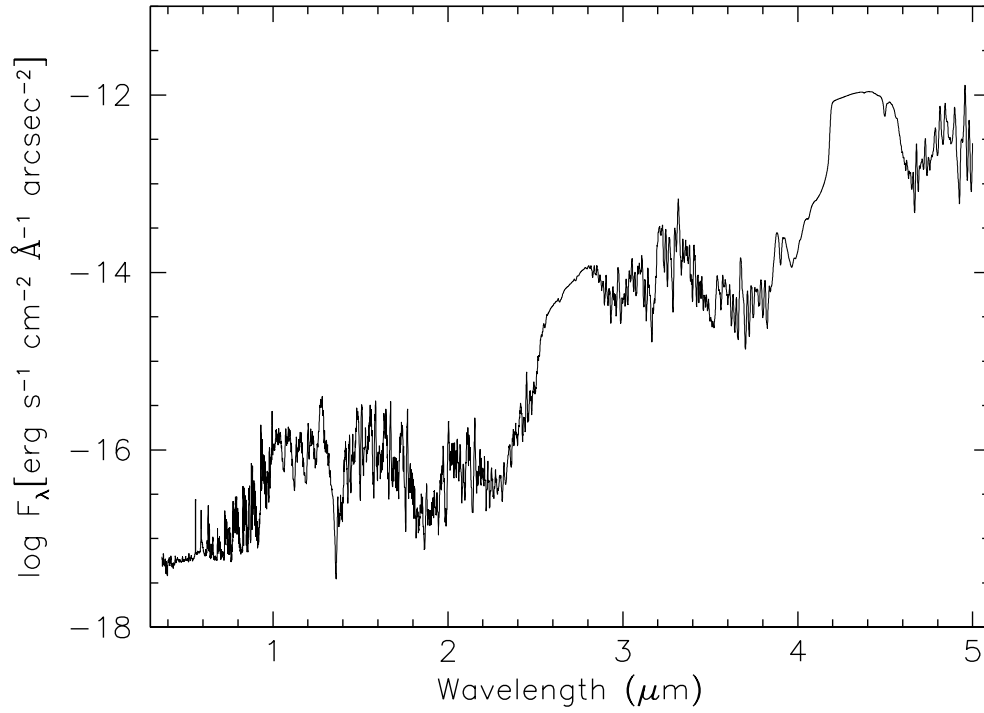


Figure 3: Optical-IR night sky spectrum. For $\lambda < 1\mu\text{m}$ the spectrum is that presented in Fig. 2 while for $\lambda > 1\mu\text{m}$ the synthetic model used in Gemini Exposure Time Calculator was adopted.

The lack of measurements at high latitudes is essentially due to the fact that most observatories are placed at equatorial or tropical latitudes. The few available data, however, seem to indicate that there is no strong dependency on the geomagnetic latitude, at variance with what happens for auroral activity.

As far as the satellite observations are concerned, the data provided by the Improved Stratospheric and Mesospheric Sounder on the UARS satellite show no differences (within the errors) between high and mid-latitudes in the average intensities of OH nightglow [22]. Also, the ground-based measurements of OH emission between 837.5 nm and 856.0 nm obtained at Davis, Antarctica (68 degrees south) do not show significant differences with respect to low-latitude sites (see [10] and references therein).

The conclusion of my search in the literature is that there is no clear indication of a geomagnetic latitude dependency of the airglow, while this is more firmly established for auroral emission. In this respect, it is worth noting that two experiments are being setup at Dome C, namely *Gattini* and *Nigel* (J. Storey and A. Moore, private communication). Those instruments are going to provide spectrophotometry both during twilight and night time.

As far as the site dependency of IR background is concerned, the situation is less clear. The background at 1.7 μm on Paranal has been reported to be a factor 4 brighter than in Mauna Kea [6]. Since at this wavelength the thermal emission is still negligible (see Fig. 7), the difference is indeed difficult to explain. However, this is in conflict with the values reported by UKIRT¹, which are in good agreement with those measured at Paranal².

2.1.1 The case of NaI D lines

While all night sky emission lines are indeed hindering astronomical observations, there is one remarkable exception, namely the Sodium D lines (5890, 5896 Å), on which the whole LGS technique is based.

Monitoring of the sodium layer is usually done with a laser and provides knowledge of the sodium variability on the shortest time scales. There is also another technique, which relies on medium-high resolution spectroscopy of the sodium doublet. Due to the required exposure times this is of course not going to give information on the variations on times scales of seconds, but it can provide an alternative monitoring tool. Experiments have been done in the past in order to inter-calibrate laser measurements with spectroscopic observations [7]. The relevant spectral region is shown in the left panel of Fig. 4 (UVES, resolving power 42,000). The sodium D lines appear to be close to two of the OH (8-2) emission lines (marked as A and B). As it is shown in the upper left insert, the four lines appear to be blended at a resolution of about 1200. Nevertheless, A (5888.2Å) and B (5894.5Å) features account for $\sim 12\%$ of the total flux carried by the D lines. Therefore, medium resolution spectroscopy might still be a potential source of information on the sodium layer.

For the sake of completeness, we mention here the possibility of doing the same kind of analysis using the observations of the D lines *in absorption* against a bright star, as proposed in [15]. However, this method is probably going to be affected by the presence of the ubiquitous sodium lines in the stellar spectrum and in the interstellar environment and, due to the very small equivalent width of atmospheric Na I D lines, indeed requires higher resolution (and

¹See <http://www.jach.hawaii.edu/UKIRT/astronomy/sky/skies.html>

²See <http://www.eso.org/gen-fac/pubs/astclim/paranal/skybackground/>

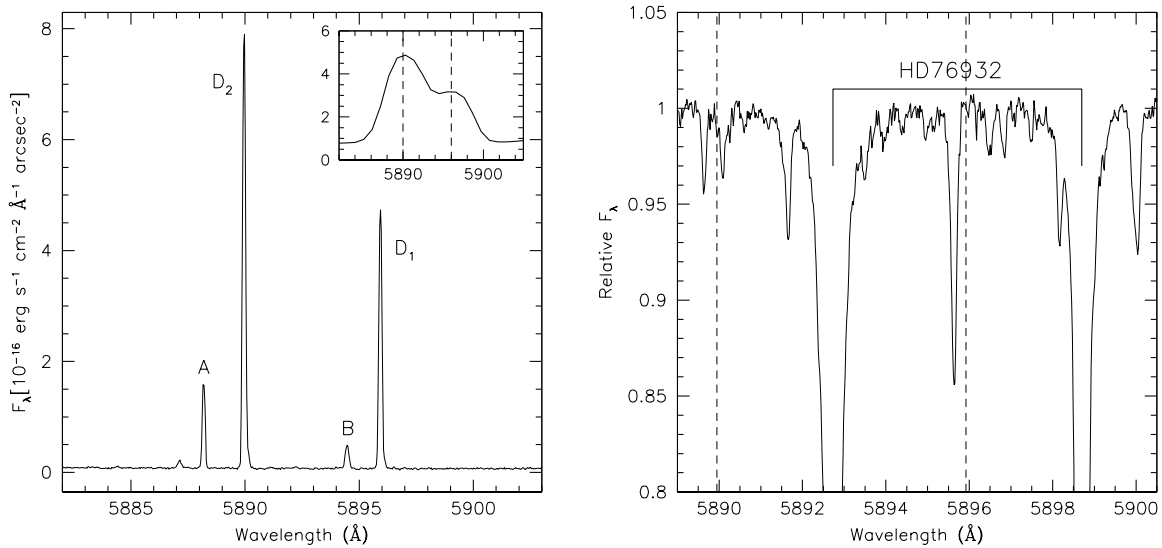


Figure 4: Left panel: Night sky UVES spectrum in the region of the NaI D lines (resolution of $\sim 0.15\text{\AA}$ FWHM; [9]). The upper insert shows the appearance of the same region in low resolution (FORS1, $\sim 5\text{\AA}$). Right panel: UVES spectrum of the bright F7 star HD 76932 ($V \sim 5.5$), courtesy of F. Primas. The vertical dashed lines mark the rest frame D lines wavelengths.

hence higher exposure times and/or large telescopes). An example is shown in the right panel of Fig. 4, where the identification of rest frame absorption D lines is actually not clear. Obviously, degrading the resolution to a few thousands would absolutely not allow this kind of analysis.

An example application of Na I D line intensity monitoring, using FORS1 archival data, will be presented soon (Patat, 2006, in preparation).

2.2 Aurorae

Aurorae are generated by the excitation of upper-atmosphere atoms and molecules by energetic particles, in atmospheric layer at 250-300 km. The main parameters that govern the auroral brightness are the following:

- geomagnetic latitude, season, solar activity, magnetic activity, wavelength

2.3 Polar aurorae

Aurorae are a serious problem for ground-based astronomy only at high latitudes, within what is generally indicated as the auroral zone. This extends from 15 to 25 degrees from the geomagnetic pole, a region which is called the auroral oval. A monitoring of the auroral oval size and position is provided by OVATION (Oval Variation, Assessment, Tracking, Intensity,

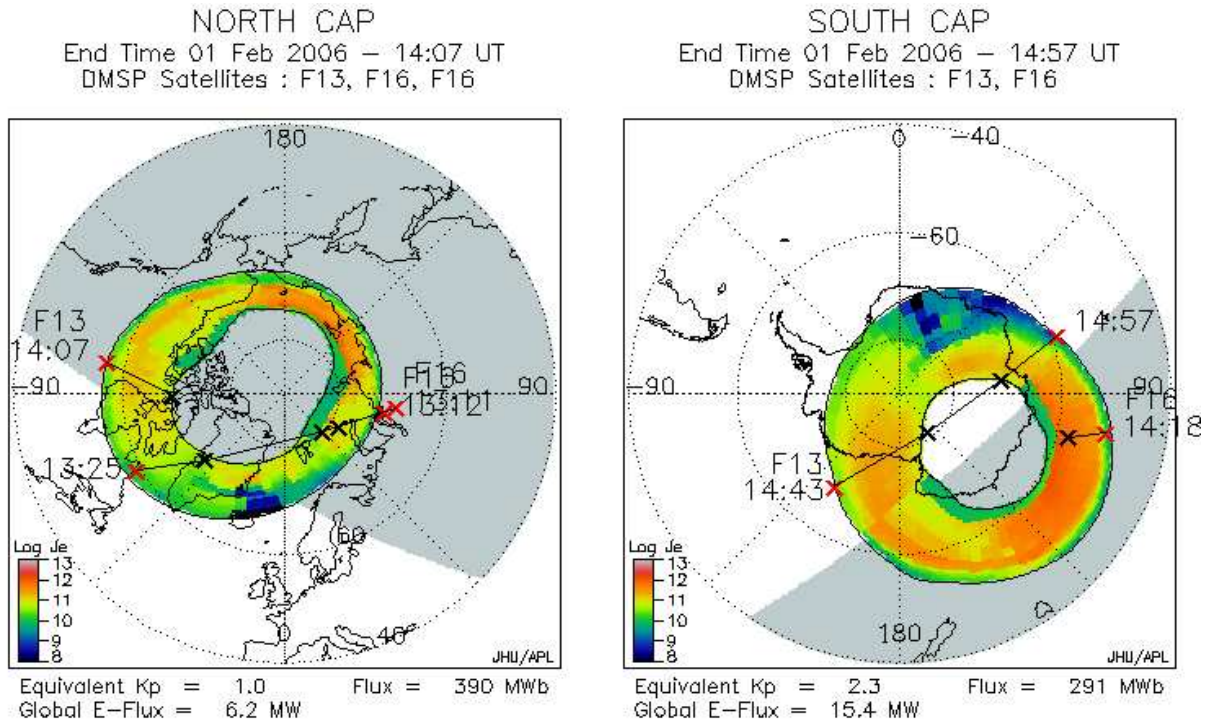


Figure 5: OVATION North (left) and South (right) polar cap plots.

and Online Nowcasting)³. An example is shown in Fig. 5.

Aurorae typically take place in atmospheric layers between 100 and 250 km above the ground, with occasional peaks up to 1000 km (see for example [20]). This potential problem for high latitude sites has been analyzed and discussed in [10] in connection to the Dome C case. The conclusion is that aurorae at 100 km (or below) are not visible from Dome C, while for an height of 250 km they would be visible at elevation of about 7 degrees above the horizon and therefore would only weakly increase the night sky brightness (see also Fig. 6). Nevertheless, this conclusion must be taken with care. Direct measurements are still missing, but they will be soon provided by the two experiments previously mentioned.

2.4 Micro-auroral activity

Sites located at $\pm 20^\circ$ from the geomagnetic equator are known to show micro-auroral activities [18], with sudden variations of emission lines like [OI] 6300, 6364 Å. However, the impact in terms of night sky brightness enhancement is negligible (see for example [13]).

3 Thermal emission in the IR

At wavelengths longer than about 2 μm the atmospheric thermal emission becomes relevant (see Figs. 7 and 8). There are two windows centered at 3.5 and 10 μm where the thermal background is minimum, while maxima are reached at about 7.5 and 14 μm .

³See <http://sd-www.jhuapl.edu/Aurora/ovation>

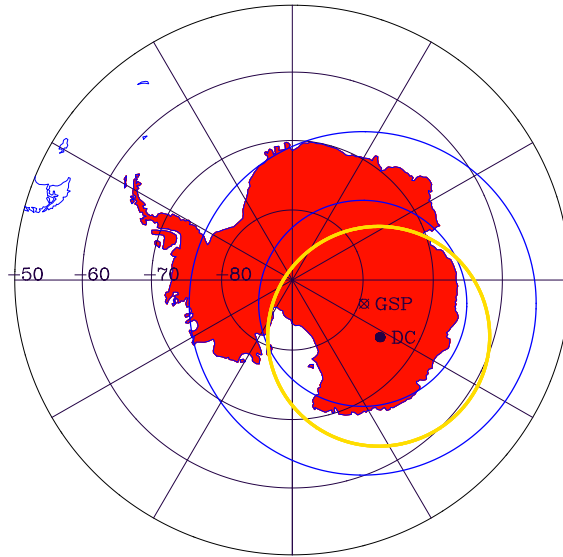


Figure 6: Schematic representation of the typical southern auroral oval, showing the geomagnetic South Pole (GSP) and Dome C (DC). The auroral oval boundaries, marked by the two blue circles, typically extends from 15 to 25 degrees from the GSP. Aurorae at 250 km altitude will be above the horizon at Dome C only if they line within the thick yellow circle (adapted from [10]).

There is a clear dependence on the site elevation, since the temperature of the lower atmospheric layers decreases very rapidly with altitude. At about 4000 m the thermal background in the window centered at $10 \mu\text{m}$ becomes almost a factor 5 weaker.

There are no clear indication about latitude dependency, while very cold sites show exceptionally low sky backgrounds, as it is the case for Dome C, both in the IR and in the sub-millimeter domain (see [10] and references therein).

4 Scattered moonlight

Scattered moonlight contributes in a dominant way to the optical night sky background when the Moon is above the horizon (at Paranal this is about 40% of the total twilight-to-twilight night time). Even though this is an unavoidable fact, different sites can show different amounts of scattered light, mainly for two reasons. The first is a different content in the aerosols, which can indeed change the impact. The other is the geographic latitude. In fact, for a given alt-az position in the sky, the background enhancement grows with the Moon height above the horizon. Therefore, at high latitude sites the moon impact is smaller than at equatorial sites, where the Moon can actually pass through zenith (see also the discussion in [10]).

The presence of scattered moonlight, which has essentially a blue spectrum peaking at 4500\AA , becomes of course progressively irrelevant as one goes into the IR domain.

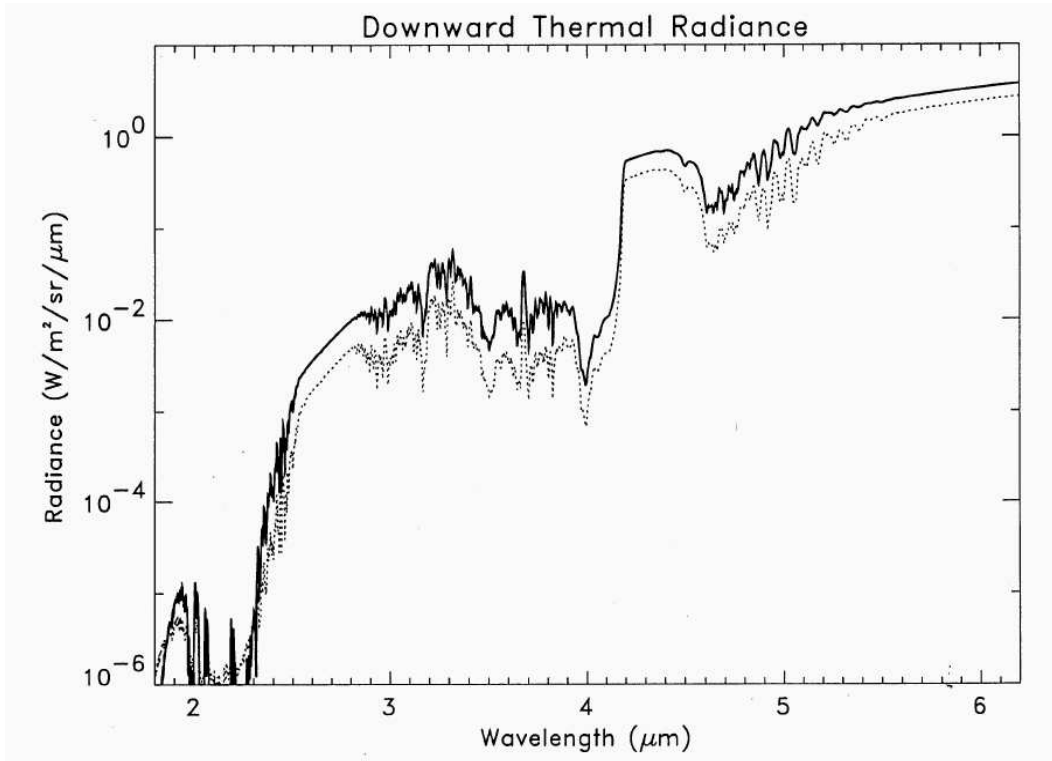


Figure 7: Downward thermal radiance in the near-IR at sea level (solid) and 4000 m a.s.l. (dotted) (from [20]).

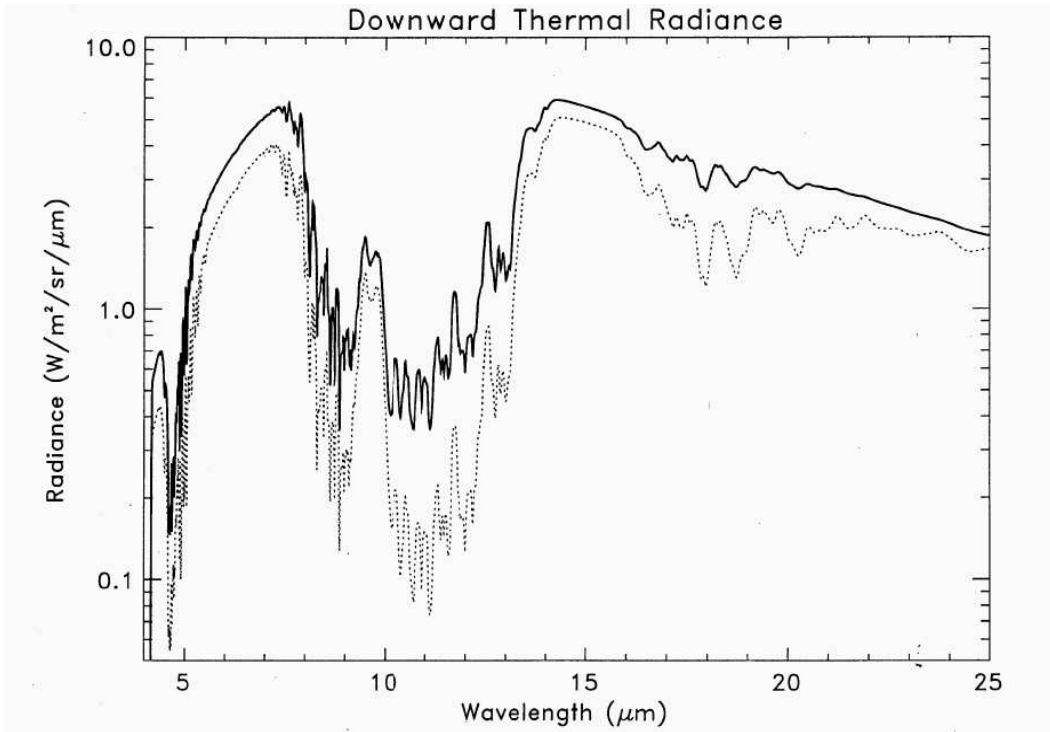


Figure 8: Downward thermal radiance in the IR at sea level (solid) and 4000 m a.s.l. (dotted) (from [20]).

4.1 Contrails

The problem of contrails is quite extensively discussed in [16]. The effects of contrails are temporary increased extinction, degradation of seeing and possible disturbs in high resolution spectra in the form of absorption lines/bands. I deem that the stronger effect comes in the form of an enhanced sky background in the presence of Moon light, as it is the case when thin/thick cirrus are present. See the discussion in [16] for more details.

5 Light Pollution

In addition to the *natural* components, human activity has added an extra source, namely the artificial light scattered by the troposphere, mostly in the form of Hg-Na emission lines in the blue-visible part of the optical spectrum (vapor lamps) and a weak continuum (incandescent lamps) [1]. With the advent and the diffusion of Compact Fluorescent Lamps, the situation has become even worse, since these lamps tend to reproduce the solar spectrum by emitting a forest of emission lines across the whole optical spectrum (see Fig. 9).

Nighttime optical images of the Earth at night have been obtained from the Defense Meteorological Satellite Program (DMSP). These data have been used to estimate the upward light flux of sources on the Earth surface and to compute the effects on the night sky modeling the light propagation in the atmosphere [4]. A world map is shown in Fig. 10.

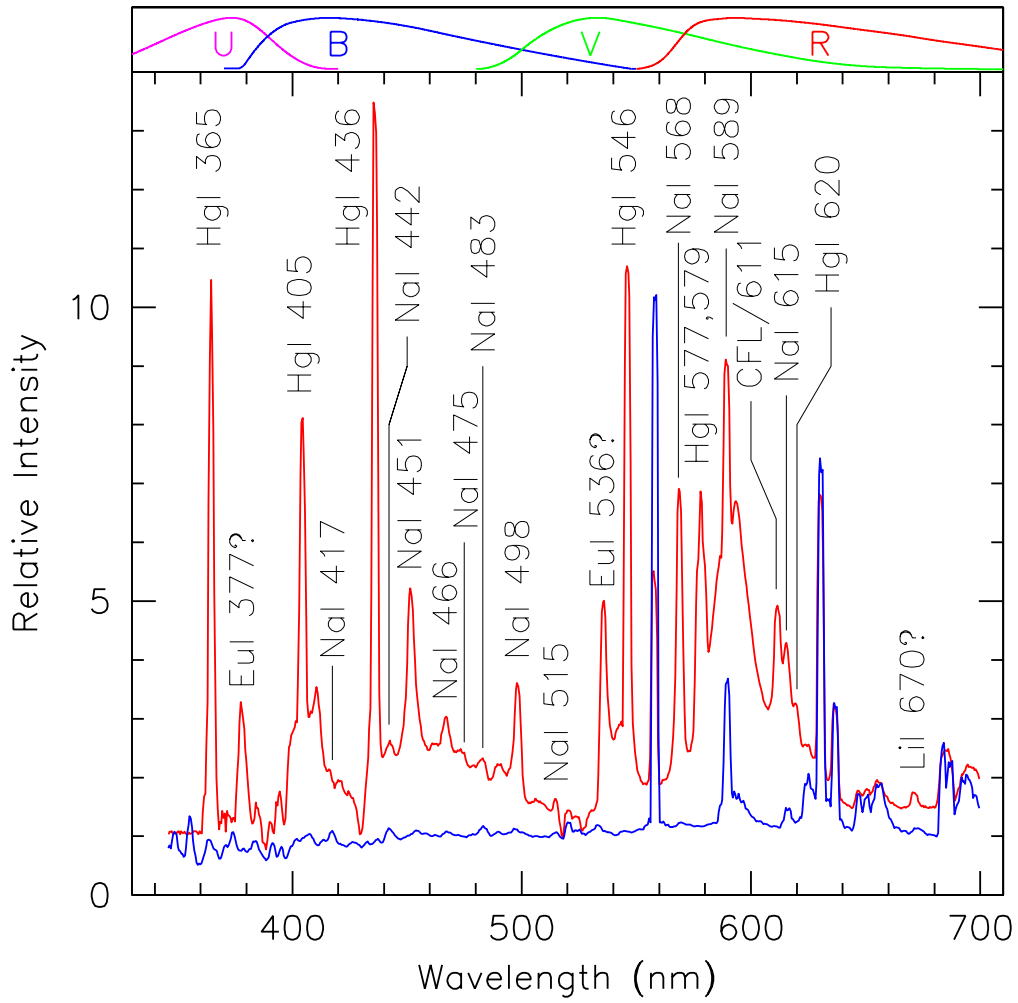


Figure 9: Comparison between night sky spectra obtained at Paranal (blue) and in a light-polluted site (red, Asiago Observatory, Italy).

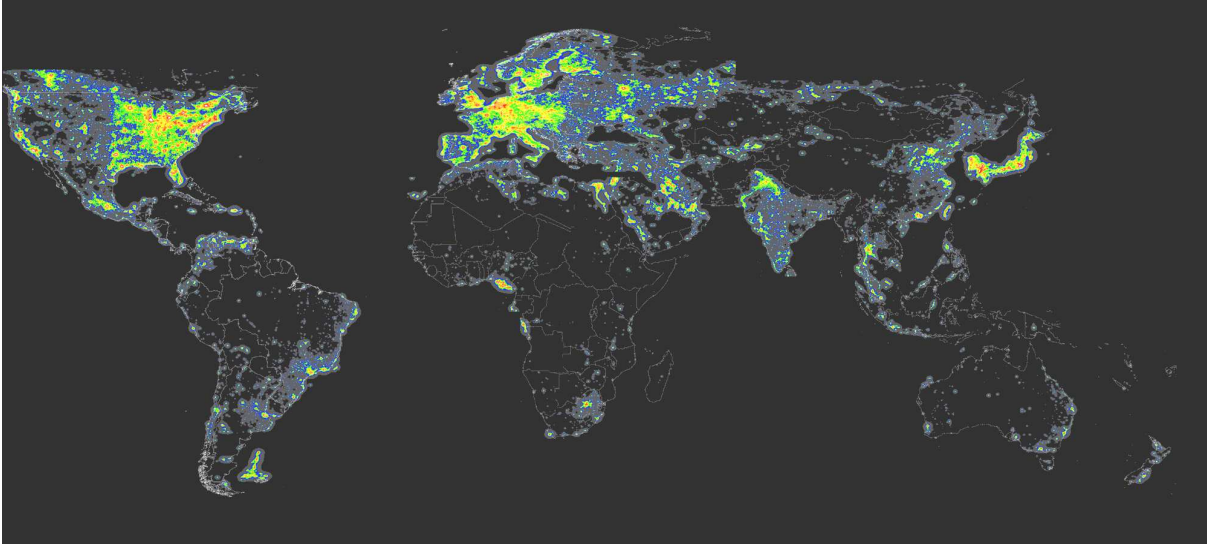


Figure 10: Artificial V sky brightness at zenith in clean nights, obtained by Cinzano et al. [4]. The mas has been computed using Garstang [8] models and measurements obtained by the Operational Linescan System of US Air Force DMSP satellites. The effects of extinction along light paths, double scattering of light from atmospheric molecules and aerosols, Earth curvature and aerosol content of the atmosphere are included.

6 Extra-terrestrial background

The extra-terrestrial background is generated by unresolved stars and galaxies and, most important, by the sun light scattered by the interplanetary dust, also known as zodiacal light. The latter contributes to about half of the brightness of the night sky in the visible, it peaks at about 4500\AA and at 8000\AA becomes only 10% of the OH airglow. At longer wavelengths, the interplanetary dust gives a contribution to the background in the form of thermal radiation, with a spectrum that peaks at about $12\ \mu\text{m}$ (see [11] and references therein).

Of course the contribution depends on ecliptic latitude and helioecliptic longitude. Therefore, equatorial sites, for which the ecliptic is rather high in the sky, do show a higher zenith background than high latitude sites. Strictly speaking, this is not an intrinsic feature of the site but rather of the typical portion of the sky observable from that site. In general, when comparing different sites, the contribution of the zodiacal light has to be taken into account, as it is the case for the solar cycle phase.

Finally, the different apparent positions of the ecliptic plane during the year can mimic intrinsic seasonal variations.

7 Conclusions

- In light pollution-free sites the optical night sky brightness due to airglow is in general independent from the geographical position. Altitude is not expected to play a role in this respect. The night sky brightnesses in V at Crimean Observatory (600m), Paranal (2600m) and Mauna Kea (4200m) are comparable.

- The situation is less clear in the OH dominated near-IR region, since not many measurements at non-tropical sites are available. In principle, no difference is expected.
- In the IR the background is definitely lower in colder sites and at higher altitudes, due to the decreased thermal emission.
- Small micro-auroral effects at sites close to the geomagnetic equator do exist, but their contribution to the global background is negligible.
- Auroral activity is a serious issue for locations at high latitudes and the effects in the optical can be rather severe. The motion of the magnetic poles can cause problems in sites where this used not to be a problem.
- The contribution to the background by the extra-terrestrial component changes with the site latitude. But this is related to the different regions of the sky which are accessible from a given site rather than to the characteristic of the site itself.

8 Appendix - Measuring the sky background

One important issue with the site testing is the inclusion of sky background measurements. For obvious reasons, any instrumentation designed for this purpose has to be simple, compact, light and must operate in a fully automatic way. As far as the spectro-photometric accuracy is concerned, 10 to 15% is sufficient.

The ideal solution should be searched within commercial products, especially for what concerns telescopes, mounts and detectors⁴.

Normally, sky brightness surveys are operated using small size telescopes (0.3-0.4m) coupled to a diaphragm photoelectric photometer with broad band filters. In this case, the operator has to chose a star-free area and this makes the operation slow and not viable for automatic campaigns. Therefore it is clear that one needs panoramic detectors in order to be able, in the data reduction phase, to reject stars and other bright astronomical objects that may fall in the field of view. Algorithms specifically designed for this purpose are available (see for example [14] and references therein).

Different degrees of complexity can be considered, all including Peltier-cooled CCD detectors:

- Imaging wide field camera, at least V filter
- Imaging camera, few square deg field of view, at least V filter;
- Imaging camera, few square deg field of view, $BVRI$ filters;
- Low resolution (30-50Å) spectrograph, covering 500-1000 nm.

In the following subsections, the single cases are discussed separately.

⁴For imaging cameras and two spectrographs see for example <http://www.sbig.com/sbwhtmls/online.htm>

8.1 Wide Field camera

This is probably the simplest solution. Due to the necessarily small focal length of the camera, there is most likely no need for tracking. Therefore the telescope can simply point the zenith and images can be continuously acquired and processed online by a simple automatic pipeline. The main issue with this setup is that wide field cameras are difficult to calibrate in photometric terms. Moreover, due to the necessarily big projected pixel size, stellar crowding may become too high so that measurements *in between the stars* can be difficult and/or inaccurate.

The advantage is that a great portion of the sky is covered, and this offers the chance to detect possible light pollution effects in some specific and critical directions, or to characterize the Moonlight effect as a function of all relevant parameters in one single shot.

8.2 Few square deg camera

This requires a telescope with a larger focal length and, therefore, it has to include the possibility of pointing and tracking. Pointing does not need to be accurate and so does the guiding. Even badly guided star trailings will be removed during the reduction. Given the pointing capability, one can think about the possibility of specifying a grid of *empty-fields* across the sky, that would allow one to get sky maps.

As far as filters are concerned, the simplest solution is to have just one, the *V* filter, hence reducing the weight and complexity caused by the presence of a filter-wheel. The *V* passband includes the bright airglow lines (and the aurora lines) and also the bright light pollution Hg and Na lines. On the other hand it does not include the OH lines. For this a *R* or better *I* filter would be required.

8.3 Long slit - low resolution spectrograph

Considering the fact that portable IR instrumentation is not a viable solution, the top setup for sky brightness measurements is a low resolution spectrograph that covers the region 500-1000 nm, i.e. giving a full coverage of airglow, aurora, light pollution and OH optical features. At a resolution of 50Å the most important features would be visible (see Fig. 11) and would allow studies of seasonal/latitudinal trends of micro-auroral, auroral and OH features (for NaID studies the resolution is far too low).

There is a main problem with this, i.e. the fact that one necessarily needs to have a slit and this has to be placed in reasonably star free areas. This problem can be mitigated by a smart data processing coupled to the long slit, in the sense that one can reasonably assume that most of the pixels will be dominated by sky background.

The instrument has to be kept very compact in order to be mounted on a small telescope. An example is given in [5], even though that instrument was designed for light polluted sites, i.e. with a much brighter background.

A possible alternative is a fiber-fed spectrograph. This would greatly reduce the weight, but it would introduce the problem that during the data processing is impossible to disentangle the contribution of the background from that of possible astronomical objects falling into the fiber.

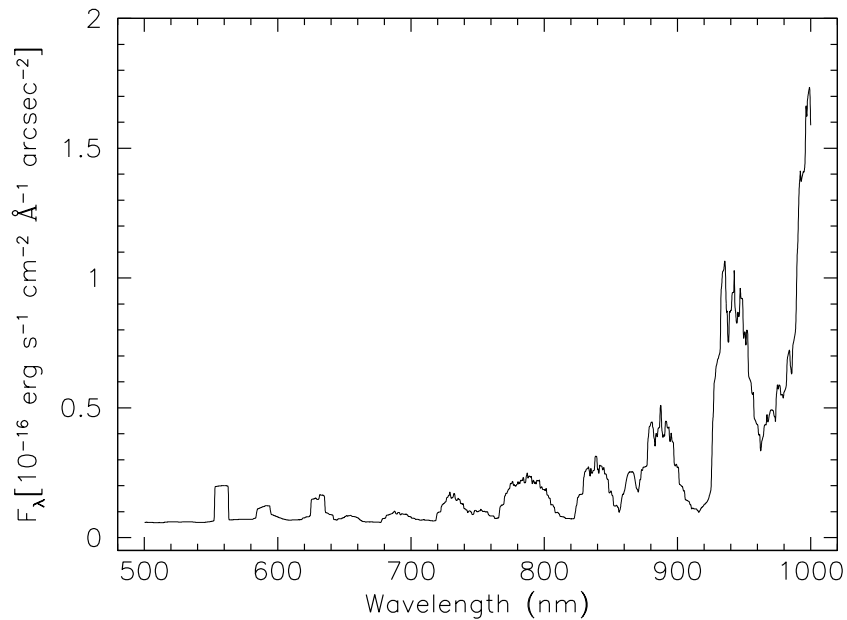


Figure 11: Optical night sky spectrum in the region 500-1000nm degraded to a resolution of 50 Å.

In all cases wavelength calibration is not an issue, since the night sky lines themselves can be used. As for the flux calibration, bright standard stars for professional instruments can be easily observed once in a while to get reference sensitivity curves.

For what concerns data processing, there is no major problem. The only real issue for the absolute fluxing is the stability of bias level and dark current. In the case of Peltier-cooled detectors this might require the need of taking calibration frames during the measuring sessions. Of course, this problem affects both imaging and spectroscopy. If the controller allows for pre/over-scan readings, this issue becomes much less important.

I believe that, in general, for imaging one can easily find all required hardware on the market. For the spectrographs there is not much available. Nevertheless, current commercial solutions should be considered. For example, the SBIG DSS-7 spectrograph covers the range 400-800 nm (see Fig. 12 for an example night sky spectra obtained with this instrument). This is a very compact and low weight instrument (~ 1.1 kg) and the price is around 1500 USD. The dispersion is $5\text{\AA}/\text{pix}$ and resolution is about 15\AA ($7 \mu\text{m px}$, ST-7 camera). Testing is of course required, but I think that such a setup would be already sufficient for our purposes.

Things get of course extremely more complicated in the case of site testing in extreme conditions, like in Antarctica. On the other hand, this site is quite unique and site testing campaigns are already in place and they should provide us with the relevant data in due time.

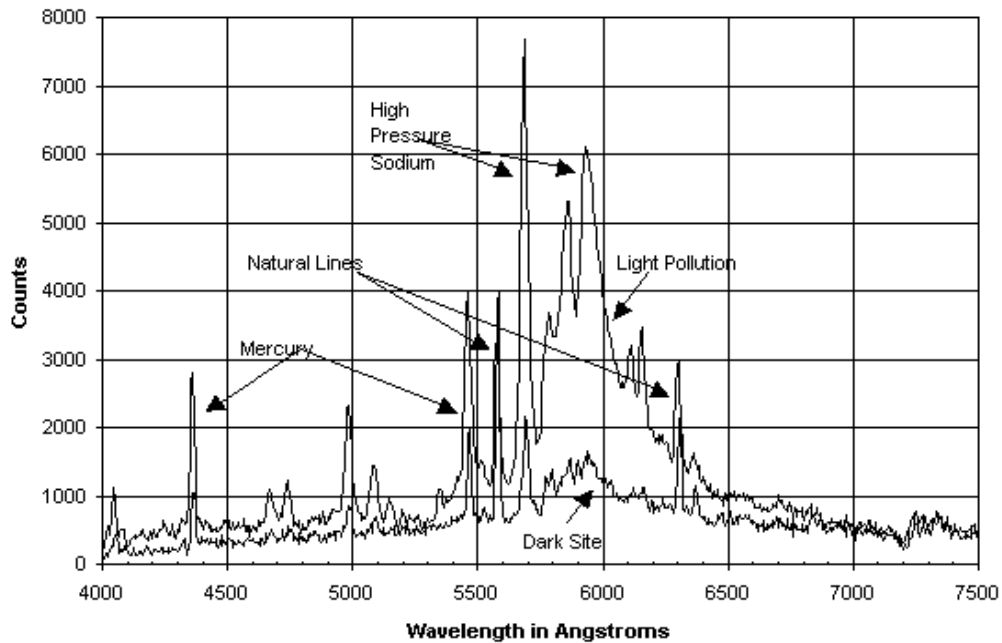


Figure 12: Optical night sky spectra obtained at two different sites with the SBIG DSS7 spectrograph (from the SBIG web site). Note that what is called here *dark* site shows clear signs of light pollution (compare with Paranal spectra).

References

- [1] Benn, C.R. & Ellison, S.L., 1998, Atmospheric extinction at the Roque de los Muchachos Observatory, La Palma Tech. Note n. 115
- [2] Broadfoot, A.L. & Kendall, K.R., 1968, J. Geophys. Res., 73, 426
- [3] Chamberlain, J.W., 1961, Physics of the Aurora and Airglow, (Academic Press: New York)
- [4] Cinzano, P., Falchi, F., Elvidge C.D. 2001, The first world atlas of the artificial night sky brightness, MNRAS, 328, 689
- [5] Cinzano, P., 2004, A portable spectrophotometer for light pollution measurements, Mem. S.A.It. Suppl. Vol. 5, 395
- [6] Cuby, J.G., Lidman, C. & Motou, C., 2000, ISAAC: 18 months of Paranal Science Operations The ESO Messenger, 101, 2
- [7] d'Orgeville, C. et al., 2003, Preliminary results of the 2001-2002 Gemini sodium monitoring campaign at Cerro Tololo, Chile, SPIE, 4839, 492D
- [8] Garstang, R.H., 1989, Night sky brightness at observatories and sites, PASP, 101, 306

- [9] Hanuschik, R., 2003, A flux calibrated, high resolution atlas of optical sky emission from UVES, *A&A*, 407, 1157
- [10] Kenyon, S.L. & Storey, J.W.V., A review of optical sky brightness and extinction at Dome C-Antarctica, 2005, *PASP*, in press, astro-ph/0511510
- [11] Leinert, Ch. et al., 1998, The 1997 reference of diffuse night sky brightness, *A&ASS*, 127, 1
- [12] Le Texier, H., Solomon, S. & Garcia, R.R., 1987, Seasonal variability of the OH Meinel bands, *Planet. Space Sci.*, 35, 977
- [13] Patat, F., 2003a, UBVRI night sky brightness at sunspot maximum at ESO-Paranal, *A&A*, 400, 1183
- [14] Patat, F., 2003b, A robust algorithm for sky background computation in CCD images, *A&A*, 401, 797
- [15] Patriarchi, P. & Cacciani, A., 2000, Monitoring of the mesospheric sodium layer using a magneto-optical filter, *SPIE*, 4007, 368
- [16] Pedersen, H., 1998, VLT observing conditions monitor, ESO internal document
- [17] Ramsay, S.K., Mountain, C.M. & Geballe, T.R., 1992, Non-thermal emission in the atmosphere above Mauna Kea *PASP*, 259, 751
- [18] Roach, F.E. & Gordon, J.L., 1973, *The light of the night sky*, Dordrecht-Reidel
- [19] Rousselot, P., Lidman, C., Cuby, J.G., Moreels, G. & Monnet, G., 2000, Night-sky spectral atlas of OH emission lines in the near-IR, *A&A*, 354, 1134
- [20] Schubert, G. & Walterscheid, R.L., 2000, Earth, in *Allen's Astrophysical Quantities*, ed. A. Cox (New York: AIP Press; Springer), 4th edition, 239
- [21] Walker, A. & Schwarz, H.E., 2005, Night Sky Brightness at Cerro Pachon, http://www.ctio.noao.edu/site/pachon_sky
- [22] Zaragoza, G., Taylor, F.W. & Lopez-Puertas, M., 2001, Latitudinal and longitudinal behaviour of the mesospheric OH nightglow as observed by UARS/ISAMS *J. Geophys. Res.*, 106, 8027

UV OBSERVATIONS SITE REQUIREMENTS

Sergio Ortolani

Department of Astronomy, University of Padova

Roberto Gilmozzi

European Southern Observatory

The UV region between 280 and 380 nm is of special astrophysical interest because there are important emission and absorption lines and peculiar spectral features including several metallic lines such as [Ne V] lines at 342 nm, the O III at 344, the [OII] doublet at 372.7-372.9 and the Balmer jump (365). Furthermore there is a specific interest for some coronal lines such as the He II at 303 nm, Fe XII at 284 and Fe XVI at 335 while OH lines around 283, 308 and 314 are of interest to solar system astrophysics.

Furthermore in this range we have the U standard Johnson band, centered around 360 nm and 50 nm wide (Bessell, 1990), and the Gunn u band (Thuan and Gunn, 1976), centered at 353 nm and 40 nm wide. Interesting features of the UV continuum can be detected from the thermal component of neutron stars and from accretion disks.

Archive UV high resolution spectra taken with medium size telescopes from moderate altitude sites (Kitt Peak, Calar Alto, Mt. Wilson) are extended to 304-305 nm, indicating that this limit can be currently obtained when an appropriate UV sensitive detector is used (Griffin, 2005). UVES at the VLT reaches 300 nm in its blue arm.

The shortward limit at 280 nm corresponds to the limit where the Sun radiation can be detected. The atmospheric absorption in this region is the major limitation for the observations. It is dominated by two contributions:

- (1) the Rayleigh scattering, dominating at wavelengths longer than about 310 nm;
- (2) the absorption by ozone molecules, at shorter wavelengths.

The Mie scattering due to the aerosols in a clear night, below 380 nm is negligible compared to the Rayleigh scattering and the ozone absorption. The three separated components are plotted in Fig. 1 (Tug et al., 1977) as a function of the wavelength.

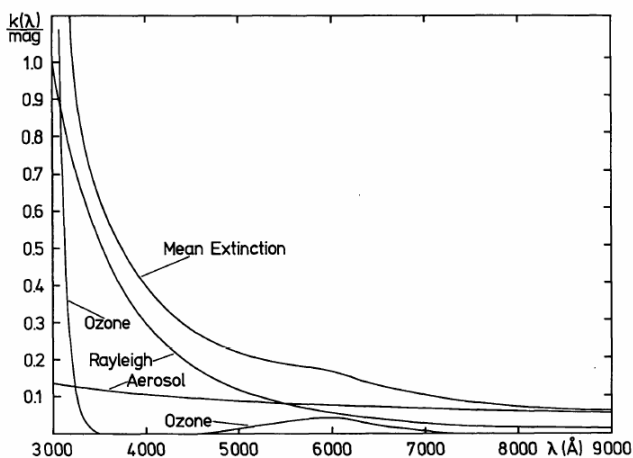


Fig. 1. Mean vertical extinction at Flagstaff, Arizona, in May-June, 1976. The Rayleigh, ozone and aerosol contributions are shown separately (from Tug et al., 1977)

1) The Rayleigh scattering

The Rayleigh scattering is proportional to the number of the molecules of the atmosphere along the optical path. It decreases approximately with the fourth power of the wavelength and, at a fixed wavelength, it decreases with an exponential law of the altitude of the observing site (barometric law), with an average height scale of 7.99 km (Hayes and Latham, 1975), very close to the atmospheric pressure height scale. The absolute value of the Rayleigh optical depth τ_R can be expressed, in a first approximation by the following equation:

$$\tau_R = P(h)/P_0 (0.0086/\lambda^4) \quad (1)$$

(for details see http://fedwww.gsfc.nasa.gov/html/fedmac/opt_thic/opt_thic.html), where $P(h)$ is the local pressure at the height h , P_0 the pressure at the sea level and λ is measured in microns. In a given site it can vary with the local pressure, typically by about 1%. It is evident that the proportion of the Rayleigh scattering contribution to the total extinction, at a given wavelength, depends on the site.

For example, in the U band (mean wavelength $\lambda_0 = 346.4$ nm), the extinction at La Silla calculated by Burki et al. (1995) is 0.61 mag./airmass, with the 82% due to the Rayleigh scattering and 10% to the ozone.

Starting from a contribution of 0.55 mag./airmass extinction at the altitude of La Silla (2400 m), it is easy to calculate a decrease to 0.30 mag./airmass at an altitude of 4400 m, still higher than the 0.06 mag. absorption due to ozone.

In a detailed analysis of the UV transmission from 308 to 382 nm Boulade et al. (private communication, 2002) show that at high altitude sites such as Mauna Kea the UV transmission is from 15 to 20% higher, in the 310 - 330 nm range, than in lower sites such as La Palma (King, 1985), Kitt Peak, Tololo and La Silla, confirming the expected decreasing scattering with the height. Another way to quantify the gain of the UV transmission with the altitude is the wavelength limit corresponding to an extinction of less than 1.0 mag./airmass, which is about 310 nm. The gain in the short wavelength cutoff at 4200m compared to 2400m is about 1.5 nm.

Similar conclusions can be derived from the analysis of the theoretical models published by Nitzschelm (1988), although they predict a systematically lower transmission.

2) The ozone contribution

In the spectral region between 280 and 310-315 nm the atmospheric absorption is dominated by the ozone.

The main atmospheric ozone belt (containing the *stratospheric ozone*) is located at an height between 20 and 50 km. For this reason the ozone absorption is largely independent of the height of a ground based site, provided that the site is above the low altitude inversion layer trapping the man made smog which produces the so called "*tropospheric ozone*" via photodissociation by optical Sun radiation. The ozone content in the atmosphere is measured in Dobson unit where 100 Dobson units correspond to 3 mm of equivalent thickness in a standard atmosphere.

The main ozone absorption band (Hartley band) is extended between about 210 and 330 nm. Weaker features overlap the red side of the Hartley band between 300 and 350 nm (Huggins bands).

The absorption increases at short wavelengths much faster than the Rayleigh scattering, following the Beer law:

$$I = I_0 e^{-K m(O_3)} \quad (2)$$

Where I is the transmitted intensity, I_0 the radiation at the top of the atmosphere, K the absorption coefficient of the ozone and $m(O_3)$ the ozone atmospheric thickness (on average 0.3 cm in the reference standard atmosphere). The coefficient K can be obtained from the literature (Vigroux, 1967, Bass and Paur 1984 or Bird and Riordan, 1984 for on line data). There is a wide literature on the discussion of the K variations with temperature and pressure. Typical values are around 2.5 at 310 nm and 10 at 300 nm.

The corresponding optical thickness ($\tau = 0.3 \times K$ for standard ozone content) at 310 nm is about 0.3 and it increases above 3 at 300 nm and around 36 at 280 nm.

In a first approximation, a reduction of the ozone thickness from 300 to 200 Dobson units corresponds to a transmission increase by a factor 5 at 300 nm (from 1% to 5%) and by two orders of magnitudes at 290 nm (from 5×10^{-3} % to 4×10^{-1} %).

The ozone absorption effect can be also quantified comparing the solar intensity spectrum at the sea level, with the Sun at zenith, at 310 nm, where it is reduced to about 10% of its peak value, while at 300 nm is 2×10^{-1} % and at 290 nm is 10^{-3} % (Mason and Hughens, 2001). At 288 nm it is below 10^{-4} %.

These average values are strictly dependent on the ozone conditions in the stratosphere.

The stratospheric ozone absorption varies up to a factor 2 with latitude and season. The majority of the measurements have been done during daytime, but recent analysis of night time stellar spectra show that the day to night differences should be below 10% in the subtropical sites (Griffin, 2005).

The recent UV measurements available from the Total Ozone Mapping Spectrometer (TOMS) satellites, available on line at: <ftp://jwocky.gsfc.nasa.gov/pub/eptoms/images/global/> give the stratospheric ozone thickness, in Dobson units, covering almost all the Earth, from 1978 to now, from local daily measurements around the local noon in a grid of about 1.1×1.1 degree pixels.

Fig. 2 presents the global distribution of the average monthly total ozone from TOMS Earth Probe and OMI in June 2003 and January 2006. The minimum ozone thickness is located in a strip just below and above the equator respectively, with about 200-220 Dobson units, while it reaches 340-350 Dobson at temperate latitudes, with about a 50% difference. There are other two low ozone regions above Arctica and Antarctica (the so called *ozone hole*, where the ozone thickness can go below 200 Dobson). These two regions are displayed only during their summer seasons.

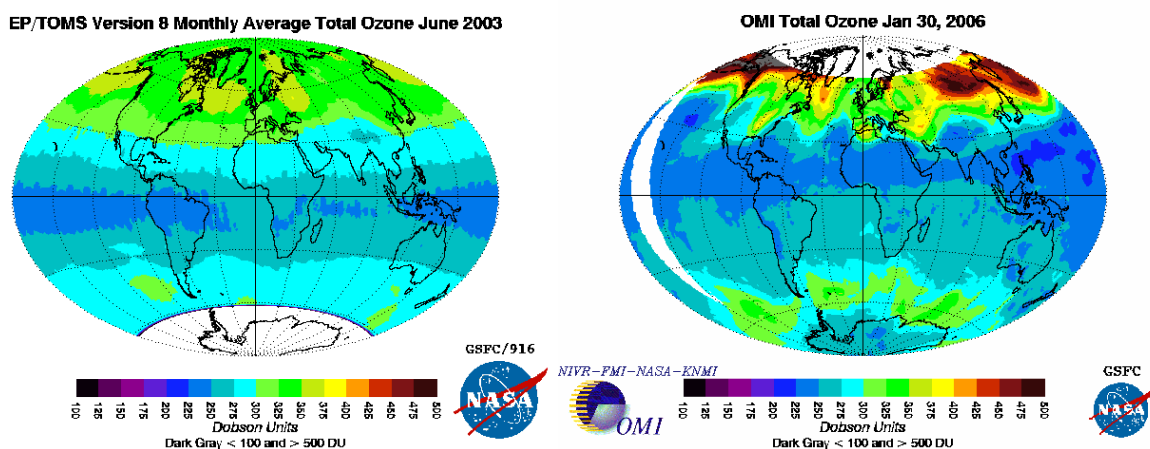


Fig. 2 Stratospheric ozone thickness in June 2003 from Earth Probe/TOMS and January 30, 2006 from OMI/TOMS

As a further example we computed the monthly average tropospheric ozone quantity from about 8000 TOMS data of Nimbus-7 (1978-1993), Meteor-3 (1993-1994) and Earth Probe (1994-2002) satellites, in order to check the potential UV observing conditions at a subtropical site such as Hawaii (Fig. 3). In all the three histograms the peak of the total ozone is below the standard 300 Dobson. The mean value is 270 +/- 20 Dobson.

This is about 10% lower than the standard atmospheric ozone thickness and should allow also a UV cutoff limit shorter by about 2 nm compared to a site with the standard ozone thickness (300 Dobson). The ozone thickness at Hawaii fluctuated, from 1978 until now, with annual median values ranging from about 270 to 290.

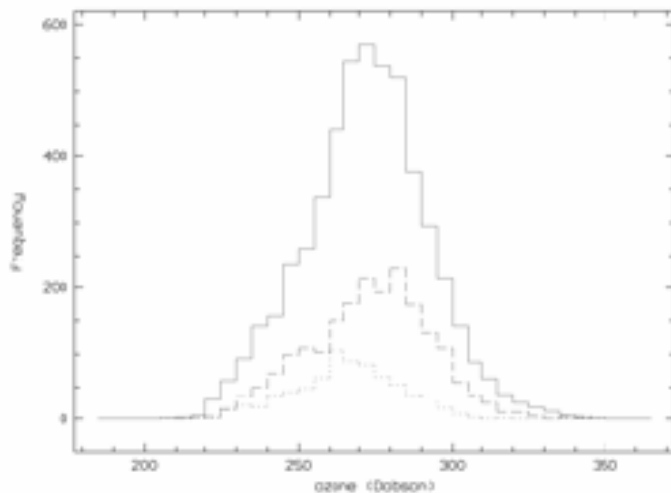


Fig. 3 Distribution of the ozone thickness above Hawaii (continuum line) in the period 1978-1993 from Nimbus-7 data, Meteor-3 (1993-1994) and Earth Probe (1994-2002)

The ozone thickness there shows a well defined seasonal trend with a sharp maximum in mid-April and a minimum in December-January, reaching the lowest values around 250 Dobson (Fig. 4).

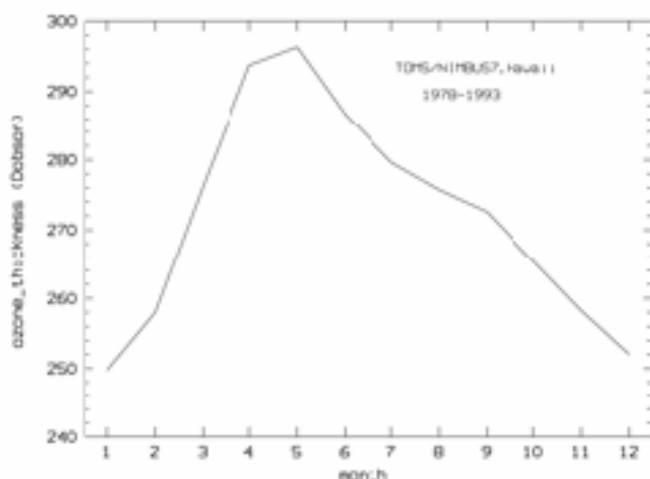


Fig.4. Mean monthly ozone total thickness at Hawaii from TOMS/NIMBUS7 in the period 1978-1993.

The secular decrease of the total ozone thickness above Dome C, in Antarctica, is shown in Fig.5.

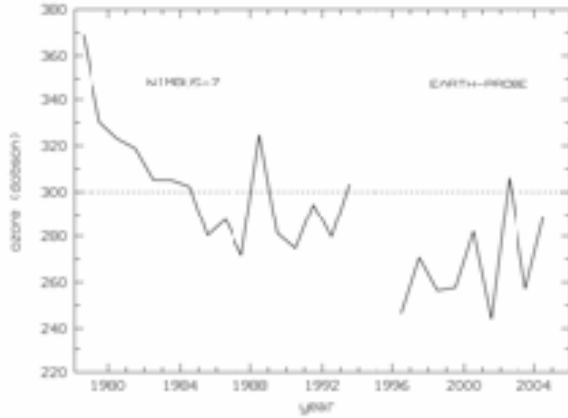


Fig. 5. Yearly mean values of the total ozone thickness at Dome C from 1978 to 2005 from TOMS Nimbus7 and Earth Probe satellites. Only daytime (summer) yearly averages are computed.

Conclusions

From the above analysis it is clear that a large telescope can realistically investigate in the UV range between 300 and 380 nm, but in some conditions the possibility to collect data near 280 nm could be investigated.

From the combined effect of the Rayleigh scattering and the ozone absorption there is a clear gain of the UV transmission with the height in the interval 310 to 380 nm. The effect of the height and a variable total ozone content from 300 to 270 Dobson is shown in Tab. 1 where the data are calculated from a simple model based on the equations (1) and (2) and compared to Boulade et al. (2003) measurements[†].

TABLE 1: calculated values of the optical depth due to Raileigh scattering at the sea level, at 4200m height, ozone optical depth, total optical depth, transmission (TR), transmission measured at Mauna Kea, transmission calculated at 4200m, transmission calculated at 4200m with 270 Dobson

Wavelength nm	τ_R	$\tau_R(4200m)$	KO_3	τ_{O_3}	τ_{tot}	TR (%)	TR (MK)	TR (4200m)	TR(4200m,270D)
330	.72	.43	0.09	0.03	0.75	47%	59%	59%	59%
310	.93	.56	2.5	0.75	1.68	19%	29%	27%	29%
308	.95	.57	3.45	1.03	1.99	14%	24%	20%	22%
300	1.06	.64	10.6	3.18	4.2	1.5%	-	2.2%	2.9%
290	1.21	0.72	29.0	8.7	9.9	5x10-3%	-	5x10-3%	0.02%
280	1.4	0.84	120	36	37.4	6x10-15%	-	-	2x10-13%

The height is also important to reduce the effects of differential refraction.

[†] It may be interesting to derive the equivalent diameter of a telescope outside the atmosphere from the data in the last column. Assuming a 50m ELT, the respective equivalent diameters would be: 38m (330), 27m (310), 23m (308), 8.5m (300), 71cm (290, comparable to the 42cm IUE), 2 μ m [!] (280).

Below 310 nm the difference with the height decreases because of the prevailing effect of the ozone. Specific studies on the variability of the ozone thickness above selected locations must be investigated because of its large variations with latitude and season.

In summary the main site quality requirements for UV observations can be prioritized in the following points:

- 1) height above the sea level (low local pressure);
- 2) low stratospheric ozone content (equatorial-subtropical sites or polar regions).

Other obvious parameters are the seeing and the fraction of clear nights.

Acknowledgements

We acknowledge NASA/GSFC TOMS Group for the use of TOMS data.

We are very grateful to Danielle Alloin for suggestions.

References

- Bass, A.M., Paur, M.J., 1984, in Atmospheric Ozone, ed. C.S. Zerefos and A. Ghazi (Dordrecht: Reidel), 606
- Bessell, M.S., 1990, UBVRI passbands, Publ. of Astronomical Soc. of Pacific, 102, 1181.
- Bird, R., Riordan, C., 1984, data on line at <http://rredc.nrel.gov/solar/pubs/spectral/model/t2-1.html>
- Boulade, O., Alloin D., Alonso M., Vigroux L., 2002, The extinction curve and night sky properties at Mauna Kea, from 308 to 382 nm, private communication.
- Burki, G., Rufener, F., Burnet, M., Richard, C., Blecha, A., Bratschi, P., 1995, A&AS, 112, 383
- Griffin, R.E., 2005, PASP, 117, 885
- King, D.L., 1985, RGO/La Palma technical note n. 31
- Mason, N., Hughens, P., 2001, Introduction to Environmental Physics, Taylor & Francis, London and New York, p. 217.
- Nitschelm, C., 1988, A&AS, 74, 67
- Thuan T.X., Gunn J.E., 1976, A new four-color intermediate band photometric system, Publ. of Astronomical Soc. of Pacific, 88, 543.
- Tug, H., White, N.M., Lockwood, G.W., 1977, A.&A., 61, 679
- Vigroux, E., 1967, Ann. Phys. B, 2, 209.

SITE REQUIREMENTS FOR QUANTEYE AT ELT

1 - Introduction

QuantEYE is an instrument conceived for extremely high time resolution, with a scale between 10^{-9} to 10^{-2} seconds. Oscillations in neutron stars (for example in the Crab pulsar) and the quantum photon bunching (for example from optical laser emission lines) are typical applications. While the latter requires a specific narrow band wavelength range, the former can include the full spectral range offered by the combination of the instrumentation and the atmosphere with the advantage to get more photons. The device is based on photon-counting avalanche photodiode detectors with a sensitivity extended from 400 to 1000 nm, but some companies are studying high speed devices in the near IR as well.

2 - Main Requirements

The need for a high number of photons and for stability at high frequencies are the main requirements for this instrument. However lower frequency modulations should be kept under control in order to minimize the noise, even if, in principle, they could be efficiently canceled using simultaneous observations with a reference star. Furthermore higher frequency harmonics and non linear propagations in the telescope should be kept under strict control.

The seeing should not affect the observations at very high frequencies, but again the residual noise can affect measurements when very high accuracy is requested. The seeing at relatively high frequency have been recently studied by Dravins and collaborators from scintillation measurements (1997, PASP, 109, 173). They found a sharp cutoff around 300 microseconds (about 3 KHz), consistent with the motion of 3 mm cells at 10 m/s (Fig.1).

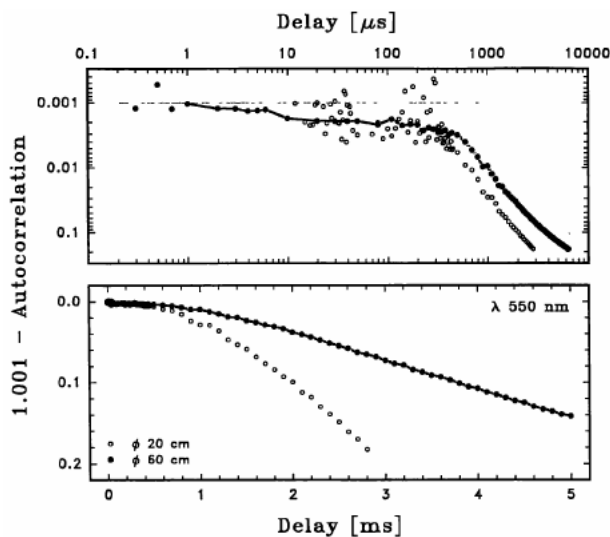


Fig. 1. Autocorrelation function of the stellar scintillation on very short time scales. The apparent break in the curves at 300 μ s may be connected to the inner scale of the atmospheric turbulence (from Dravins et al., 1997).

This spatial scale corresponds to the lower scale of the Kolmogorof cascade (Reynolds limit) in the free atmosphere. Higher frequencies have been found only in peculiar situations where the flow speed is substantially higher (for examples from airplane observations at 200-300 m/s). The same authors suggest also the possibility that high frequency components could be originated near the telescope (at about 15 m). This means that "a very good local telescope environment would be

required in order to depress the most rapid scintillation components". The noise from the scintillation itself should be as well considered. Since the effect increases with the distance of the perturbation layer from the pupil, sites with optical turbulence located near the ground (for example on the Antarctic Plateau) should be preferred (Dravins et al., 1998, PASP, 110, 610).

The frequency range of these observations, however, is some orders of magnitude lower than the planned QuantEYE performances, and further studies in the MHz frequency domain, as those planned by Barbieri and Dravins group in the next two years, are needed in order to quantify the real impact of the atmospheric effects on the performances of the instrument. It is not yet clear if high frequency components from the adaptive optics corrections can introduce some noise. QuantEYE observations "per se" do not need adaptive optics, given that the pupil image falls inside the aperture of the detector. A moderate seeing, around 0.7", is acceptable. Other high frequency noise sources should be taken into consideration, for example the wind shaking, microseismicity and thermal oscillations. A very clean electrical environment is also an important requirement.

Finally the sky coverage must be considered with high priority. The instrument primary need for a high number of photons requires relatively bright sources, which are sparse in the sky. Neutron stars, for example, are located preferentially around the galactic plane, but spread at all the declinations, including the southern and northern sky. The same for peculiar massive stars with strong emission lines.

For example the pulsar Crab is at RA 5h 34m, DEC +22 and Eta Carinae RA 10h 45m and DEC -59.

Given the importance of this aspect and the impact of the sky coverage needs on the site selection we suggest an immediate, dedicated study, in order to get quantitative data on the number and distribution of the observable targets on the sky.

3-Conclusions

In summary the main site parameter requirements can be ranked as following:

- 1) Very high sky coverage in declination (equatorial sites are better);
- 2) Seeing stability, low scintillation;
- 3) Low seismicity;
- 4) Low wind;
- 5) Low thermal gradients (in time and space);
- 5) Clean electrical environment;
- 6) Number of clear nights and stability of the sky;
- 7) High atmospheric transmission in the optical and near IR.

We suggest a urgent study of the target distribution on the sky, and a statistical analysis of the high frequency noise introduced by the seeing, mechanical parts of the telescope and adaptive optics.

ELT Site Evaluation Working Group (WG-3)

CODEX: science case and relevant site parameters

Gautier Mathys

CODEX (COsmic Dynamics EXperiment) is the name given to the high-resolution visible spectrograph whose concept has been studied by ESO and associated institutes (IoA in Cambridge, Observatoire de Genève, and INAF – Osservatorio de Trieste) in the framework of the OWL Observatory Concept Study.

Its primary scientific objective is to perform for the first time a direct dynamical measurement of the acceleration of the Universe. Other high priority scientific issues that should be addressed with such an instrument and that have been discussed in some detail are the possible variability of physical constants with time, the discovery and follow-up of exoplanets, especially earthmass planets in habitable zones around other stars, and the abundances of the elements produced in the Big Bang. Other interesting topics for which this instrument will be suitable include asteroseismology, cosmochronometers, first stars, temperature evolution of the cosmic microwave background, chemical evolution of the intergalactic medium, etc.

In order to achieve the primary scientific objective, a spectral resolving power of 150000 is needed. The wavelength domain of interest ranges from 400 to 680 nm; an extension towards the blue would add some information, but it may not be justified in view of the technical difficulties that it would involve. The intended characteristics can be achieved for a set of cross-dispersed echelle spectrographs of reasonable size working in seeing-limited regime. To achieve the primary scientific objective, a radial velocity accuracy of 1 cm s^{-1} must be achieved over 10 years. Stability is therefore paramount to the success of the experiment, and also essential for most other considered science cases. For achievement of the RV accuracy aimed at, the analysed spectra must have a S/N ratio of the order of $1-2 \cdot 10^4$. In other words, the photon noise limit must be reached. This is true not only for the primary scientific objective, but also for most of the other science objectives that have been considered.

The implications for the site selection are as follows:

- Seismic activity may jeopardise the mechanical stability of the instrument and the stability of the optical beam feeding it (especially if it has to be done through a long, multiple mirror coudé train, as seems likely), or at least it may make this stability considerably more complicated and expensive to achieve.
- Seeing constraints result from various considerations:
 - Minimising photon losses (“slit losses”) in seeing-limited observations with an entrance aperture of the order or 1 arcsec (depending on telescope diameter) does not set particularly stringent constraints on the image

quality of the site: the median seeing of most good modern observatory sites is compatible with this requirement.

- Seeing-dependent contamination of the target spectrum by faint objects close to the scientific target limits the achievable RV accuracy. For a given contaminator brightness, the better the seeing, the closer the contaminator can be to the science target without significantly degrading the determined radial velocity. Conversely, at a given distance, maximum contaminator brightness that can be tolerated increases with improving seeing. This does not set a very stringent constraint on the seeing either: at seeing of 1.5", contaminating sources at distances exceeding 2.5" should have no significant detrimental effect, independent of the magnitude difference with the science target. Again the median seeing conditions of most good modern observatory sites are generally sufficient to deal with the vast majority of plausible target configurations.
- However, under the assumption that the instrument can only be seeing-limited (because adaptive optics corrections appear unfeasible in the wavelength range that it covers), excellent seeing would allow one to build a smaller, more compact instrument, and exposure times for individual frames to be shorter. These factors would in turn allow one to have better control of the stability of the parameters critically affecting the achievement of the ultimate RV accuracy.
- Excellent sky transparency is critical to avoid contamination of the science target spectra by diffuse light (e.g. from the Moon) reflected by clouds. Of course it also benefits to maximisation of the photon collection rate.
- Spectrum contamination by telluric sky lines also limits the achievable radial velocity accuracy; spectral regions containing such lines probably need to be rejected in the analysis. Sites where the number and intensity of such lines is lower are better in this respect; in particular, low water vapour content of the atmosphere is beneficial. Quantitative evaluation of the effect would require complex numerical modelling that vastly exceeds the framework of the current assessment. If deemed necessary for final decision on site selection, a dedicated project to study this effect should be initiated, and the corresponding resources should be identified and assigned.
- Low level of light pollution is, of course, also important. More generally, a low level of diffuse light is essential, especially as far as light whose spectrum contains high-frequency features.
- Variability of the atmospheric conditions is detrimental in several respects.
 - Although their impact can be limited by optimisation of the optical design of the instrument, seeing variations can introduce variations of the illumination geometry leading to systematic errors in the radial velocity determinations.
 - In case contamination by neighbouring sources is relevant, it also varies with the seeing.
 - Transparency variations can lead to guiding errors, which in turn affect the spectrograph illumination geometry.

- Transparency variations also introduce variability in the contamination of the target spectra by e.g. reflected Moonlight.
- Furthermore, transparency and seeing variations affect the precise determination of the effective time of mid-exposure (i.e., the time at which half the total number of photons have been collected), which is critical for calculation of the barycentric radial velocity correction. It is unclear that monitoring of these variations during the exposure (e.g. diverting a small fraction of the scientific target light towards an auxiliary photometer) can be sufficient to achieve the 1 cm s^{-1} accuracy level.
- Matching of the flux of the reference source used for wavelength calibration with that of the scientific target, which is required for achievement of the ultimate RV precision, is made considerably more complicated when the sky transparency is variable during the observation.
- The intensity and wavelength variability of the atmospheric emission and absorption lines can make the affected regions of the target spectra scientifically unusable.
- The uncertainty of the Earth's rotation velocity is one of the main limiting factors on the achievable precision of the RV determinations. The absolute value of this uncertainty diminishes with increasing latitude of the observatory site. Incidentally, high-latitude sites (specifically, within the polar circles) would also be interesting for certain types of observations for which continuous time series are useful, such as asteroseismology. However, this is irrelevant for the primary scientific goals, with the possible exception of exoplanet studies in some cases.

Based on this analysis, the relevant site parameters for an ELT high-resolution spectrograph in the optical range can be classified as follows:

- **Critical:**
 - Stability of atmospheric conditions on timescales comparable to the duration of the scientific exposures (order of magnitude: hour)
- **Important:**
 - Low or (preferably) no seismicity
 - Excellent sky transparency
 - Low high frequency sky brightness (sky emission lines)
 - Low high frequency diffuse light
 - Low humidity
 - Low light pollution
 - Good seeing (exact value depends on telescope size, but order of magnitude of median seeing should be about $0.7''$). However the gain in instrument size and exposure times for individual frames that would be achievable in a site with excellent seeing would considerably ease the achievement of the critical constraint of instrumental and atmospheric stability.
- **Desirable:**
 - High geographic latitude

Note on EPICS science and site requirements

Vincent Coudé du Foresto*

16 février 2006

1 Introduction

EPICS is a focal plane coronagraph being considered for ESO's future extremely large telescope and whose conceptual study can be found as part of the OWL Blue Book (see OWL-CSR-ESO-00000-0166). Its main application is for exoplanet imaging/spectropolarimetry and its definition is driven by two objectives :

- The detection and spectro-polarimetric characterization of telluric exoplanets around nearby stars, with the possibility to discover habitable exoplanets (*primary science objective*);
- The detection and characterization of cold gas giant planets in a late evolutionary stage (*secondary science objective*).

The observational challenge resulting from these goals is best summarized by the properties of two planets from our solar system as seen from 20 pc :

- Earth : $m_v=30.6$, planet/star brightness ratio 2×10^{-10} , angular separation 50 mas;
- Jupiter : $m_v=28.8$, planet/star brightness ratio 10^{-9} , angular separation 250 mas.

It is expected that these detectivity levels can be achieved only after extensive use of differential point source extraction techniques after the starlight has been rejected. The operating wavelength range is 0.6–1.7 μm , divided among four channels, three of which are for science :

- A polarimetric differential imager in the R band;
- A spectrometric differential imager in the J band;
- An integral field spectrograph in the H band;
- A wavefront sensor in the I band.

The difficulty of the observations results more in the dynamic range that is required than in the angular separation (the diffraction limit λ/D of a 20 m telescope is 6 mas at $\lambda = 0.6 \mu\text{m}$). The general system requirements call for an intrinsic coronagraph performance of better than 10^{-9} for separations larger than $10\lambda/D$, which includes a drastic control of telescope diffraction effects

*Observatoire de Paris

(segments and gaps) to the 10^{-9} level, as well as static errors across the pupil (0.3 nm rms on the 10–75 cycles/pupil frequency range).

Because of the of the high Strehl ratios (>90 %) that are required to maintain the halo at an acceptable level within 0.03 – 2 arcsec of the central source, adaptive optics is one of the major and most critical components of EPICS. Due to limitations in (even extrapolated) computing power, it is anticipated that the XAO system for EPICS will be based on two stages : a first system is an extrapolation of the VLT-PF concept with a classical Shack-Hartmann controlling a 1.7×10^5 actuators system at 1 kHz. A second system in cascade with the first one is based on 1.5×10^4 actuators controlled at 3 kHz with a Pyramid sensor.

2 EPICS science

The primary science objectives of EPICS are very similar to those of the DARWIN space mission (census and characterization of habitable earth-like planets in the nearby 25 pc) under consideration by ESA. The complementarity resides in the spectral domain considered (0.6–1.7 μm for EPICS, 6–18 μm for DARWIN), which drives the physics accessible for the main targets :

- EPICS will detect the light reflected by the planet, which depends on many aspects of the planetary surface, such as the albedo, phase effects, Rayleigh diffusion, seasonal effects etc. . .
- DARWIN will detect the thermal light emitted by the planet, which gives access to the thermal properties of the atmosphere (inertia, circulation) and also to a clear set of biomarkers (the $\text{O}_3/\text{H}_2\text{O}/\text{CO}_2$ criterion).

Still, because of the very strong commonality of objectives between the two programs, their similar time frames (2020) and political contexts (European), it is important to articulate both projects while they are being defined in order to avoid undue competition. More specifically, common sense suggests that whatever can be done from the ground *should* be done from the ground. This may be the case of the detection of habitable telluric planets in the solar vicinity. A ground-based detection would provide a strong impetus to a space spectroscopic mission, which would be relieved from time-extensive survey part of its program to be able concentrate, for specified planetary targets, on the more challenging task that represents the detection of biological markers.

Therefore if the feasibility of nearby exoearths detection with a ground based coronagraph can be established, this would provide a compelling science case for an EPICS-like instrument attached to a ground-based ELT, but also impose strict dimensionning constraints and specifications. Conversely, if the primary science objective is out of reach, a “best effort” approach could be acceptable for the achievement of the secondary goals (Jupiter-like planets detection).

3 Site requirements

3.1 Critical characteristics

The methodology followed to establish the site requirements is to start from the list of major risk areas that could be potential show stoppers for the most demanding science goal, as identified in the EPICS concept study, and review how they are impacted by the site.

3.1.1 High density deformable mirror

The density of actuators is related to the width of the correction zone. In the case of OWL more than 10^5 actuators are expected for the deformable mirror. All things else being equal, the number of actuators scales as D^2 . This favors sites for which an equivalent performance can be obtained with a smaller telescope diameter.

3.1.2 Computing power

The computing power required for AO scales somewhere between $\tau_0(D/r_0)^2$ and $\tau_0(D/r_0)^4$, depending on the algorithms used for wavefront reconstruction (from fully diagonal to full matrix). A site with a longer coherence time or seeing cell size will therefore be favored.

3.1.3 Coronagraph (complex Lyot stop for segmentation effects rejection)

This risk increases with the number of segments in the pupil, which is linked to the size of the pupil. Therefore a site that can provide an equivalent SNR with a smaller telescope diameter would reduce the risk.

3.1.4 Tight error budget

Some key optical elements need nanometric or subnanometric precision and/or stability. No impact of the site selection is foreseen here.

3.1.5 Atmospheric dispersion compensation

Adaptive atmospheric dispersion compensation is needed as upstream as possible to avoid chromatic beam shifts. A low water vapor content is preferred in the atmosphere to reduce the amplitude of the atmospheric dispersion compensation.

3.1.6 Telescope stability, wind effects

Telescope should be atmospheric limited with respect to wind shake effects. A site with lower surface wind speeds is therefore preferred.

3.1.7 Scattering by dust particles

The scattering by dust particles must not degrade the goal contrast. A clean site is therefore to be preferred.

3.1.8 CCD flat fielding

CCD flat fielding must be done accurately enough to not degrade the goal contrast. No impact of the site selection is foreseen here.

3.1.9 Pyramid WFS

Risk associated with a non mature technology. No impact of the site selection is foreseen here.

3.1.10 Focal plane WFS

Risk associated with the complexity of the focal plane wavefront sensor, which scales as D^2/r_0^2 . This favors sites with the highest r_0 or those for which an equivalent performance can be obtained with a smaller telescope diameter.

3.1.11 Differential imager

Cross-talk, diffraction effects must not degrade the goal contrast. No impact of the site selection is foreseen here.

3.1.12 Differential polarimeter

Differential errors must not degrade the goal contrast. No impact of the site selection is foreseen here.

3.2 Other (non critical) characteristics

A *small external scale* for the turbulence would help reduce the excursion of the adaptive optics actuators. *Long coherence times* are crucial to increase the number of photons available for wavefront correction (and, ultimately, the wavefront residual errors). On the other hand, because the correction is to be performed for a bright source on-axis, the isoplanetic angle is of little relevance to the performance of the instrument.

Sky brightness (diffusion, emission, aurorae, light pollution) should be lower than the level of residual halo in the beam étendue corresponding to a point source detection (λ^2). The possibility to perform continuous *very long integration times* (>10 hours) may be an asset to relax stability requirements while building up SNR in the most extreme cases. A *dry atmosphere* is required if H₂O and O₂ spectroscopic detection is sought. Access to the same sources as the DARWIN space mission may be an asset if a synergy between the two programmes is articulated.

4 Conclusion

EPICS has two science objectives with requirements of a different nature, and the site selection will have a different impact depending on the chosen scenario for the instrument. An evaluation for EPICS should therefore first establish which sites (if any) enable the detection of habitable telluric exoplanets. If it turns out that no ground-based site can meet the requirements for this primary science objective, then the weight on the parameters that are most responsible for the performance of an EPICS-like instrument can be somewhat relaxed.

This being said, the most important site parameters to take into account are :

- Seeing : large size of the coherence cells, and as important, slow evolution times
- Low atmospheric water vapor content
- Low surface winds
- Clean (non dusty) local environment

ELT Atmospheric Parameters between 1 – 1000 μm

R. Siebenmorgen & H.U. Käufel (ESO)

Draft 30.01.06

1 Introduction

The main deleterious effects of the Earth atmosphere on astronomy consist of reduced transparency by photons, degradation of image quality and increase of diffuse background.

In the near IR the principle source of atmospheric background during the night is airglow. Airglow results from transitions between vibrational states of OH^- radical, which discharge energy stored during daytime from solar radiation through dissociation of ozone ($\text{H} + \text{O}_3 \rightarrow \text{O}_2 + \text{OH}^*$). Airglow originates at heights of 70 – 90km and affects all ground based locations.

Molecules in the atmosphere are responsible for absorption bands for cosmic radiation. In such bands the atmosphere becomes opaque and a maximum background flux is reached: cosmic photons cannot penetrate. Redwood of $2\mu\text{m}$ thermal emission by lines (Kirchhoff law) becomes more important than airglow. For spectral regions of partial transparency and opacity produced near ground layers the background can be approximated to first order by a blackbody attenuated by a factor which is related to the transparency. The effective temperature of most relevant atmospheric layers is in the 200 – 300K range so that the atmospheric thermal emission peaks near $12\mu\text{m}$. The atmospheric transparency between 1 – 1000 μm is dominated by water absorption followed by other molecules such as: O_3 , CO_2 , N_xO_y or CH_4 .

In Fig. 1 the zenith optical thickness spectrum for wavelengths $\geq 4\mu\text{m}$ is shown. One notices the overall dominance of H_2O but also sees that CO_2 is the major absorber at $4.2\mu\text{m}$ and 13 to $17\mu\text{m}$. Interestingly there is a local minimum of the optical thickness of water in the N band near $10\mu\text{m}$ where ozone absorption with a peak at $9.5\mu\text{m}$ dominates. Another disturbing effect of the atmospheric absorption is the fact that water concentration can be highly variable and on timescale of several minutes.

Nevertheless as argued in the following sections the 1 ~ 1000 μm atmospheric opacity and emissivity can be minimized by placing observatories at dry and cold sites. Such sites are generally located at high ($\sim 5\text{km}$) altitudes.

2 Radiosonde data

Atmospheric opacities are measured with automated tipping radiometers at 225GHz and 183GHz, 1.3mm and 1.6mm, respectively or sky dips. They give estimates of the precipitable amount of water vapor (PWV) above the radiometer location. Radiosonde data from balloon launches provide vertical profiles of atmospheric parameters such as the temperature, pressure, relative humidity and wind (speed and direction). This allows estimates of the distribution of water vapor concentration with height.

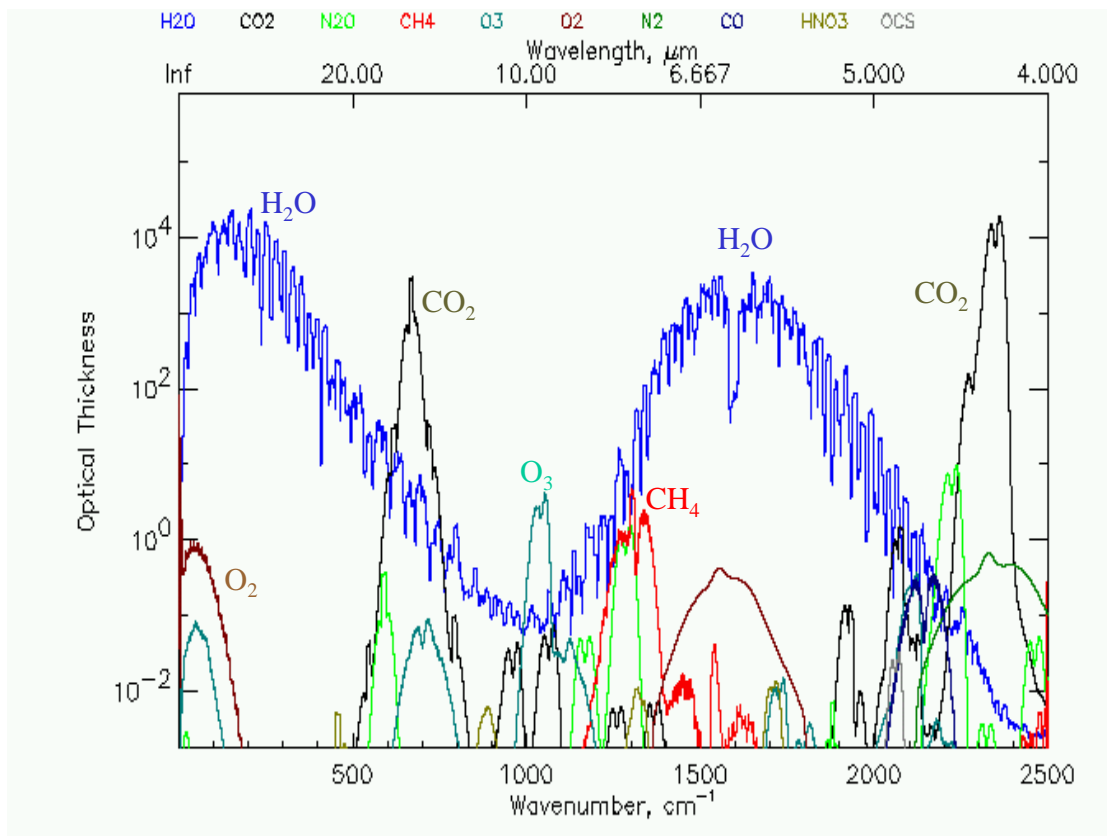


Figure 1: Zenith optical thickness spectrum of the atmosphere showing absorption features of each molecule. Spectra are calculated using the RFM line-by-line model with HITRAN line data and US Standard Atmosphere absorber profiles.

Adopted from: <http://www-atm.physics.ox.ac.uk/group/mipas/atlas/>

For example more than 100 radiosonde data over the Atacama desert were analysed by Giovanni et al. (2001). They show:

- conspicuous seasonal variations in PWV. During the 'Bolivian winter', January and February, PWV is about twice as large than median values and from April to November 30% lower.
- Diurnal cycles also effects the PWV to within variations of 20%. Such changes are phase lagged to about 4h behind that of sunlight: minimum PWV between midnight to noon and maximum PWV at sunset.
- Typically PWV height distribution is close to be exponential. But when temperature inversions occur the water vapor distribution departs quite severely from an exponential shape.

Temperature inversions impact not only the PWV and thus the transparency of a site but also the quality of astronomical seeing. In layers with temperature inversions the refractive index structure constant is increased and therefore the seeing disk of point source images (Hufnagel 1978). Hence observatory sites above inversion layers would not only yield lower PWV but also much better astronomical image quality at all wavelengths.

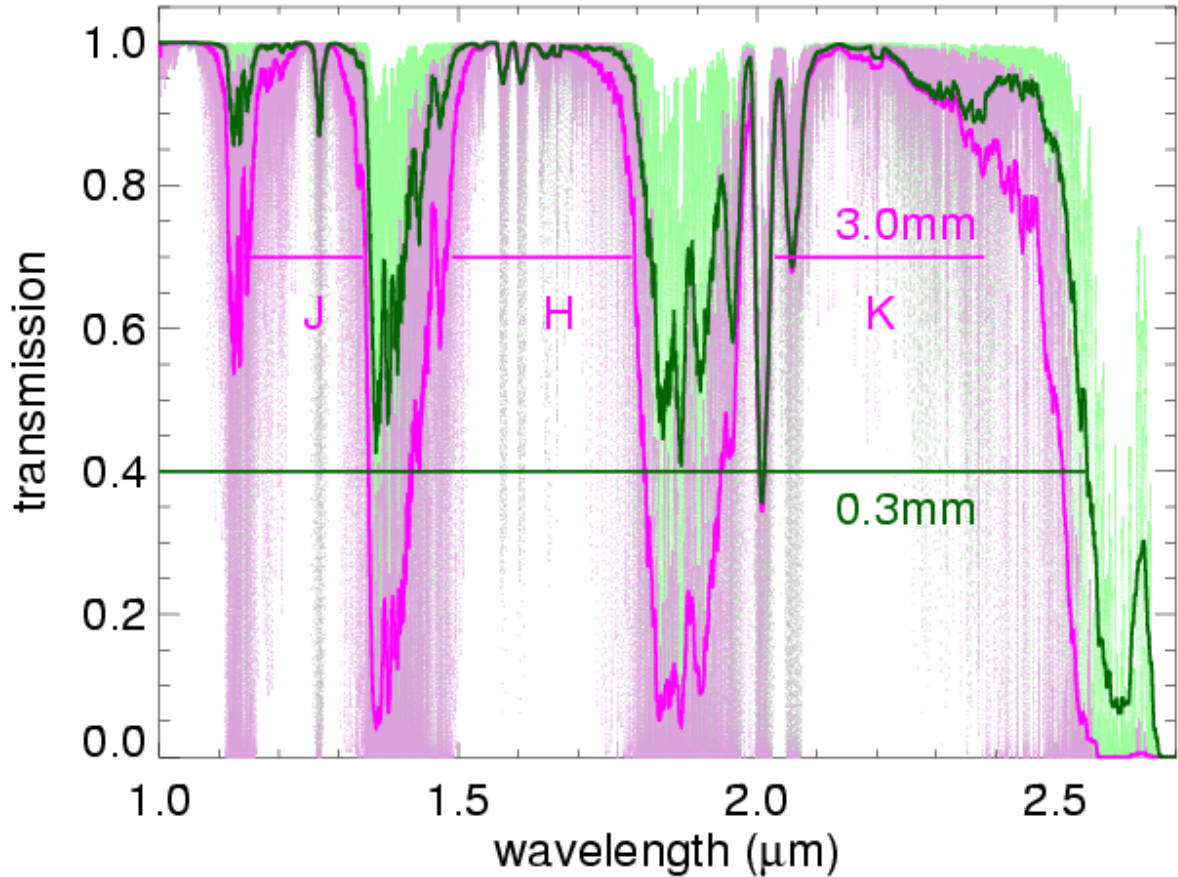


Figure 2: The atmospheric transparency between 1 – 2.7 μm computed with HITRAN line data and US Standard Atmosphere for a zenith angle of 45° and precipitable water vapor (PWV) of 0.3mm (green, ALMA site) and 3mm (red, Paranal site). Shaded areas are calculated at spectral resolution of $R = 100,000$ while full lines are for $R \sim 250$. For both sites the wavelengths regions where the transparency exceeds 40%, so where ground based observations are possible, are indicated by horizontal lines .

3 Atmospheric transparency

The atmospheric transparency between 1 – 25 μm is calculated with HITRAN line data and US Standard Atmosphere for a zenith angle of 45° and precipitable water vapor (PWV) of 0.3mm and 3mm. A PWV of 3mm is quoted for Paranal. From 108 radiosondes at Atacama, Giovanelli et al. (2001) found PWV of 0.3mm within the 25% quartiles during night and 5 – 13 UT hours for 5400m and during day time for 5750m altitude. Such low PWV is slightly compensated using an airmass of 1.4 in the computations. Results are shown for J,H,K (Fig.2) and L,M and N,Q bands (Fig.3).

The complete NIR atmospheric window from 1 – 2.55 μm is opening up for ground based observations at high and dry sites: Observations in between the standard J, H, K atmospheric windows become feasible (Fig.2). An example of continuous 1 – 2.55 μm spectroscopy of stars performed from Mauna Kea site under good conditions is published by Jones et al. (1994, MNRAS 267,413).

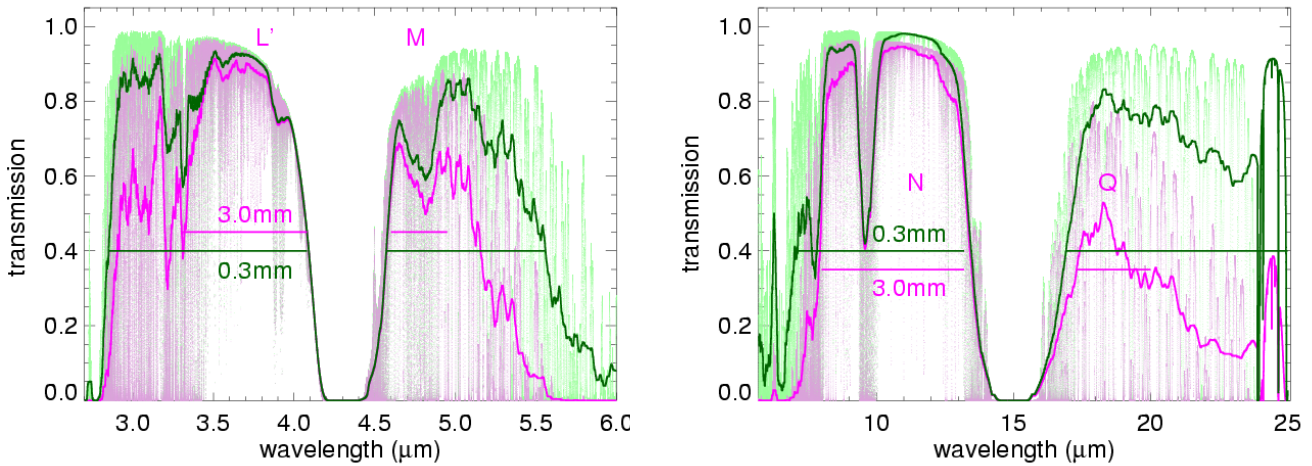


Figure 3: As Fig.2 but for L,M (left) and N,Q bands (right) .

Similar trends can be seen in the L and M band (Fig.3): From a high and dry site observations in the L band become possible below $3\mu\text{m}$ which is of particular importance for measuring water ice bands from astronomical dust. The M band at high and dry sites has much higher overall transmission and extends to longer wavelengths. The site and its humidity will ultimately be the decisive factor whether an ELT is competitive or exceeds the JWST in the $3\mu\text{m}$ range. A higher site is also beneficial for CH_4 as the opacity and the pressure broadening become more favorable. This holds also for the N band (Fig.3): higher overall transmission and extend of the window down to shorter wavelengths when compared to less dry sites. The later is of interest as observations of the $7.7\mu\text{m}$ PAH band become possible at high altitudes. Although between $7.6 - 8.0\mu\text{m}$ telluric absorption by methane may become as important as water. One also notices that the reduced transmission within the $9.55\mu\text{m}$ ozone feature is independent on PWV which is true for any ground based observatory. Finally the Q band is strongly effected by PWV of the observatory site. In the far IR and longword of $25\mu\text{m}$ numerous atmospheric windows appear for $\text{PWV} \leq 0.5\text{mm}$, beside others, notably near 32, 34, 38, 42 and $46\mu\text{m}$.

In the submillimeter results are shown for PWV of 0.2, 0.5 and 1mm (Fig.4). They correspond to best and median atmospheric conditions at the ALMA site and Mauna Kea, respectively. The ALMA site has close to 100% transmission at $\sim 1\text{mm}$. A strong rise of more than a factor two of the transmission in the 350 and $450\mu\text{m}$ atmospheric windows is noted when Atacama is compared with Mauna Kea. Strikingly also at 290 , 240 and $200\mu\text{m}$ new atmospheric windows open up. Those have under best ALMA conditions higher transmission than Mauna Kea in the standard submm windows at 350 and $450\mu\text{m}$. Matsushita et al. (1999) estimated that for about half a winter season and $\text{PWV} \leq 1\text{mm}$ such FIR windows may become already open from the "Pampa la Bola" site located 4800m above sea level, 7km apart from ALMA at Chajnantor.

The influence of PWV on the submm sensitivity limit for observations at airmass 1.2 at an ELT with 50m diameter is given in the table below. For comparison the point source sensitivity of ALMA at $450\mu\text{m}$ is about $2.5\text{mJy}/10\sigma/1\text{h}$ so a factor 5 less sensitive than is possible with ELT. The Herschel Space Observatory which will operate in the FIR/submm will be confusion limited already at $\sim 40\text{mJy}$ at $450\mu\text{m}$.

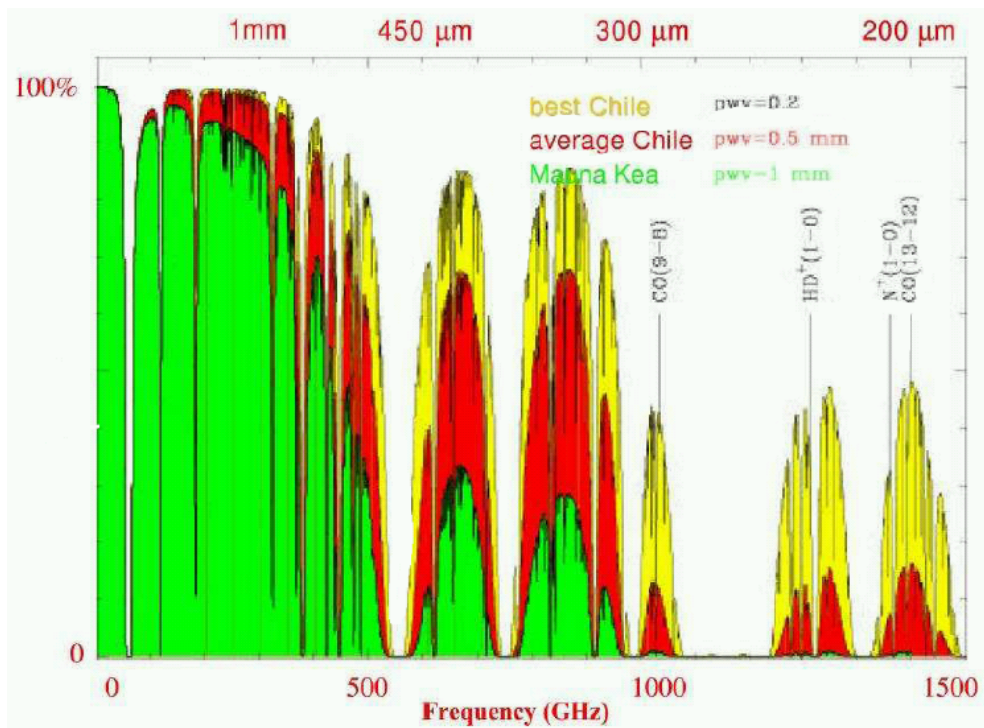


Figure 4: Atmospheric transmission in the submm for PWV = 0.2, 0.5 and 1mm.

Estimated sensitivities of SCEL T as a function of precipitable water vapour.

(NB: these sensitivities are for a perfect 50m telescope at airmass 1.2)

PWV content (mm)	Optical depth at zenith at 225GHz	Sensitivity ¹ 850 μ m	Sensitivity ¹ 450 μ m	Sensitivity ¹ 350 μ m	Sensitivity ^{1,2} 200 μ m
0.3mm	$\tau_{225}=0.02$	0.19	0.32	0.52	1.6
0.5mm	$\tau_{225}=0.03$	0.2	0.44	0.72	4.4
1mm	$\tau_{225}=0.06$	0.24	0.92	1.7	64
2mm	$\tau_{225}=0.1$	0.32	2.0	8	12000
4mm	$\tau_{225}=0.19$	0.6	80	19	>>

Notes:

- 1) sensitivity is 10σ 1hr, in mJy, in 1 beam
- 2) 200 μ m sensitivity is uncertain
- 3) Green is good, yellow is acceptable, and red is poor!

Courtesy of B. Dent.

4 MIR site stability

Short time fluctuations of the atmosphere are studied with ESO's mid infrared instruments (Käufl et al. 1991) in the so called burst mode. In those observations for example sky exposures are taken with detector integration time (DIT) of several msec over a period of ~ 3 minutes. The total exposure time is limited by the memory of the instrument work station. The signal is then analysed in Fourier space. The power spectrum allows separation of artifacts from instrument, atmosphere and the $1/f$ noise. Such observations can be performed in spectroscopy resulting in a two dimensional distribution of the power spectrum with frequency of the noise components and observing wavelengths as axes. One example is given in Fig.5 where ~ 2000 N band ($7.7 - 13.3\mu\text{m}$) spectroscopic images are taken with DIT of 10msec for two airmass of 1 and 1.6 with the TIMMI2 instrument mounted on the 3.6m at La Silla (courtesy of M. Sterzik). The measurements sample frequencies of the noise components between $0.1 - 50\text{Hz}$. One notices that the amplitude of the power spectrum is correlated with atmospheric molecular absorption bands. Also in the N band water is often the most dominating absorber. Example of water features are at $7.9, 8.3, 8.5, 11.76\mu\text{m}, \dots$ CO_2 is important redword of $13\mu\text{m}$ and between $13.3 - 15\mu\text{m}$ it makes ground based observations from any site impossible. CO_2 also contributes near $10\mu\text{m}$, methane near $8.6\mu\text{m}$ and below $8\mu\text{m}$, ozone dominates between $9.4 - 9.9\mu\text{m}$.

Overall when one compares TIMMI2 burst spectra at different zenith angles, one notices that the same amplitude of the noise components is seen at higher frequencies when one observers at higher airmass. The atmosphere appears more stable when observing close to zenith. This may be explained by the lower PWV. In the same way a site at higher altitude shall be more stable and fluctuate with higher power at lower frequencies. This behaviour of the power spectral density of the IR sky brightness fluctuations is qualitatively in agreement with the experience in adaptive optics where one finds that the atmospheric coherence time rapidly degrades with airmass.

In the MIR changes of the atmosphere are compensated by chopping. Originally chopper frequencies were chosen such that they would exceed frequencies where the power spectral density of the sky brightness fluctuations is noticeable. With the advent of detector arrays this requirement could be relaxed as the sky brightness fluctuations produce on the detectors only a signal with very low spatial frequencies, basically a common mode signal. The chopping frequency is determined by the combination of the power spectrum of the sky, the detector linearity and ability to flat field. Experience with 4m to 8m telescopes on La Silla and Paranal in the MIR ($5 - 25\mu\text{m}$) has shown that the optimum chopping frequency is $\sim 1\text{Hz}$ or larger. This issue will be further elaborated with next generation detector MIR devices.

5 MIR site monitoring

MIR observations of astronomical standard stars provide conversion factors for absolute photometry and give the sensitivity limit which can be reached during the night. Both parameters are monitored and stored in calibration data base for ESO's mid infrared instruments:

- TIMMI2 mounted at the 3.6m on La Silla (see: <http://www.ls.eso.org/lasilla/sciops/3p6/timmi/html/calmeas.html>)
- and VISIR mounted at Melipal/VLT on Paranal (see: http://www.eso.org/observing/dfo/quality/VISIR/img/trend/trend_STD_IMG_current.asc).

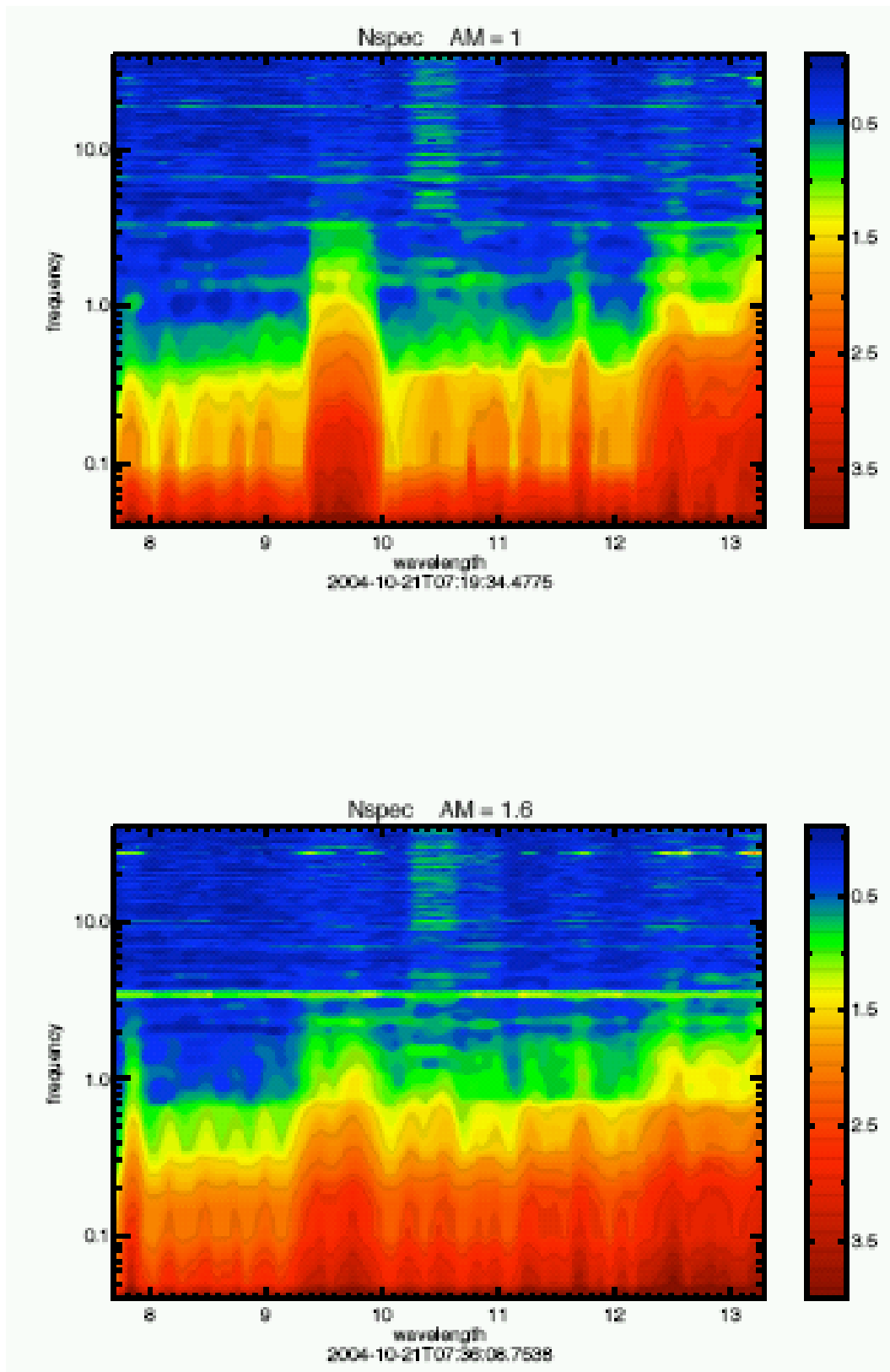


Figure 5: Power spectral analysis of TIMMI2 burst mode spectra at airmass 1 (top) followed by observations with airmass 1.6 (bottom). *Courtesy of M. Sterzik.* One shall notice: i) a correlation of atmospheric absorption bands with the power amplitude. ii) Lower airmass and therefore lower PWV or higher altitude of the site requires a lower chopping frequency which impact chopper design.

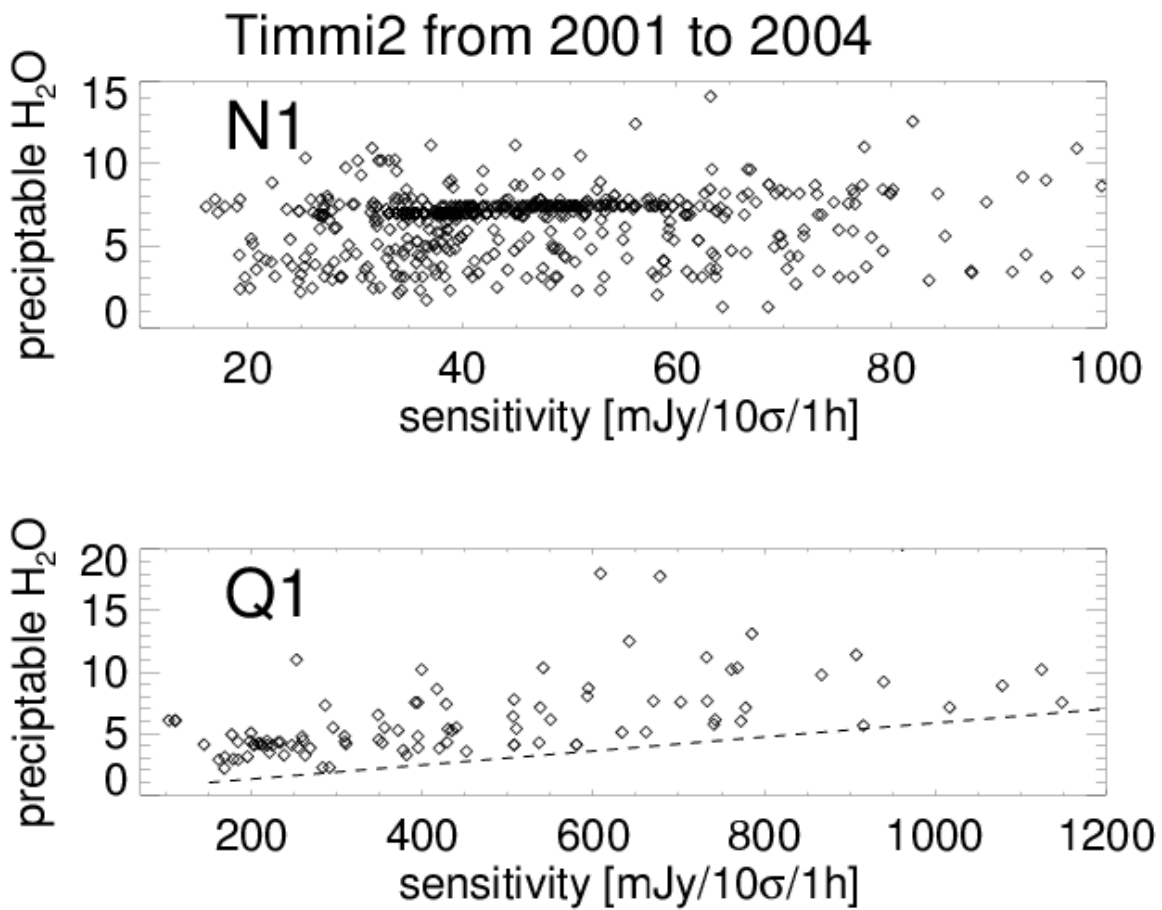


Figure 6: Variation of point source sensitivity with PWV as observed between 2001 – 2004 with TIMMI2: N1 (top) and Q1 filter (bottom).

At the same time ERASMUS satellite data are available ¹ and provide PWV measurements with a pixel resolution of ~ 10 km.

A cross correlation of PWV with TIMMI2 data for years 2001 – 2004 in filters: N1 ($7.47 - 9.93\mu\text{m}$) and Q1 ($16.9 - 18.54\mu\text{m}$) is shown in Fig. 6. For Q1 an obvious correlation with PWV can be noticed: High water content gives poor Q1 sensitivity. On the other hand for the N1 filter no trend is visible. This holds also for other N band filters. This trend is confirmed by VISIR data as available from year 2004. Both results can be understood by looking back to Fig.1: The major atmospheric absorber in the Q1 filter is water while in the N1 filter beside H₂O also other molecules contribute.

The conversion factor and the measured background is also correlated with PWV but to some degree in all filters. It is also suspected that the sensitivity in all N,Q filters depends on the local amount of dust (A. Smette & L. Vanzi, priv. com.). The idea behind is that dust in the local atmosphere would re-radiate principally in the N and Q band, therefore increasing the background and decreasing the sensitivity. At present the VISIR team is undertaking further studies. It is proposed to monitor the dust and aerosol content of the atmosphere at potential ELT sites. This is also considered of high importance for high contrast imaging at all wavelengths but especially in the near IR.

When a few (2–3) potential ELT sites may be selected some monitoring of the MIR sensitivity measurements shall be performed as well. Such observations in the Q band would answer the question on how often there are non-photometric conditions in the optical/NIR but good observing conditions in the Q band and submm with low and stable PWV.

Acknowledgments

The support by A. Seifahrt on HITRAN calculations, M. Sterzik providing TIMMI2 burst mode observations and analysis, A. Smette and L. Vanzi on VISIR results and B. Dent for sensitivity estimates of SCELTE is thankfully acknowledged.

References

- Giovanni R., Darling J., Henderson C., et al., 2001, PASP 113, 803
Hufnagel R.E., 1978, in: The Infrared Handbook, eds. W.L. Wolfe & G.J. Zissis
Käufel H.U., Bouchet P., van Dijsseldonk A., Weilemann, 1991, Exp. Astronomy 2, 115
Matsushita S., Matsuo H., Pardo J.R., Radford S.J.E., 1999, PASJ 51, 603

¹ <http://www.esoa.org/gen-fac/pubs/astclim/forecast/meteo/ERASMUS/archive/>

Comments on Minutes from Meeting on 01/13/06

I presume that in the second paragraph “privatised” should read “prioritized”.

On the issue of climate change: I can imagine two types of changes occurring at a given site on the time scale of several years to decades. The first type would be a change (such as a decrease of the number of clear nights) affecting a large area, but with spatial gradients remaining more or less the same. This type of change would affect neighboring sites in a rather similar way, and would not change the ranking between sites in some local area. There is probably little one could do to anticipate and mitigate the effects of such changes. The second type of change would be a shift of a climate zone or typical weather pattern with time. (One might for example very naively expect that to first order global warming should move all climate zones to larger absolute latitudes.) If this type of change occurs, the ranking between sites in a local area would change, as the “sweet spot” moves across them. Furthermore, this type of behavior might be at least partly predictable in that a strong local gradient of the typical conditions, or proximity to an area with a different typical weather pattern, might be warning signs. One could speculate that the correlation of both Paranal and La Silla conditions with ENSO is somewhat similar to the first phenomenon (a whole area becoming better or worse simultaneously), whereas the long-term deterioration of Paranal both in cloud coverage and Fried parameter, which is not seen at more Southern Chilean sites (e.g., La Silla and Las Campanas), might be indicative of a shift of the whole “Atacama” climate zone towards the South. Questions: Is there sufficient information (e.g. from satellite data) to confirm or reject that speculation? Would it make sense to include information about the local gradients of conditions / size of an area with good conditions / proximity to areas with substantially worse conditions among the site selection criteria? If so, how can this be done? Taking into account orography will probably not be trivial – for example, weather patterns could easily shift along the Andes, but the coast will certainly stay where it is.

There is a somewhat cryptic remark that “differential refraction ... is latitude-dependent”. Should this be “altitude-dependent”? That would make more sense – differential refraction actually depends on barometric pressure at the observatory.

Thinking about the “latitude dependence”, another effect related to sky coverage came to my mind: the larger the absolute latitude, the less sky is accessible at small air mass, which probably means that the mean air mass of all observations increases with absolute latitude (depending somewhat on the science being done). This should be factored into performance comparisons. Another rather trivial (but important) parameter, which I have not seen listed, is the strong dependence of nighttime hours on absolute latitude.

On instrumentation for site evaluation: We have very little information on the outer scale of turbulence from direct measurements on the relevant scales of tens of meters. Extrapolations from measurements on much smaller scales are very model dependent, and there is little evidence favoring one model over the other (e.g., Greenwood-Tarazano versus von Karman cut-off). This can be resolved by interferometry with simultaneous fringe tracking on two baselines of different lengths. The VLTI should soon be able to take such data. This will only provide data for Cerro Paranal and thus not help to select an ELT site, but it will provide valuable information for the design of AO systems for ELTs.

On measurements of the sodium layer: It is rather simple to measure the sodium density profile with a 589nm cw laser – one just has to look at the elongated sodium “spot” from the side

(e.g., Butler et al. 2003, A&A 403, 775; Michaille et al. 2001, MNRAS 328, 993). I think that such measurements should be part of any ELT site evaluation campaign. There are also recent Na measurements from ODIN and ENVISAT (several publications by Gumbel et al. and Fussen et al., respectively), which could help in constructing “global” models of the Na layer. One would probably have to contact these groups in order to find out how detailed and how useful their data are for our purposes.

Relevant Parameters for ONIRICA

As far as criteria for the site selection are concerned, the requirements of ONIRICA are very similar to those of MOMFIS. The AO concepts of these instruments are different, but the general parameters are rather similar (identical wavelength range, similar field, use of multiple LGS). There is a difference regarding the sky background: Being an imager, ONIRICA cannot look between the airglow lines. But since MOMFIS will also need low airglow background, the two instruments have similar requirements even in this respect.

It should be pointed out the ONIRICA description in the “Blue Book” contains a statement that the instrument may work only in the 10% – 30% best seeing. This raises a number of operational issues (number of instruments available on the telescope simultaneously, time needed for switching between instruments), but may also have a number of consequences for the site requirements:

- How exactly will the seeing parameters be specified (e.g., mean and variation, median, quartiles)?
- If two sites have the same median seeing, is it better to have a small variation (giving rather consistent conditions) or a large variation (giving spectacular seeing once in a while, but also rather poor seeing more often)?
- Is there a criterion that captures how fast the seeing changes, and how well it can be predicted for a few hours? It is probably desirable (not only for ONIRICA) that the seeing is quite stable over a night, and that it can be predicted a few hours in advance.
- What is the relation between the methods and instrumentation used for site selection and those used for site monitoring during operations?

Site Requirements for a Multi-Object Multi-Field Near IR Spectrograph (MOMFIS)

1 Introduction

Among the focal plane instruments which have been suggested for ESO's future extremely large telescope is a multi-object multi-field near-IR spectrograph ('MOMFIS'). A conceptual study of such an instrument has been carried out by a consortium of French laboratories (LAM, CNRS/CRA Lyon, CNRS GEPI, CNRS LESIA, and ONERA) in the context of the OWL project. This study, described in the OWL Blue Book, is used as a basis for the following analysis of the site requirements for this type of instruments. Following the study, it will be assumed that MOMFIS is operating in the wavelength range $0.8 \mu m$ to $2.5 \mu m$, and that it will consist of a system of 30 integral field units (IFUs) which can be individually positioned in a 5 arc-minute field. The spectral resolution is assumed to be at least $R \approx 4000$. MOMFIS has been designed to be operated in diffraction-limited mode and (at least as a back-up) also at a seeing limited angular resolution. The diffraction-limited mode over the whole 5 arc minutes FOV will require a multi-object adaptive optics (MOAO) system, covering the individual IFUs within the FOV. Multiple laser guide stars will be needed for this purpose. An AO system providing fully diffraction limited images for the central 1 - 2 arc minutes only and a degradation towards the field edges has been suggested as a back-up solution, if a full MOAO system cannot be realized.

2 MOMFIS Scientific Objectives

As described in the OWL Blue Book the main scientific objective of MOMFIS is the spectroscopy of high-redshift galaxies at the epoch of re-ionization of the universe. An explicit aim of MOMFIS is 'to push back as early as possible into the Dark Ages' of cosmic evolution. This will require the spectroscopy of small (≈ 1 arc-second), but extended, objects of very low surface brightness. However, it is obvious that such an instrument at a 30 - 60 m ELT will have many additional important scientific applications as well. Examples for such other applications are studies of the physics of AGN, the physics of very cool stars and investigations of circumstellar matter.

3 Site Requirements

The scientific objectives of MOMFIS require good S/N NIR observations of very faint extended objects. The sensitivity of groundbased observation of this type is normally limited by the NIR absorption and emission of the earth atmosphere. The main cause of the atmospheric NIR absorption is water vapor, which restrict groundbased NIR observations to a few distinct wavelength bands. The width and transparency of these 'atmospheric windows' depend on the absolute water vapor content above the site.

At low geographic latitudes the atmospheric NIR emission is normally dominated by OH airglow emission bands. At absolute latitudes $> 60^\circ$ auroral emission lines (of N_2 , N_2^+ , NI, OI, and [NI]) will often dominate the NIR sky emission. In addition to the line emission, thermal continuum emission by aerosols may contribute to the NIR sky

background. All three types of night sky emission (air glow, aurora, and aerosol emission) vary strongly with geographic location and with time.

The proposed spectral resolution of MOMFIS will allow to resolve the OH bands. Thus, it will in principle be possible to obtain deep observations of the spectral regions falling between the OH lines. However, at the proposed spectral resolution for very faint objects the wings and straylight of the strong OH lines (and the even stronger auroral lines) will affect the spectroscopy even between the nightsky lines in much of the MOMFIS wavelength range. Therefore, in most of the spectral range the flux limit of MOMFIS for extended objects will depend linearly on the night sky emission. The S/N will be either inversely proportional to the square root of the spectral flux from the sky (if the noise is dominated by the photon statistics) or inversely proportional to the sky emission (if spatial and temporal variations dominate the noise). Thus, a low NIR sky emission appears to be the most important and critical site selection criterion for MOMFIS and similar instruments. At least in the case of potential high-latitude sites (for which less information is available than on the conventional observatory sites at moderate latitudes) careful test observations of the sky emission, its spectrum, and its temporal and spatial variability must be carried out before such sites are seriously considered for ESO's ELT.

As noted above, the width and transparency of the NIR atmospheric windows depend critically on the atmospheric water vapor content. Any decrease of the atmospheric precipitable water vapor content will directly increase the usable wavelength range(s) of MOMFIS. Therefore, another important site criterion for MOMFIS will be a low amount of precipitable water vapor above the telescope site. (For quantitative information on this effect see Ralf Siebenmorgen's contribution).

Many of the main scientific objectives of MOMFIS require a diffraction limited angular resolution. Therefore, atmospheric turbulence conditions suitable for a multi-object adaptive optics system covering the 5 arc minutes FOV are another important site constraint for MOMFIS and its scientific aims. Obviously, a large isoplanatic angle and/or a small contribution to the seeing of high atmospheric layers would be of advantage for the operation of MOMFIS.

A modest amount of atmospheric extinction will not have a significant direct impact on the spectroscopic observations of MOMFIS, if the extinction does not affect the sky emission. However, since the diffraction limited observations with MOMFIS will normally require laser guide stars, significant and variable atmospheric extinction of any kind may hamper the MOMFIS operation via the dimming and straylight effects of the guide star radiation.

4 Conclusions

As pointed out above, the most critical site requirement for optimal scientific results with instruments like MOMFIS will be a low NIR line and continuum emission of the atmosphere above the telescope. The quality of the spectroscopic data and the usable wavelength range will also be strongly affected by the atmospheric precipitable water vapor content of the site. Local atmospheric turbulence conditions allowing an efficient MOAO system will be a prerequisite for the diffraction limited operation of MOMFIS over the proposed 5 arc minutes FOV. The operation of the AO system will require a low and stable atmospheric extinction. Apart from trivial considerations (such as the absence of clouds and precipitation) other site criteria will be less important for MOMFIS.

ELT Site Evaluation Working Group (WG-3)

Second Meeting, 7/1/06.

Richard Wilson, University of Durham.

Influence of Site Properties for MOAO (+GLAO).

MOMFIS parameters:

- 30 integral field ‘buttons’, 40x20mas image slices over a 5’ patrol field
- Spectral bands: Y,J,H,K.
- Required image quality: <50mas image width (50% EED).
- MOAO correction, one DM per button, 10K actuators each.
- Multi NGS (first generation) or LGS tomographic (?) wavefront sensing.
- Independent (common) GLAO correction of the patrol field.

Key site parameters for MOAO (+GLAO) on ELT

Fried parameter. As for all astronomical applications of adaptive optics, the statistics of the total integrated turbulence at the site, in terms of r_0 , will be key in defining the main AO system parameters: spatial order of sampling for the wavefront sensors (WFS), required actuator density and stroke of deformable mirrors (DM).

Outer scale of turbulence. For a telescope aperture diameter $\sim 50\text{m}$, the outer scale length associated with the turbulence will also be critical in specifying DM parameters. For the von Karman turbulence spectrum with an outer scale length L_0 in the region of 20m (typical of values measured at Paranal, La Palma and elsewhere), the structure function of atmospheric phase perturbations at the ground will saturate at length scales much smaller than the aperture diameter, with the saturation level depending on the actual values of r_0 and L_0 . A change of r_0 (at 500nm) from 16cm to 12cm (the approx. range of median r_0 values for the best sites) results in a change of the structure function saturation level by a factor 1.6. Increasing L_0 from 20m to 26m produces the same change. This highlights the sensitivity of the power in large-scale aberrations (and hence the required DM actuator stroke) to L_0 . The high sensitivity to L_0 suggests that the *actual* form of the structure function on length scales up to 50m will be important - i.e. we should not simply assume a von Karman spectrum and extrapolate from measurements made on 8m telescopes.

$L_0(h)$. Assuming effective GLAO correction for low altitude turbulent layers, the required stroke for the MOAO button DMs will then depend on the L_0 of the higher layers only, so that measurements of L_0 with (even very crude) altitude resolution would allow more appropriate specification of the individual DMs for button AO and GLAO.

Ground layer turbulence profile. GLAO may provide significant reduction of the demands on the button-AO systems, through decreased actuator density and stroke, improved SNR for tomographic wavefront sensing. Also a more stable $C_n^2(h)$ profile for reconstructor optimisation due to the reduced impact of ground layer fluctuations, which can be very rapid – e.g. see figure 2, example SLODAR turbulence profile sequences below).

The effectiveness of GLAO correction naturally depends on the statistics of the fraction of the total $C_n^2(h)$ in the ground layer (<1km altitude for the sake of argument). This is thought to be ~50% or more at typical sites, but more statistics are required. Assuming perfect GLAO correction of the ground layer, a fixed total turbulence strength and a constant L_0 with altitude, then reducing the GL fraction from 60% to 40% of the total $C_n^2(h)$ results in a factor 1.5 increase in the structure function saturation level on long baselines, i.e. a similar factor as for the variation of r_0 from 16cm-12cm.

Modeling of GLAO will also require an exploration of the trade-off for delivered image quality versus corrected field size. The field diameter over which GLAO delivers approximately constant partial image correction will be limited by the fraction and distribution of turbulence in the ‘gray zone’ of altitudes of a few hundred meters (Tokovinin, PASP 116, 824). The required altitude resolution of $C_n^2(h)$ measurements for modeling of the GLAO PSF is given approximately by the ratio of the DM pitch to the required field radius. For a 5 arcmin (max) field radius for GLAO correction in the IR this implies a sampling resolution of ~200m over the first 1km.

Surface layer turbulence profile. The actual ground layer fraction will depend substantially on what fraction of the (often very strong) surface layer (<~50m) turbulence is actually ‘seen’ by the ELT. Hence detailed profiling of $C_n^2(h)$ up to the height of the ELT and its enclosure will be important, as well as modeling to indicate the extent to which the telescope and its enclosure will create their own ‘surface layer’ turbulence.

Free atmosphere turbulence profile. The residual uncorrected phase variance for AO with multi-LGS or multi-NGS wavefront sensing (including tomography) increases with the separation of copies of the telescope pupil function projected onto the turbulent layers, in the directions of the reference targets. Hence a site with weak high altitude turbulence is favorable - as for all AO. Statistics of $C_n^2(h)$ for the whole atmosphere, with good vertical resolution, are required for accurate system modeling and performance prediction.

$C_n^2(\mathbf{h}, \mathbf{t})$. Fluctuations of the turbulence profile will result in temporal variations of the corrected PSF, to some degree, for all AO corrected observations – e.g. the field of view for GLAO correction will vary according to the profile of the turbulence in the first km altitude. For tomography, some knowledge of the turbulence profile is required in order to optimize the control matrix. The delivered image quality will be degraded when the actual profile differs from that assumed for the operating control matrix. There will be a practical limit to the frequency with the reconstructor can be re-optimized for changes of

ambient $C_n^2(h)$ profile (e.g. the time required to measure the profile to some level of statistical accuracy), so that temporal fluctuations of the profile will be a limitation on the performance of MOAO.

Assemat (PhD thesis: <http://www.dur.ac.uk/francois.assemat/these-francois-assemat.pdf>) has modeled the effect of variations of the altitude and strength of turbulent layers on MOAO correction in the H band for the 8m-telescope case (the FALCON instrument concept). The spatial correction for FALCON is similar to that required by MOMFIS (partial correction in the IR, moderate Strehl ratio, 50%EED \sim 50mas), so that the sensitivity of the MOAO corrected image quality for MOMFIS to changes of the turbulence profile is likely to be of the same order of magnitude. Figure 1(a) indicates sensitivity to the altitude of a dominant turbulent layer. In this example a change of 1km in the *altitude* of the layer reduces the delivered Strehl by approx 15%. From figure 1b, a 20% change in the *relative strength* of the dominant layer reduces the Strehl by 40%.

Coherence time, turbulence wind speed. Statistics of the atmospheric coherence time τ_0 define the required AO system bandwidths. Wind speeds in the free atmosphere will dominate the coherence time relevant to MOAO button system bandwidths. Ground layer wind speeds are typically lower, so that GLAO bandwidths may be relaxed. GLAO correction will not greatly reduce bandwidth requirements for the button AO systems.

Sodium layer profile. For sodium laser beacons, the integrated column density of the sodium layer defines minimum laser power requirements. The sodium layer strength and profile with altitude shows seasonal variations as well as substantial fluctuations during a single night (e.g. see Michaille et al. MNRAS 328, 993). Statistics of the sodium layer profile and its variation are required with reference to the laser specification as well as for modeling of the stability of the AO corrected PSF, also for example impacting on requirements for the measurement and correction of low-order aberrations via natural guide stars. The brightness of the Rayleigh back-scatter plumes for the Sodium beacon uplink will also be site dependent, with the degree of contamination of the science field determining notch filter requirements in the science instrument.

Ranked List of Site Properties for MOAO & GLAO.

Key areas of impact; required spatial and temporal resolution of parameters for system design & modeling; suitable or possible site monitoring instruments.

Rank	Site Property	Impacts on:	Required Resolution	Site testing Instruments
1	Integrated seeing, r_0	AO system order, DM actuator density + stroke	1 min	DIMM, WFS on 8m, ...
2	Coherence time, τ_0	AO system bandwidths	1 min	DIMM, WFS on 8m
3	Free atmosphere turbulence profile (>1km)	MOAO PSF (field dependent)	0.5-2km	SCIDAR, SSS, MASS, SLODAR,...
4	Ground layer turbulence profile (<1km)	Achievable correction & FOV for GLAO	50m	SLODAR LOLAS SoDAR
5	Surface layer turbulence profile (to ELT height)	Achievable correction & FOV for GLAO	5m	Mast, Kite? Laser interferometer ?
6	L_0 (H ?), Actual structure-function on scales up to 50m	Required actuator stroke for GLAO DM & MOAO button DMs	SL/GL/FA ? 2km ?	WFS on 8m, Portable fiber-linked transit interferometer ??
7	Sodium density & profile variation nightly, seasonal	Laser beacon power requirements. AO PSF stability.	1 min ?	PARSEC + off-axis telescope ?
8	Temporal variation of $C_n^2(h)$ profile	Performance of tomographic reconstruction	1 min	Assorted profilers
9	Turbulence wind-speed altitude profile, $V_w(h)$	Individual bandwidths for GLAO & MOAO/button systems	2 km ?	SSS SCIDAR SLODAR
10	Frozen turbulence (or not...)	Use of prediction to reduce AO bandwidth	SL/GL/FA ?	WFS on 8m
11	LGS Rayleigh scattering into science field	Science limiting magnitude, notch filter requirements	Samples ?	VLT + PARSEC ?

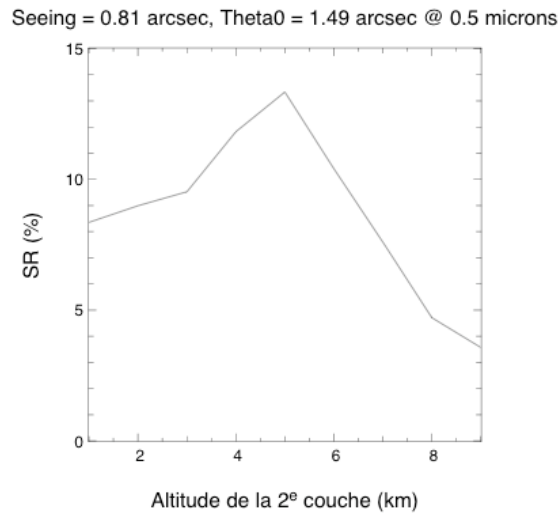


FIG. 5.9 – Evolution du rapport de Strehl en fonction de l'altitude de la deuxième couche. La matrice de reconstruction suppose une altitude $h_2 = 5$ kilomètres. Analyse et correction des polynômes de Zernike 2 à 120.

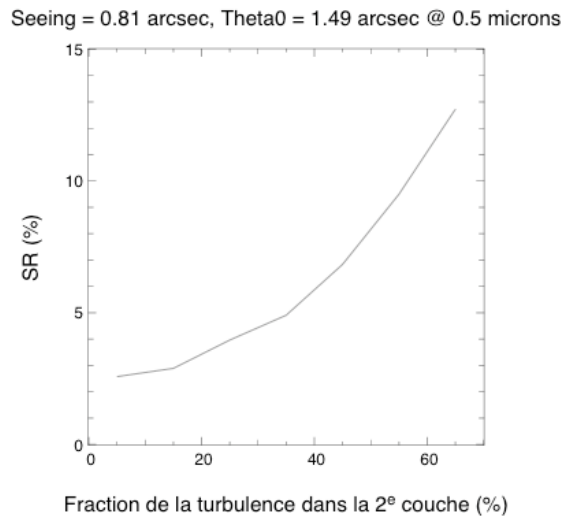


FIG. 5.10 – Evolution du rapport de Strehl en fonction de la fraction de la turbulence totale dans la deuxième couche d'altitude $h_2 = 5$ kilomètres. La matrice de reconstruction suppose 65% de la turbulence dans cette couche et 15% dans la troisième couche d'altitude $h_3 = 10$ kilomètres. Analyse et correction des polynômes de Zernike 2 à 120.

Figure 1. Example exploration of the sensitivity of MOAO delivered PSF Strehl ratio to fluctuations of the turbulence profile, in the 8-m telescope case (F. Assemat, PhD thesis). (a) top – the effect of changes in the altitude of the dominant turbulent layer. (b) bottom – the effect of changes in the relative strength of the dominant layer.

Technical note on SLODAR characterisation of the ground-layer turbulence profile.

The ESO prototype (small telescope) SLODAR system measures the $C_n^2(h)$ profile in 8 altitude bands, each approximately 140m in thickness, plus a measure of the total turbulence above ~1km. Hence the data is suited to modeling of GLAO for an ELT. The first altitude bin is centered at the instrument altitude (currently ground level), and so is effectively one half bin (70m) in height. The altitude resolution is currently limited by the CCD detector size, and can be improved to ~60m - spanning the first ~500m - if a larger format detector is used to accept wider double star targets (the planned SLODAR system for the Gemini GLAO study will have this capability). The first resolution element will then encompass 0m to 30m above the instrument.

The prototype instrument is at ground level, and employs a closed tube telescope and a fixed enclosure. As a result, the first 'layer' measurement (0-70m altitude) is 'contaminated' by turbulence in the first few meters and possibly some internal enclosure and/or mirror seeing - a contribution that is certainly not relevant to an ELT. Compared to the ASM DIMM on a 6m tower adjacent to SLODAR, we find that the difference of the DIMM and SLODAR integrated seeing values is correlated with the strength of the first SLODAR layer. Typically 50% of this surface layer is not 'seen' by DIMM.

The current integrated SLODAR + MASS median profile for Paranal suggests that the ground layer (<1km) contributes approx. 60% of the total turbulence. This is likely to be an over-estimate, since a large fraction of the first layer contribution is not relevant to an ELT. If one half of the SLODAR first layer strength is excluded, then the median GL fraction reduces to ~50% of the total $C_n^2(h)$. The first layer is also typically found to be highly non-Kolmogorov in nature, with excess power on centimeter scales. This complicates the SLODAR data reduction process. Mounting on a tower platform, use of an open-tube telescope, as well as a larger format detector are therefore recommended for any future SLODAR implementation.

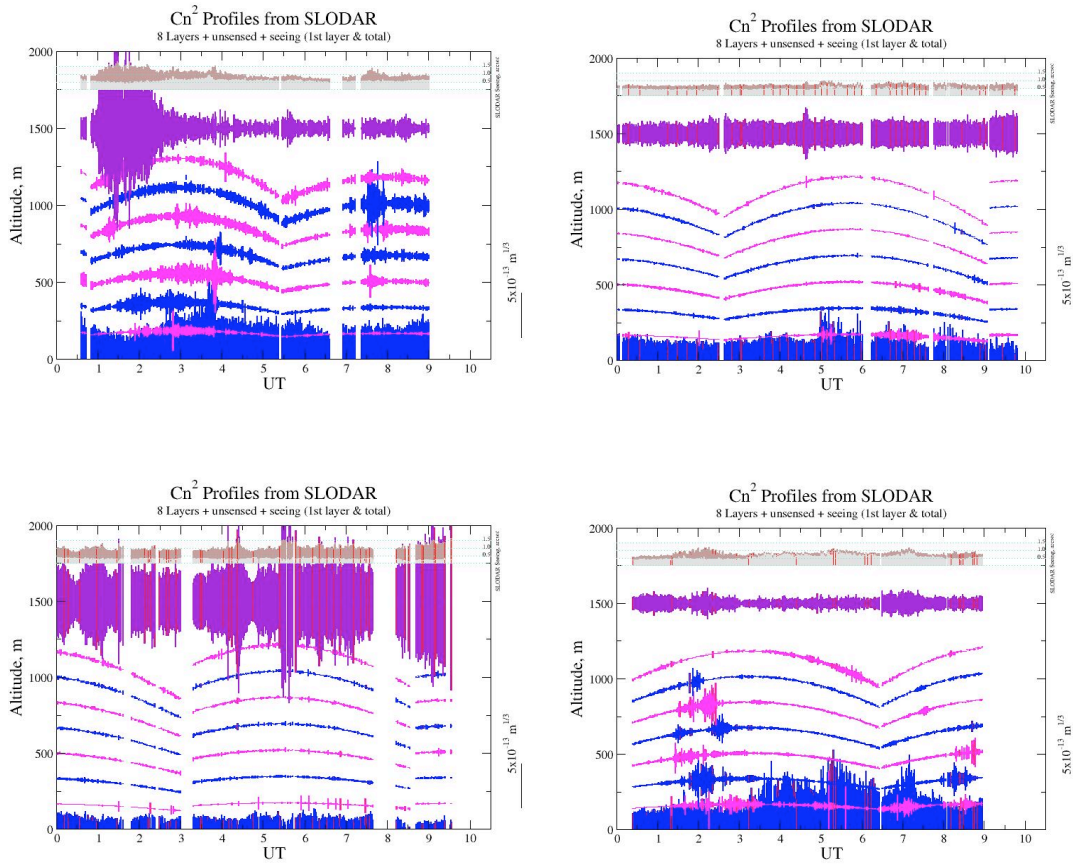


Figure 2. Contrasting example SLODAR nightly ground-layer $C_n^2(h)$ profile sequences for Cerro Paranal (2005): 8 sensed layers up to approx 1200m in altitude, plus the total contribution from all higher altitudes (purple bar centered at 1500m). Bar widths indicate turbulence strength. Layer altitudes vary with elevation of the target star - hence the traces are curved. The first layer (blue) is centered at the ground. The sampling interval is approx. 1 minute. The first km is often stable, but note examples of short-lived turbulent activity, with changes on timescales of minutes. Turbulence in the first (surface) layer (<80m) is usually significant.

Contrails

The condensation trails -contrails- that often form behind aircraft at flight altitude are more than a nuisance to ground-based astronomy. While these man-made clouds share with natural clouds the positive quality of being grey, they are highly structured, making proper calibration of the astronomical observation difficult. Aviation has been rising for decades, almost without cessation, and most scenarios (see below) predict that this will continue. Since the basic means of propulsion - the burning of kerosene, leading to the formation of water - will remain the same for decades to come, contrails present a problem for the location of the ELT, and a challenge for its operation.

Contrails form and persist when certain conditions of relative humidity and temperature exist in the flight altitude (Schmidt 1941, Appleman 1953). This may happen in areas of cirrus, or in air-masses with no preexisting cloudiness. Regions prone to contrail formation are often up to 1000 km across (Figure 1); they may total some 20-30 percent of the globe. Contrail formation in air-masses that are already supersaturated with respect to water-ice may cause the contrail to grow further and last very long. Individual contrails have been tracked (by satellite observation) for as long as 17 hours (Minnis et al. 1997); clusters of contrails can often be followed for two days or more (Bakan et al. 1994). The affected zones of the globe are therefore the areas directly below and to the East of air-routes. Contrails generally sink through the atmosphere (partly due to the down-wash from the aircraft, partly due to particle size). Under typical vertical wind shear conditions, the horizontal expansion rate is of the order of 3 km per hour (Jensen et al. 1998; Duda et al. 2004). During its hour-long persistence, a contrail may entirely lose the original, line-shaped characteristics, to become indistinguishable from natural cirrus. A number of studies have indeed pointed to increased cirrus-cloudiness below air-routes (e.g. Boucher 1999; Zerefos et al. 2003; Palikonda et al. 1996; Stordal et al. 2005). In areas of high air-traffic, contrails may form an unbroken pattern of cloudiness (Figure 2). The ratio between the area covered by line-shaped contrails (detectable by automated search routines working on 1 km resolution satellite imagery) and that of contrail-cirrus, is a matter of debate. While values of 2 to 3 have been quoted, this may indeed be too low, if contrail-cirrus of low optical depth ($\tau < 0.02$) is taken into account.

For wide regions of the globe, aviation is expected to increase by 3 - 5 percent annually¹. The predictions by the Intergovernmental Panel on Climate Change, up to 2050 (Penner et al. 1999), may be on the conservative side, in particular what regards Chinese and Indian aviation. Although the densely populated regions of the Northern hemisphere will remain the most heavily travelled, it is noteworthy, that few regions are currently void of aviation, hence exempt from contrail formation (Figure 3). Thinking decades ahead, it is almost inconceivable, that the contrail formation rate should lessen. Marquart et al. (2003) have concluded, that the growth of contrail-cover at northern latitudes, away from the tropics, will be

¹ By 2030 British aviation is expected to rise to 2 - 4 times above the 2003-level, ref.

http://www.dft.gov.uk/stellent/groups/dft_aviation/documents/page/dft_aviation_031493.hcsp and

http://ncas.nerc.ac.uk/meetings/past/aviation_impacts/talks/poll.pdf

determined by growth of aviation, while at tropical latitudes, it will, additionally, be highly affected by climate change. The generally warmer climate expected during the 21st century will tend to reduce the contrail cover (Sausen 2000).

For reason of their climatic impact, contrails are an intensely studied field in geophysics. Recent works on contrail-cirrus coverage include those of Travis et al. (2002 & 2004), Minnis et al. (2005), and Duda et al. (2005).

Contained in the exhaust from jet engines is a tiny proportion of soot, engine oil and metallic particles from general engine wear. Possibly in unison with emitted Sulphur, these particles act as cloud condensation nuclei for the immediate contrail formation. Settling slowly, they may cause cloudiness or atmospheric haze (Hofmann et al. 1998) during weeks to months ahead. From the point of view of astronomical observations, it is not meaningful to distinguish such emissions from a host of other anthropogenic sources, such as rocketry, diesel exhausts and soot from forest clearing. The general trend is to increase astronomical extinction (the night-time version of 'global dimming', ref. Liepert 2002), in particular near the blue limit.

Dominant effects

The most obvious action of a contrail in the field of view of a telescope is to cause loss of signal strength. The optical depths are mostly in the range $\tau = 0.15 - 0.30$ and may reach 0.5 (Minnis et al. 2004). This absorption is spatially and temporally variable, meaning that an imaging telescope will suffer from non-uniform absorption across the field of view, with little possibility to calibrate using preceding or subsequent exposures. In the presence of contrails, spectrophotometry cannot depend on standard calibrations.

On moon-lit nights, contrail-cirrus will generally act to increase the sky background. Minor effects of polarization cannot be excluded (Sussmann 1997).

In the rare instance, that an aircraft should pass very close to a telescope's field of view, the hot exhaust gasses may leave an infrared emission signal; its general shape has been modeled by Beier and Schreier (1994).

Mitigatory initiatives

Already years ago, the International Astronomical Union made recommendations regarding aviation near prime site observatories², but these are not widely known to pilots or aviation authorities. Spain regulates aviation around the Canary Islands³, with the aim to protect the observing sites against contrails and other detrimental effects of direct overflights. Neither set of rules will protect observatories from hour-old contrail-cirrus.

Unfortunately, technological developments do not necessarily lead to weaker or lesser contrails. The higher flight altitudes realized during recent years means more contrails and longer residence time for particles. The concern for NOx emissions, coupled with demand for high fuel efficiency, may lead to engines emitting water vapor at lower temperatures. In this tradeoff, an increase in contrail cover is likely

² Distance limit 60 km, ref. IAU Transactions, vol. XVIB, p.320 (1977).

³ Distance limit 38 nautical miles, ref. http://www.iac.es/proyect/otpc/esp_prot.pdf

(Marquart et al. 2003). The eventual deployment of Hydrogen-powered aircraft will lead to denser contrails⁴.

To some extent, astronomy can benefit from the concern often expressed for the contrails' climate signal. The UK's Royal Commission on Environmental Pollution has suggested that aircraft "could be routed to avoid areas where contrails or cirrus are likely to form, or to minimise the greenhouse effect of water vapour released"⁵. Fichter et al. (2005) have shown that a modest change of flight altitude (~ 2000 feet) is often sufficient to inhibit contrail formation. A British engineering group⁶ has concluded, that the penalty of higher fuel consumption at lower flight altitudes (20,000 feet) is less damaging for the environment, than the radiative forcing due to contrails generated at 35,000 feet.

While the operational use of the Schmidt-Appleman criterion is common to military aviation, it was only recently introduced to general aviation. Pilots flying over Alaska⁷, contiguous USA⁸, and Europe⁹ can now use this methodology to seek routes and flight altitudes, with less chance of 'pulling contrails'. The on-board instrumentation is sufficient to finally decide upon the conditions.

Contrail detection at ELT

The loss of statistical significance, caused by a contrail drifting through the ELT field of view, can, in many cases, be compensated by a slightly extended exposure duration. More serious is, perhaps, the potential for the introduction of non-statistical, gross, errors, in certain types of observations (e.g. time-series measurements and wide-field imagery). In the extreme, these can be interpreted as genuine discoveries. It is, of course, an open question, which effort to put into a system, which can protect the ELT against this.

While all-sky cameras using fish-eye optics are in use at many observatories, these are insufficient to quantify the presence and angular motion of contrails. For that to come true, it will be necessary to employ mosaic imaging, larger format CCDs, and mass-photometry of thousands of stars. To fully locate the contrail in three dimensions, two such instruments should be operated in a stereoscopic detection mode. That done, the ELT observer could be supplied with warnings of upcoming contrail passages.

In the mean-time, contrails would appear to be an important issue for the ELT site selection.

Holger Pedersen
Niels Bohr Institute
Copenhagen, Denmark

⁴ http://www.mpimet.mpg.de/en/depts/dep1/acc/hycare/presentations/22_zerefos.pdf

⁵ <http://www.parliament.uk/post/pr195.pdf>

⁶ <http://www.epsrc.ac.uk/PressReleases/ClimateChangeAndTheFutureOfAirTravel.htm>

⁷ http://contrail.gi.alaska.edu/frame/MM5_section2.html

⁸ http://www-pm.larc.nasa.gov/sass/contrail_forecast/contrail_prediction.html

⁹ http://www.pa.op.dlr.de/arctic/pazi/fc_today.html

References

- Appleman, H., "The formation of exhaust condensation trails by jet aircraft", Bull. Amer. Meteor. Soc. vol. 34, p.14-20 (1953).
- Bakan, S., et al.: "Contrail frequency over Europe from NOAA-satellite images", Annales Geophysicae, vol. 12, p.962-968 (1994).
- Beier, K., and Schreier, F.: "Modeling of aircraft exhaust emissions and infrared spectra for remote measurement of nitrogen oxides", Annales Geophysicae, vol. 12, p.920-943 (1994).
- Boucher, O.: "Air traffic may increase cirrus cloudiness", Nature, vol. 397, p.30-31 (1999).
http://www.nature.com/nature/journal/v397/n6714/abs/397030a0_fs.html
- Duda, D.P., et al.: "A case study of the development of contrail clusters over the Great Lakes", J. of the Atm. Sci., vol. 61, p.1132-1146 (2004).
- Duda, D.P., et al.: "CONUS contrail frequency and coverage estimated from RUC and flight track data", Meteorologische Zeitschrift, vol. 14, p.537-548 (2005).
- Fichter, C., et al.: "The impact of cruise altitude on contrails and related radiative forcing", Meteorologische Zeitschrift, vol. 14, p.563-572 (2005).
- Hofmann, D.J., et al.: "An analysis of 25 years of balloonborne aerosol data in search of a signature of the subsonic commercial aircraft fleet", Geophys. Res. Letters, vol. 25, p.2433-2436 (1998).
- Jensen, E. J., et al.: 1998: "Spreading and Growth of Contrails in a Sheared Environment", J. Geophys. Res., vol. 103, p.31,557-31,568 (1998).
- Liepert, B.G.: "Observed reductions of surface solar radiation at Sites in the United States and worldwide from 1961 to 1990", Geoph. Research Letters, vol. 29, p.1421-1433 (2002).
http://www.ldeo.columbia.edu/~liepert/papers/liepert_GRL2002.pdf
- Marquart, S., et al.: "Future Development of Contrail Cover, Optical Depth, and Radiative Forcing: Impacts of Increasing Air Traffic and Climate Change", Journal of Climate, vol. 16, p.2890-2904 (2003).
- Minnis, P., et al.: "Transformation of Contrails into Cirrus during SUCCESS", Geophysical Res. Letters, vol. 25, p.1157 (1997).
<http://www-pm.larc.nasa.gov/data/success/auxiliary/Transformation.pdf>
- Minnis, P., et al.: "Contrails, Cirrus Change and Climate", Journal of Climate, vol. 17 p.1671-1685 (2004).
- Minnis, P., et al.: "Contrail coverage over the North Pacific from AVHRR data", Meteorologische Zeitschrift, vol. 14, p.515-523 (2005).
- Palikonda, R., et al.: "Remote Sensing of Contrails and Aircraft Altered Cirrus Clouds", Proceeding of Impact of Aircraft Emissions upon the Atmosphere International Colloquium, Volume II, Paris, France, October 15-18, 1996, p.439-444 (1996).
<http://www-pm.larc.nasa.gov/sass/pub/conference/Rabi.ONERA.abs.pdf>
- Penner, J.E., et al.: "Aviation and the Global Atmosphere", Intergovernmental Panel on Climate Change, Cambridge University Press, 365p (1999).
<http://www.grida.no/climate/ipcc/aviation/index.htm>
- Sausen, R.: "Aviation impact as part of global climate change". Proc. Conf. on Aviation, Aerosols, Contrails and Cirrus Clouds, Seeheim, Germany, European Commission, p.275-280 (2000).
- Schmidt, E.: "Die Entstehung von Eisnebel aus den Auspuffgasen von Flugmotoren". Schriften der Deutschen Akademie der Luftfahrtforschung, Verlag R. Oldenbourg, München und Berlin, Heft 44, S.1-15 (1941).

- Stordal, F., et al.: "Is there a trend in cirrus cloud cover due to aircraft traffic?", Atmos. Chem. Phys, vol. 5, p.2155-2162 (2005).
- Sussmann, R.: "Optical properties of contrail-induced cirrus: discussion of unusual halo phenomena", Applied Optics, vol. 36, p.4195-4201 (1997).
- Travis, D. J., et al.: "Contrails reduce daily temperature range", Nature, vol. 418, p.601 (2002).
- Travis, D.J., et al.: "Regional variations in US diurnal temperature range for the 11-14 September 2001 aircraft groundings: Evidence of jet contrail influence on climate", Journal of Climate vol. 17, p.1123-1134 (2004)
- Zerefos, C.S., et al.: "Evidence of impact of aviation on cirrus cloud formation", Atmos. Chem. Phys. vol. 3, p.3335-3359 (2003).
- <http://www.copernicus.org/EGU/acp/acpd/3/3335/acpd-3-3335.pdf>

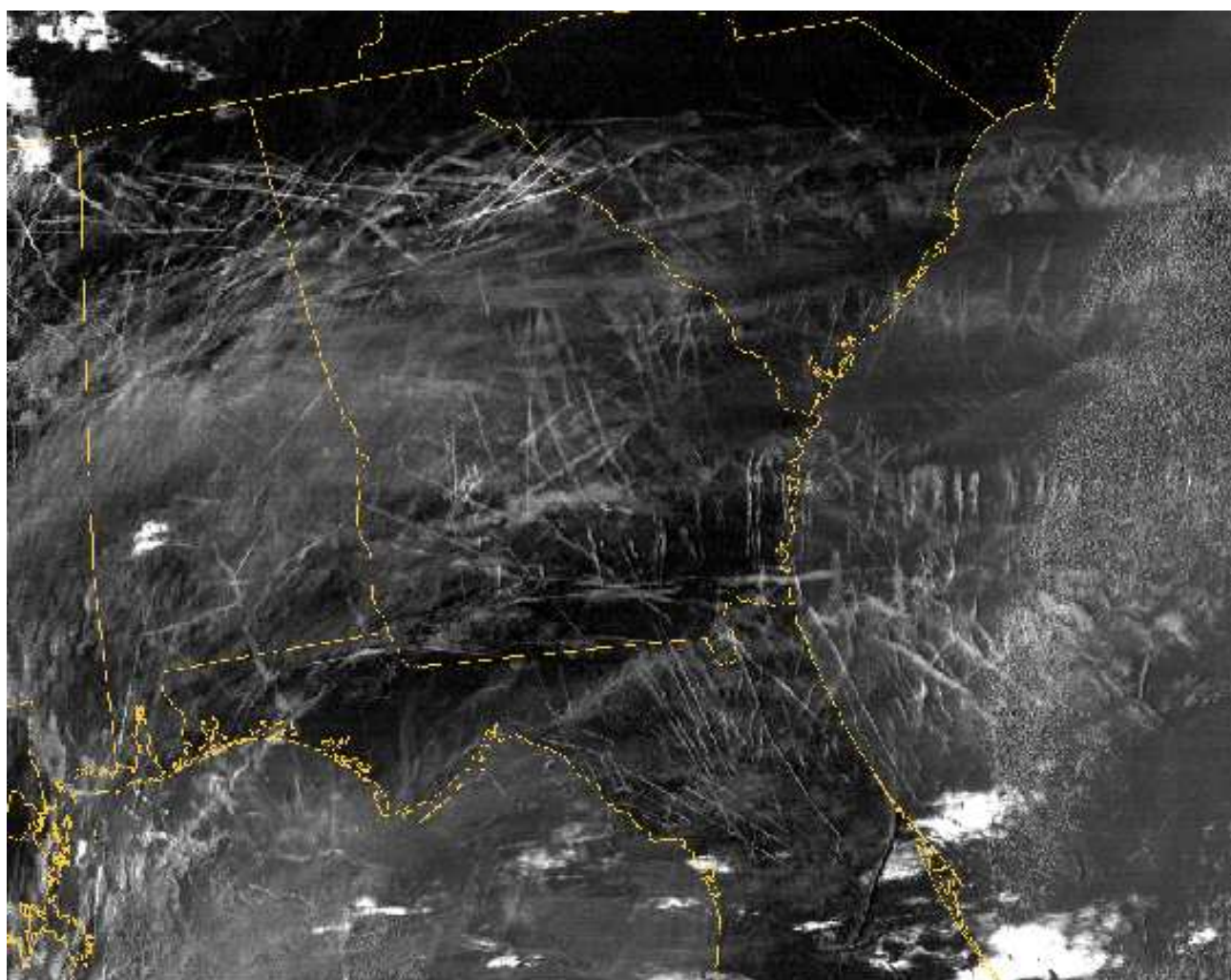


Figure 1. Contrails over North America, as detected by NASA's Terra satellite on January 29, 2004.

http://earthobservatory.nasa.gov/Newsroom/NewImages/Images/contrails_southeast_lrg.gif



Figure 2. Contrails at sunrise. Photo: Jim Kaler (with permission).



Figure 3. An isolated contrail over the Greenland ice cap (North GRIP photo).

DRAFT

Synergy considerations for the ELT site

Summary

Given the distribution of potential sites around the world, the ELT will be located either within a few degrees of ALMA or more than 40-50 degrees away in geographical latitude. A large latitude difference will have serious negative consequences for scientific synergy between the two facilities. Considering the importance of both facilities in the coming decades, this should be a major factor in selecting the site for the ELT.

Latitude distribution of sites

In terms of latitude difference from ALMA, the distribution of potential ELT sites is effectively bimodal - the sites are either within a few degrees of ALMA, or over 40-50 degrees away.

ALMA is being built on the Llano de Chajnantor in the Atacama region of Chile, at a latitude of -23 degrees. Several potential sites for the ELT are within a few degrees of this latitude. Almost all the others are in the northern hemisphere, at latitudes ranging from 43 to 62

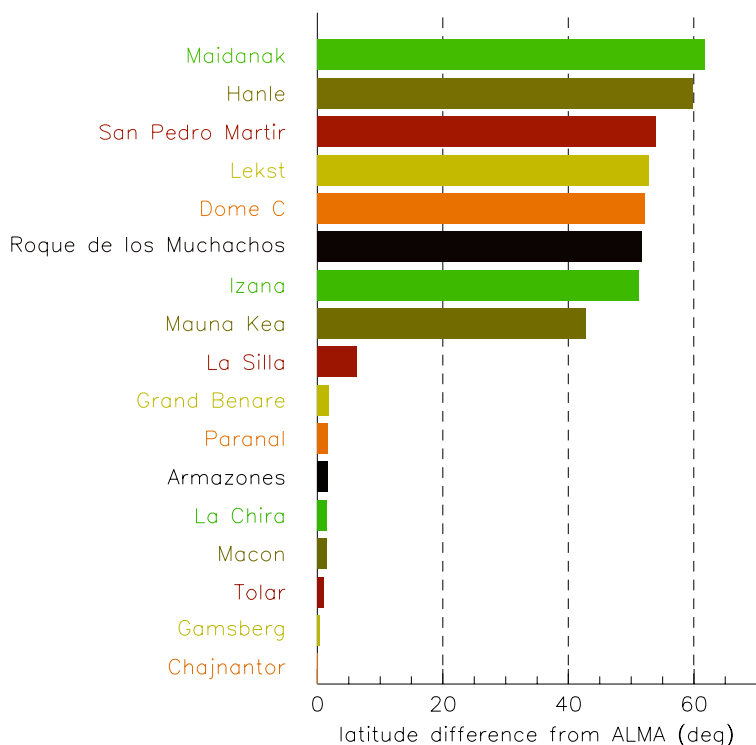


Fig 1 - Distribution of latitude difference between ALMA and possible ELT sites. Note that the distribution is bimodal: the ELT latitude is either within 5 deg of that of ALMA, or more than 40 deg away

deg north of ALMA (all but one (Mauna Kea) are more than 50 deg away from ALMA in latitude). The only site significantly to the south of ALMA is Dome C in the Antarctic, 52 degrees away. Thus, the sites under consideration for the ELT are either optimally placed in latitude for scientific synergy with ALMA, or very far away. This is illustrated in fig. 1.

Effect of latitude difference on observational efficiency

At 50 deg. zenith distance, at optical and near-infrared wavelengths, an ELT would only achieve 65% to 70% of the S/N that would be achieved at zenith

– it would require 2.2 times longer integration time to achieve the same S/N as at zenith (see fig. 2). Thus, for a source that transits overhead of ALMA, observations using an ELT located 50 deg away would be 2.2 times less efficient than if the ELT were located at the same latitude as ALMA. In addition, the image quality (seeing) would be worse by 30%, and there would be serious consequences for the performance of adaptive optics.

Conversely, for a source that transits overhead of an ELT located 50 deg away from ALMA, the S/N achieved by ALMA would be only 40% and 72% of that at zenith for 650 and 345 GHz respectively – the integration times would have to be 6 and 1.9 times longer at 650 and 345 GHz respectively to achieve the same sensitivity as at zenith (fig. 3). In addition, the phase stability for ALMA observations at 50 deg ZD would be about 25% worse than at zenith, further diminishing both the S/N and the image quality. (Phase errors cause a loss of coherence of visibilities and limit the spatial resolution.)

Suppose one were to choose an optimal field for a joint ALMA-ELT deep survey. If the latitude difference between ALMA and an ELT were small, such a field would likely be chosen at a declination close to -23 deg. If one observed this field for four hours centered around transit (HA from -30 to +30 deg), the total S/N ratios relative to observing a source at 0 deg ZD would be between 97% to 98% for the optical to near-IR, and between 94% and 99% for ALMA frequencies ranging from 650 GHz to 100GHz. Obviously, the total efficiency of such an experiment would be very high.

Now consider an ELT located at +27 degrees latitude, i.e., 50 deg away from ALMA. In this case the survey field would probably be chosen close to the equator. Taking the same observational strategy as above, the integrated S/N ratios would drop to between 86% and 88% in the optical/near-IR, and the S/N ratios in the ALMA band would be 77% in at 650 GHz, 91% at 345 GHz, and 96% at 100 GHz. A combined I-band – 650 GHz survey would have a S/N ratio of 69% compared to 91% for a survey with ALMA and ELT at the same latitude. This translates into a difference of factor 1.7 in the combined ALMA-ELT observing time. For a combined I-band – 100 GHz survey, this difference would be a factor 1.2. Of course, one would not want to restrict all observations to this narrow declination band.

As another example therefore, we consider what the effect on efficiency would be if the ELT were to observe ‘typical’ ALMA sources. Suppose that ALMA will typically observe sources over the declination range -50 to 0 deg, with hour angles between -30 and 30 deg. The inte-

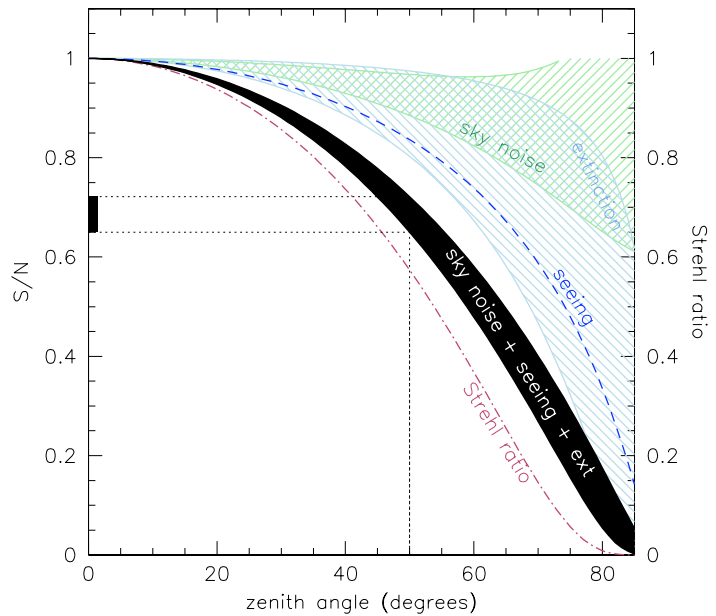


Fig 2 - Signal-to-noise ratios of an ELT normalised to that maximally achieved at zenith. The shaded areas show the effects of atmospheric extinction and sky brightness, ranging from U-band to I-band, and the dashed line shows the effect of seeing. The black band shows the combined effect. The dash-dot line indicates the AO performance as a function of zenith distance. Projected on the y-axis is the expected S/N at 50 deg zenith distance.

grated S/N ratios compared to observing at zenith are high, between 88% and 98%, for the 650 GHz to 100 GHz bands, respectively. If an ELT at latitude -23 deg were to observe the same sources, the integrated S/N ratios would be approximately 95% of those at zenith. However, if the ELT were at +27 deg, the relative S/N ratios would drop by a factor 1.5, corresponding to a factor 2.2 in integration time.

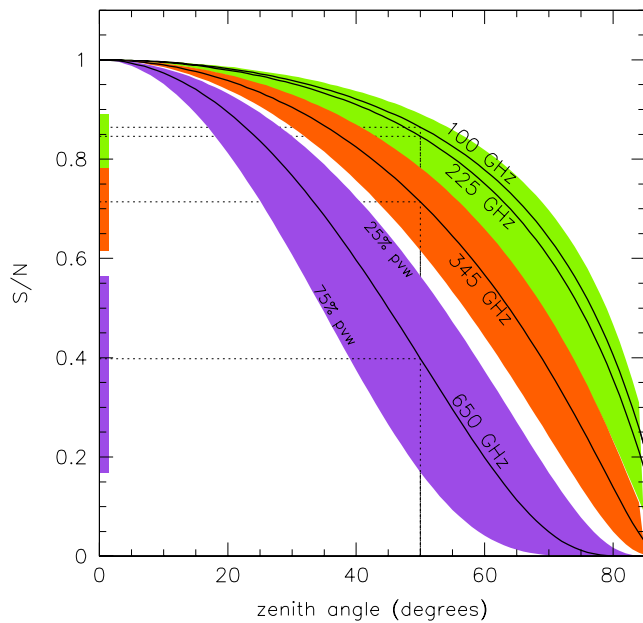


Fig 3 - Signal-to-noise ratios for four ALMA bands, normalised to that maximally achieved at zenith. Both the effect on optical depth and the tropospheric effect on system temperature are taken into account. The bands indicate the range between the 25th and 75th percentiles of the precipitable water vapour (pwv) at Chajnantor. Projected on the y-axis are the expected S/N values at 50 deg zenith distance.

corresponding to a factor 2.2 in integration time.

It should be noted that all of these estimates are optimistic because not all observational factors have been taken into account – any others can only make matters worse.

Discussion

The scientific synergies between ALMA and an ELT cover most of the science cases of each, ranging from the first objects that reionized the Universe and the entire subsequent evolution of galaxies, to the formation of stars and planets in our own Galaxy. It is therefore important that these two facilities be able to work together as efficiently as possible, and this requires that they be located at similar latitudes. The VLT, and three of the four sites currently under study for the SKA, are also located within a few

degrees of the latitude of ALMA; if future synergy with these facilities is also considered desirable, this adds further to the case for the ELT site being in that latitude range – not to mention the many unique features of the southern sky.

Acknowledgements

We are grateful to F. Patat, J. Richer, M. Le Louarn and M. Sarazin for essential input on which this study is based. We would also like to thank several others for helpful discussions, including M. Casali, U. Kaeufl, M. Kissler-Patig, R. Siebenmorgen and T. Wilson.

NaI column densities

It has been suggested that the NaI column densities suffer from strong seasonal variations (Ageorges & Els, SPIE Vol 5490, 1041 (2004)). NaI profiles are retrieved from ODIN by measurements of the sodium dayglow at 589 nm. In a first step, Dr. Gumbel (MISU Stockholm) has retrieved NaI column densities as a function of time (see figure). There is no geographical longitude dependence of NaI column densities. The group at MISU is in progress to construct a sodium reference atmosphere, based on satellite and LIDAR measurements and on numerical modeling. The model is to be prepared for the upcoming COSPAR conference in July and will be made available to this group.

